STREAMLINE-BASED TRANSPORT TOMOGRAPHY AND HISTORY MATCHING FOR THREE-PHASE FLOW

A Dissertation

by

DONGJAE KAM

Submitted to the Office of Graduate and Professional Studies of
Texas A&M University
in partial fulfillment of the requirements for the degree of

DOCTOR OF PHILOSOPHY

Chair of Committee,	Akhil Datta-Gupta
Committee Members,	Michael J. King
	Eduardo Gildin
	Yalchin Efendiev
Head of Department,	A. Daniel Hill

August 2015

Major Subject: Petroleum Engineering

ABSTRACT

Reconciling a geological static model to the available dynamic information, known as history matching, is an essential procedure for the decision-making through predictions of fluid displacement in a reservoir. However, there are several challenges in the history matching workflow because the geologic models are becoming complex and more detailed with a large number of grids. Recently, streamline-based inverse modeling has shown great promise for the high resolution geologic model because of many advantages in terms of computational efficiency and applicability. However, the current approach is primarily focused on handling the water-cut and tracer test data. This dissertation presents a novel streamline-based approach to incorporate a variety of dynamic information into the history matching process for the forecasting of reservoir behavior with increased confidence.

We first develop the streamline-based transport tomography by incorporating novel tracer technology. The distributed arrival time made available by a novel tracer provides a significantly improved flow resolution for reservoir characterization. We demonstrate the new approach for streamline-based history matching of distributed water arrival time together with aggregated well production data that clearly shows the benefits of the transport tomography using novel tracers.

Second, we propose a new methodology to incorporate bottom-hole pressure data into the geologic model using the streamline-based approach. This approach overcomes the limitation of the sequential process used in previous applications by facilitating the joint inversion, while reproducing reservoir energy during the flow rate matching. The joint

inversion with a multiscale approach is suggested to account for the disparity in resolution of different types of data. It leads to capturing of the large- and fine-scale heterogeneity and reproducing the pressure and water-cut responses efficiently.

Finally, we extend the streamline-based inverse modeling to the three-phase system by adding gas-oil ratio data simultaneously. We validate that the streamline-based analytical sensitivity of the gas-oil ratio can provide reasonable approximations for the purpose of inverse modeling. The Pareto-front concept is introduced for a multiscale multiobjective approach in combination with the streamline approach to overcome the challenges in the streamline-based three-phase joint inversion.

In addition to demonstration of the streamline-based history matching method with a variety of dynamic data, we emphasize the applicability of our approach to the field-scale reservoir model to satisfy the industry demands.

DEDICATION

I dedicate this dissertation to the Lord, my wife, and my family including my parents in law.

ACKNOWLEDGEMENTS

I would like to express my sincere gratitude to my committee chair, Dr. Datta-Gupta for his academic guidance and financial support throughout the course of this research. His continuous encouragement and teaching assisted me to finish my PhD degree. Also his support for industry opportunities through internship was extremely helpful for my future career.

I would also like to extend my sincere appreciation to my committee members, Dr. King, Dr. Gildin, and Dr. Efendiev for their thoughtful discussions and suggestions that improved the contents of this research.

Thanks also go to MCERI alumni and current students for their mentorship and friendship.

Finally, special thanks to my beloved family.

TABLE OF CONTENTS

Page

LIST OF FIGURES

Page

LIST OF TABLES

Page

CHAPTER I

INTRODUCTION AND STUDY OBJECTIVES

The reservoir property models will always have considerable uncertainty because of the complexity of reservoirs and limited amount of information. Optimal use of all available data will contribute to reducing this uncertainty in the reservoir model. Thus, history matching with a variety of information is critical in building reliable reservoir models and prediction of future behavior with increased confidence.

The history matching is the process to reconcile geological models to the dynamic data such as production history, well test and time-lapse seismic measurement data. In general, the objective of history matching is minimization of data misfit between observed historical data and calculated response from the forward simulator by calibrating the reservoir properties. There are several approaches to such minimization, in this dissertation, we focus on the streamline-based approach.

1.1 Overview of History Matching and Research Objectives

Over the decades of the history matching technologies development, various automatic history matching methods have been developed. They are mainly categorized in deterministic (Vega el al. 2004, Hoffman et al. 2006) and stochastic method (Hastings 1970, Granville et al. 1994). The other classification is gradient and non-gradient (derivative-free) method. First, the stochastic method is typically a non-gradient method such as evolutionary algorithm (simulated annealing, genetic algorithm etc.), Monte-Carlo

methods, and Ensemble Kalman Filter. These methods generally generate multiple history matched static models to cover the solution space in a probabilistic manner that can be used for uncertainty quantification of future reservoir performance. However, they are limited to relatively small number of parameters because of the computational burden (Oliver et al. 2008). Secondly, deterministic methods utilize the model sensitivity, which is the partial derivative relates the reservoir properties to the well responses, to find a solution from a given single prior model. The perturbation method, adjoint method, and streamline-based method are belong to this category. The perturbation method is computationally prohibitive for large number of parameters because it requires ($N+1$) forward simulation where N is the number of parameters. Adjoint method (Li et al. 2003) uses the optimal control theory and mathematically complex and typically requires access to the source code of the forward simulator which may not be available (Rey et al. 2009).

Recently, streamline-based history matching techniques have shown great promise for integrating field-scale water-cut and tracer data into high resolution geologic models. This approach has many advantages in terms of computational efficiency and applicability (Datta-Gupta and King 2007). The main advantage of the streamline-based method is that it is able to calculate parameter sensitivity with a single streamline simulation and a post process of the finite difference simulation results. The approach can be extended to account for the gravity and changing field conditions (He et al. 2002).

The current status of the streamline-based history matching is mainly focused on the water-cut matching (Rey et al. 2009; Hohl et al. 2006; Cheng et al. 2004). However, dealing with uncertainties in reservoir models and making reliable static models

essentially requires integration of all available dynamic data in the field. Thus, our goal in this research is to develop an efficient approach to incorporate the surveillance data from novel tracer technology that provides distributed water arrival time along the wellbore (transport tomography), three-phase production and pressure data such as water-cut, bottom-hole pressure, and gas-oil ratio into geologic model utilizing streamline information.

1.2 Dissertation Outline

This research focuses on the development of the novel streamline-based algorithms to establish the history matching process with a variety of dynamic information and the applicability to the field-scale reservoir model. Main objectives and corresponding chapters of this dissertation are as follows.

- Develop the streamline-based transport tomography using novel tracer technology (Chapter II)
- Present the pressure sensitivity with respect to reservoir properties and develop a joint inversion for water-cut and pressure data with a multiscale approach (Chapter III)
- Extend streamline-based approach to the three-phase flow system by integrating pressure and production data (water-cut and gas-oil ratio) simultaneously and field application with a multiscale multiobjective approach (Chapter IV)

1.3 Software Prototype

The primary deliverable of this work will be a software prototype called "DESTINY" for streamline tracing, streamline-based history matching, and optimization algorithm. All of the proposed methods, transport tomography using novel tracer and streamline-based history matching for water-cut, bottom-hole pressure, and gas-oil ratio (with a multiscale approach), are implemented in this software. The applications in this dissertation have been carried out using DESTINY (Appendix B).

CHAPTER II

STREAMLINE-BASED TRANSPORT TOMOGRAPHY USING NOVEL TRACER TECHNOLOGY*

2.1 Chapter Summary

Traditional history matching involves calibration of reservoir models using well response such as production or tracer data aggregated over multiple producing intervals. With the advent of novel tracer technologies, we can now obtain distributed water or tracer arrival time information along the length of horizontal or vertical wellbores. This provides significantly improved flow resolution for detailed reservoir characterization through inversion of distributed water or tracer arrival times in a manner analogous to travel tomography in Geophysics.

In this chapter, we present an efficient approach to incorporate novel tracer surveillance data and distributed water arrival time information during history matching of high resolution reservoir models. Our approach relies on a novel streamline-based workflow that analytically computes the sensitivity of the arrival time with respect to reservoir heterogeneity, specifically porosity and permeability variations. The sensitivities relate the changes in arrival time to small perturbations in reservoir properties and can be obtained efficiently using the streamline-based approach with a single flow simulation.

* Part of data reported in this chapter is reprinted with permission from "Streamline-based Transport Tomography Using Novel Tracer Technologies" by Kam, D., and Datta-Gupta, A. 2014, Paper SPE 169105 Presented at the SPE Improved Oil Recovery Symposium, 12-16 April, Tulsa, Oklahoma, U.S.A.

This makes the approach particularly well-suited for high resolution reservoir characterization. Finally, the sensitivities are used in conjunction with an iterative inversion algorithm to update the reservoir models using existing and proven techniques from seismic tomography.

The power and utility of our proposed approach is demonstrated using both synthetic and field examples. These include the SPE benchmark Brugge field, Hill Air Force at Utah, and an offshore field in North America. Compared to traditional history matching techniques, the proposed tomographic approach is shown to result in improved resolution of heterogeneity through matching of water arrival time at individual completions in addition to the aggregated well production response. This results in improved performance predictions and better identification of bypassed oil for infill targeting and EOR applications.

2.2 Introduction

Integration of dynamic data such as well water-cut, production rate and bottom-hole pressure requires least-squares-based minimization to match the observed and calculated response (Vasco et al. 1999). There are several approaches to such minimization, and we reviewed them in chapter I. Oliver and Chen (2011) summarized the details of the current minimization methods for reservoir history matching. In this research, we use sensitivity-based methods using streamlines that analytically compute the parameter sensitivities which are partial derivatives defined as the change in production response because of small changes in reservoir parameters.

The streamline approach has provided an extremely efficient means for computing parameter sensitivities. The parameter sensitivities are formulated in terms of one-dimensional integrals of analytical functions along the streamlines. Specifically, the streamline-based generalized travel time inversion (GTTI) technique has proved to be an efficient means for computing parameter sensitivities under changing well conditions as commonly encountered in field applications (Cheng et al. 2005; Cheng et al. 2004; He et al. 2002). The GTTI history matching approach has been utilized in a large number of field applications (Rey et al. 2009; Hohl et al. 2006; Cheng et al. 2004). These applications have effectively matched the well water-cut response based on aggregated production data from the wellbore. However, it is very common to have multiple producing intervals along the wellbore and multiple completions are widely prevalent in horizontal and multi-segmented wells. Thus, matching the aggregated well response is often inadequate to get the high resolution reservoir model constrained to reservoir fluid movements.

Recently, several novel tracer technologies have been developed and implemented in oil and gas fields. In one such approach, the tracer is installed within the completion and each well segment can have a different chemical tracer (Figure 2.1) (Williams and Vilela 2012; Napalowski et al. 2012). With such novel technologies analysis of the effluent tracer information can now indicate the location and the timing of water breakthrough at each completion along the wellbore. It is similar to vertical tracer profiling (VTP) discussed by Maroongroge et al. (1995). For inter-well tracer tests, they demonstrated the advantages of sampling tracers at different completions along the depth of the reservoir instead of the

conventional tracer tests that measure a single integrated tracer concentration history at a well.

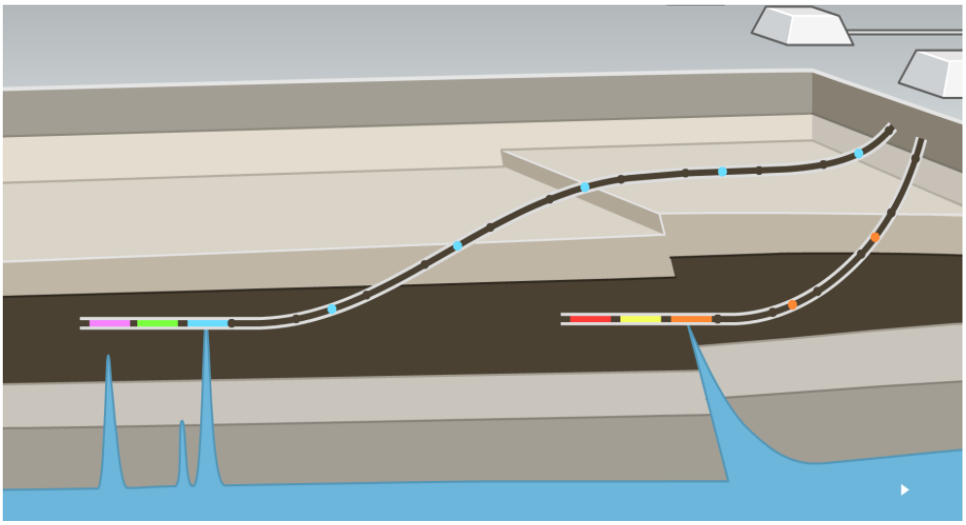

Figure 2.1 Operation of the novel tracer technology in a reservoir. *(http://www.resman.no)*

In this chapter, we focus on the reservoir characterization by matching distributed water arrival time information along the wellbore. Specifically, we formulate the inverse problem related to history matching to combine aggregated well water-cut information that is commonly used together with distributed water arrival time data that is now provided by the novel tracer technology. We demonstrate that the additional information can significantly improve the flow resolution in streamline-based history matching. The outline of this chapter is as follows. To start with, we discuss how the novel tracer technology is combined to the conventional history matching based on the aggregated well response. We then illustrate the approach using a two-dimensional synthetic model. Next, we describe the mathematical background for computing the streamline-based analytic

sensitivities for aggregated water-cut response and distributed water arrival time. In addition, we analyze the effect of the quality and quantity of the tracer data on the inversion results. Finally, we demonstrate the history matching applications using SPE benchmark Brugge field model, Hill Air Force base, and an offshore field model that the novel tracer technology is implemented in. These applications demonstrate the power, utility, and effectiveness of our new approach.

2.3 Background and Methodology

An outline of the procedure for streamline-based inverse modeling approach is given in the flow chart in Figure 2.2. We have used a commercial finite-difference simulator (ECLIPSE, Schlumberger 2012b) for modeling fluid flow in the reservoir including comprehensive physical mechanisms such as compressibility, gravity and crossflow effects. The main difference of our proposed approach compared to the previous ones (Cheng et al. 2005; He et al. 2002) is in sensitivity computation because we need to calculate two different types of sensitivities. For aggregated well water-cut match, we implement the generalized travel time inversion (GTTI) technique. The generalized travel time is computed by systematically shifting the computed production response toward the observed data until the cross correlation between the two is maximized (He et al. 2002). The distributed water arrival time at individual completions provided from novel tracer technology is matched using travel time inversion (TTI) technique at the specific time that water breakthrough happens (Cheng et al. 2005). Note that unlike the well water-cut response, the distributed information is not a time series but a single arrival time data at

each completion. We will explain in more detail later. Using these two groups of sensitivities, we minimize the difference between the observed and calculated response for the well water-cut and water arrival times at each completion. Because our approach utilizes streamlines for sensitivity calculations, we can easily distinguish the streamlines from each well and each completion. Thus, we calculate well sensitivity by GTTI method using streamlines from each well and completion sensitivity by TTI method based on streamlines from each completion separately without much additional computation time.

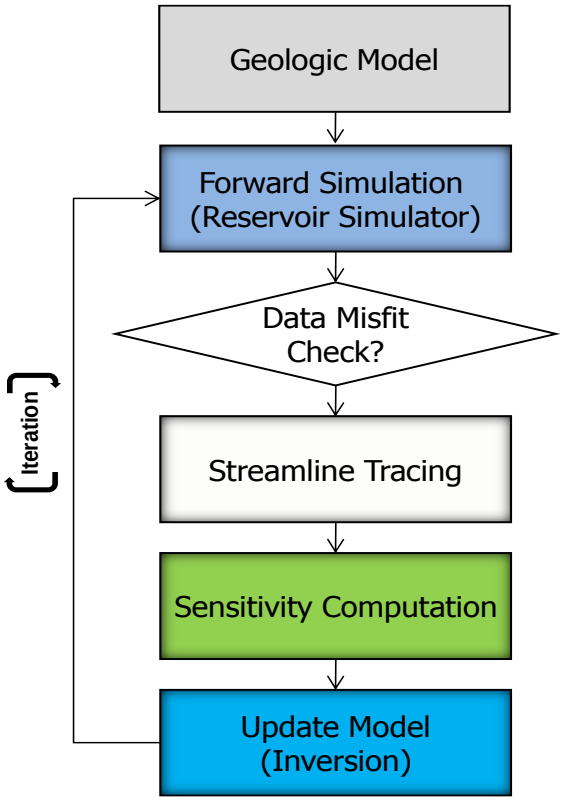

Figure 2.2 Overview of the streamline-based history matching workflow.

2.3.1 Illustration of the Method

Before going into the mathematical details, we illustrate our procedure using a synthetic example, which is a two-dimensional two-phase reservoir cross-section consisting of 100x1x50 grid blocks, with one injector and one producer. Table 2.1 shows the simulation properties used in a commercial flow simulator. The reference permeability model is generated by sequential Gaussian simulation with well permeability values as conditioning data as shown in Figure 2.3b. Location of completions is shown with a black line along the wells. The initial permeability model (Figure 2.3a) is also generated by sequential Gaussian simulation but with different geostatistical parameters from the reference model. The observation data for history matching is obtained from the reference model using a commercial reservoir simulator. These include liquid production rate, well water-cut, and water arrival time at each completion. Figure 2.3c and Figure 2.3d are the time of flight (TOF) along streamlines that reflect the difference of permeability between the initial and reference model. Because the TOF is a measure of the travel time from injector to producer, streamlines that go through high permeability layers have short TOF at producer; meanwhile streamlines that trace low permeability layers have high value of TOF.

We start with the initial model and calibrate the permeability distribution to match the aggregated well water-cut and distributed water arrival times at the completions. Two cases are compared to examine the effectiveness of our new approach.

- Case 1: It corresponds to the traditional approach whereby we calibrate the permeability model with aggregated well water-cut information only. The generalized travel time inversion method (well GTTI) is used for this purpose.
- Case 2: It updates the permeability distribution based on both the aggregated well water-cut as in Case 1 and additionally, the distributed water arrival times provided by the novel tracer technology (well GTTI + completion TTI).

Table 2.1: General parameters for numerical simulation

Parameters	Input Values
Grid number	(nx,ny,nz) = (100,1,50)
DX	10 [ft]
DY	30 [ft]
DZ	2 [ft]
Porosity	0.15
Rock compressibility	4.0 E-06 [1/psi]
Oil density	45 [lb/cf]
Water density	62.02 [lb/cf]
Oil viscosity	0.91 [cp]
Water viscosity	0.96 [cp]
Oil formation volume factor	1.12
Water formation volume factor	1.00
Total simulation time	600 [days]
Time step size	50 [days]

***PVT properties are at the reference pressure of 4000 psi**

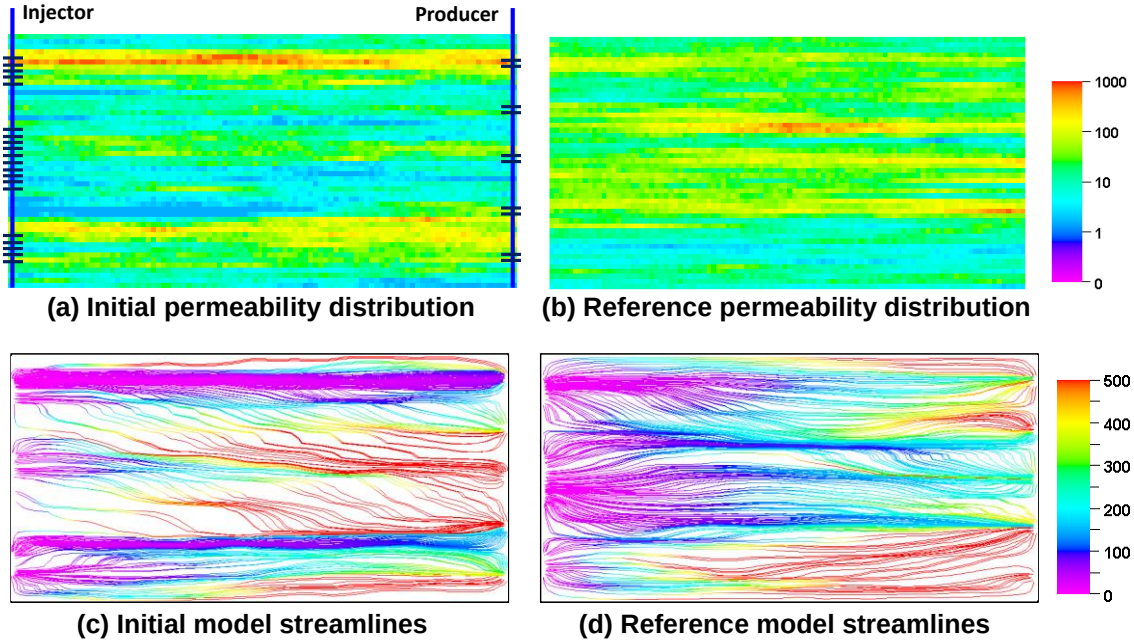

(a) Initial permeability distribution (b) Reference permeability distribution

(c) Initial model streamlines (d) Reference model streamlines

Figure 2.3 2D permeability distributions and streamlines (color shows TOF) for reference and initial models.

The history matching results are shown in Figure 2.4. Even though well GTTI method improves the match of the calculated water-cut response to the observed data (Figure 2.4a), well GTTI with completion TTI method gives better final permeability model that matches better the reference model because of the significantly improved flow resolution (Figure 2.4b). Figure 2.5 shows the cross plot of water arrival time between observed and calculated data for 1st and 2nd case after history matching. Compared to the initial model, Case 1 clearly results in improved match with the observed water arrival time. But Case 2 shows better agreement between observed and calculated response at all completions. In Figure 2.6a and Figure 2.6b, updated permeability models are shown. Streamlines based on the two updated models are shown in Figure 2.6c and Figure 2.6d. Compared to the

initial model streamlines, they are similar with the streamline and TOF color of reference model because we captured the heterogeneity during history matching process. Next, we examine if the changes made to the initial model are consistent with the reference model. Figure 2.7a is permeability change needed that is reference permeability minus the initial permeability which indicates reducing permeability at top and bottom part and increasing permeability in middle layers are required. Figure 2.7b and Figure 2.7c is permeability change made during history matching process (final model minus initial model) for the two cases. We can see that Case 2 makes permeability changes that are closer to Figure 2.7a, driving it towards the reference model particularly in the central layers. In addition, TOF color in Figure 2.6d (Case 2 streamlines) shows better agreement to the reference model streamlines at the middle and bottom part of the reservoir model compared to Case 1 final model. The effect of this permeability changes can be clearly seen in the water saturation distribution that depicts water front propagation during production. We compare the water saturation distribution in Figure 2.8. At 100 days, Case 2 final model successfully captures the low permeability at the top layers. Thus, there is no water breakthrough as in the reference model, but Case 1 has water breakthrough by this time. As we have seen in Figure 2.7c, the proposed approach increases the permeability at the middle part, causing the water saturation at 300 days for Case 2 to have water breakthrough. In contrast, in Case 1 the water front does not reach the producer in the central layers at 300 days. At 500 days, the final model with distributed water arrival time information (Case 2) shows very similar water saturation distribution when compared with the reference model. These results confirm that the integration of aggregated well water-

cut response together with water arrival time at completions constrain the history matching solution effectively with our proposed approach.

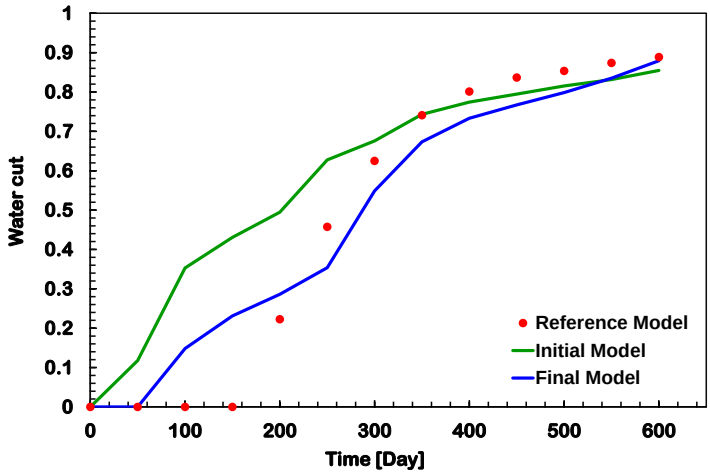

(a) Case 1: using aggregated well response

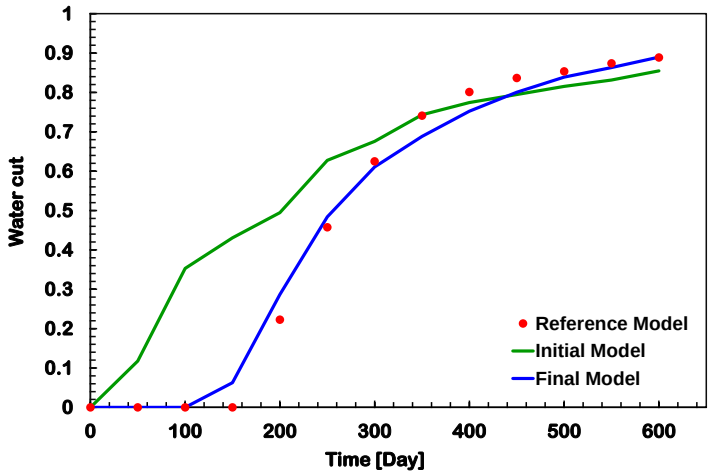

(b) Case 2: using aggregated well response and distributed water arrival time

Figure 2.4 2D simulation model water-cut history matching results.

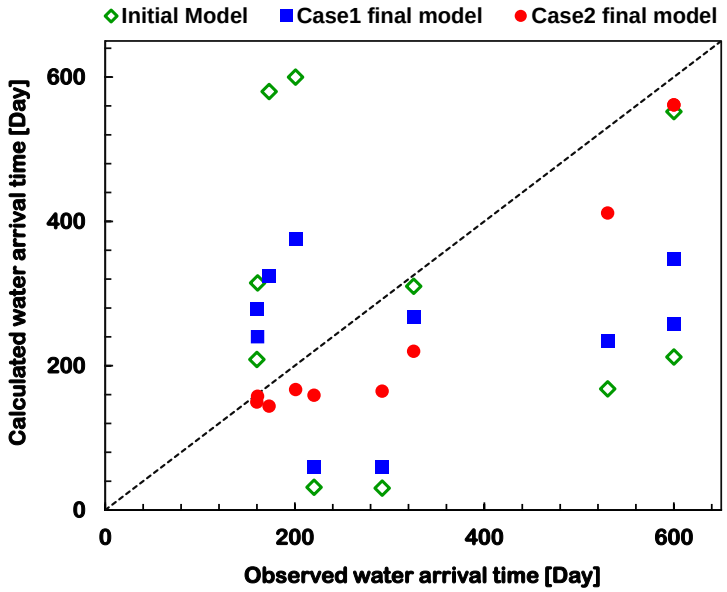

Figure 2.5 Observed and calculated water arrival time at all tracer locations before and after history matching.

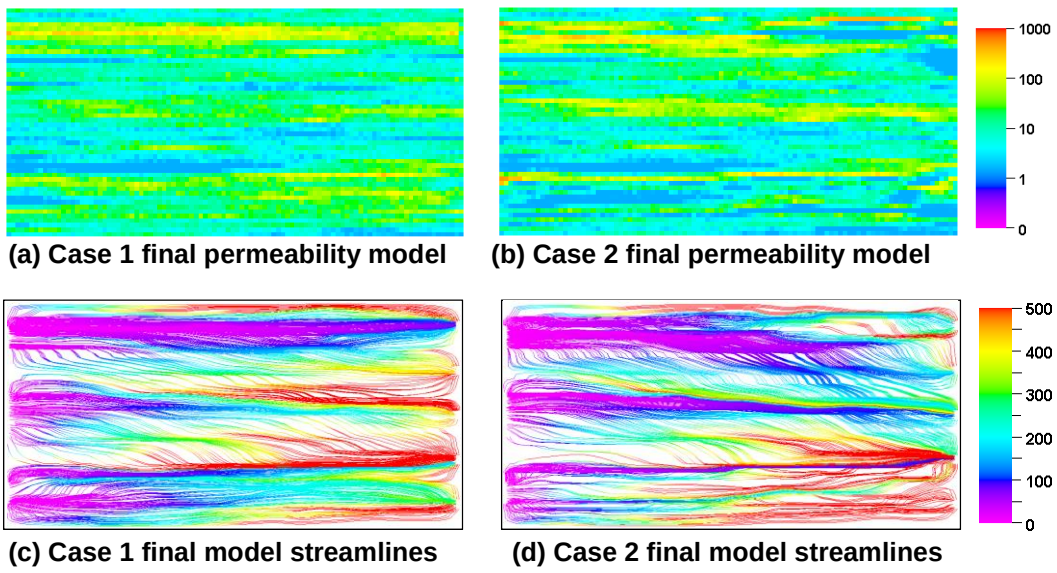

(a) Case 1 final permeability model **(b) Case 2 final permeability model**

(c) Case 1 final model streamlines **(d) Case 2 final model streamlines**

Figure 2.6 Updated permeability distribution and streamlines.

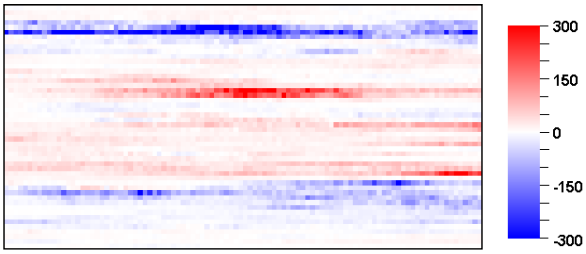

(a) Change needed

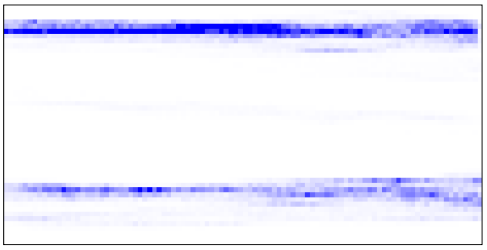

(b) Change made of Case 1

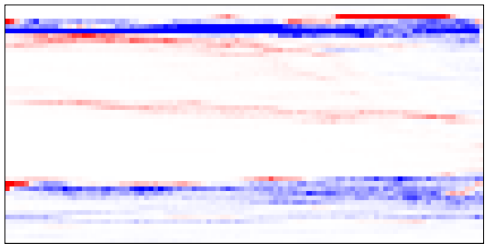

(c) Change made of Case 2

Figure 2.7 Comparison of permeability distribution changes.

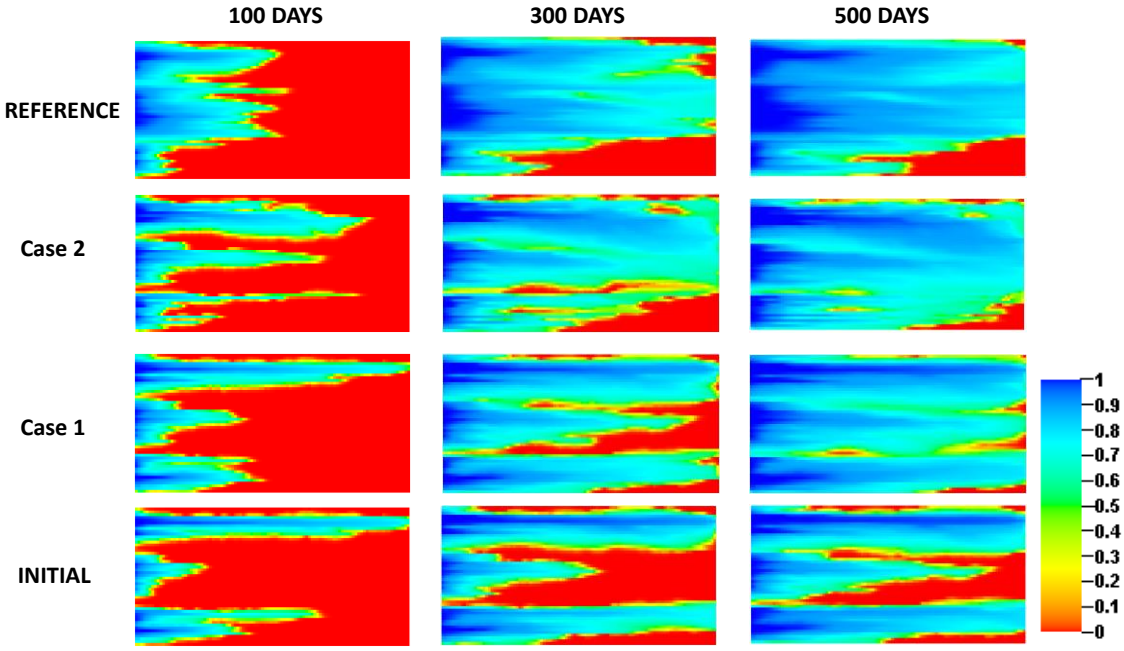

Figure 2.8 Water saturation distribution at 100 days, 300 days and 500 days after production.

2.4 Mathematical Formulations

In this section, we discuss the mathematical details related to streamline tracing, streamline-based sensitivity computations, TTI (Travel Time Inversion), GTTI (Generalized Travel Time Inversion), and the related inverse problem.

2.4.1 Time of Flight and Streamline Tracing

The basic variable in streamline simulation is the time of flight (TOF), which is the travel time of a neutral tracer along a streamline (Datta-Gupta and King, 2007). The TOF can be expressed as

$$\tau = \int_{\psi} s(x)dr \tag{2.1}$$

The integral is along the streamline trajectory ψ, r is the distance along streamline and s is the slowness defined by the reciprocal of the interstitial velocity,

$$s(\boldsymbol{x}) = \frac{1}{|\vec{v}(\boldsymbol{x})|} \tag{2. 2}$$

To compute time of flight, we essentially trace the streamline based on velocity field. A streamline is defined as the integrated curves that are locally tangential to the direction of the velocity. Tracing streamlines is based on the analytical description of a streamline path within a gridblock as described by Pollock (1988). Let us consider a gridblock in Figure 2.9 to illustrate the streamline tracing algorithm. The numerical solution gives the fluid velocities (fluxes) at the block faces.

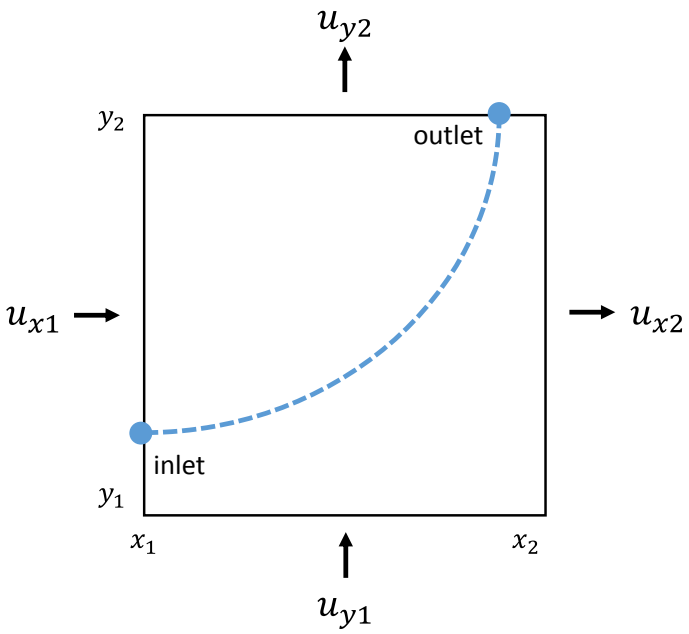

Figure 2.9 Streamline tracing in 2D single cell.

Pollock's algorithm uses a sub-gridblock velocity model with the underlying assumptions, in which a velocity in each direction varies linearly, and velocities in the other directions are independent. This leads to the following cell velocity model Eq. 2.3 and Eq. 2.4,

$$u_x = u_{x1} + c_x(x - x_1) \tag{2. 3}$$

$$c_x = \frac{u_{x2} - u_{x1}}{\Delta x} \tag{2. 4}$$

where Δx is grid size of x-direction and u is total phase velocity. Computations of the streamline trajectories and time of flight within the gridblock are available by a direct integration of the cell velocities, Eq. 2.5,

$$\frac{d\tau}{\phi} = \frac{dx}{u_x} = \frac{dy}{u_y} = \frac{dz}{u_z} \tag{2. 5}$$

where ϕ is porosity. We can integrate Eq. 2.5 explicitly, and independently, for each direction to obtain the time of flight to each of the face. The integral solution in the x-direction from location x_0 is calculated by Eq. 2.6.

$$\frac{\Delta\tau_{xi}}{\phi} = \int_{x_0}^{x_i} \frac{dx}{u_{x0} + c_x(x - x_0)} = \frac{1}{c_x} ln\left(\frac{u_{xi}}{u_{x0}}\right) \tag{2. 6}$$

The index $i = 1,2$ indicates the face of the grid block in the x-direction. We can also calculate in the y- and z-direction using Eq. 2.6. Pollock's algorithm specifies the correct exit face as the on requiring minimum positive transit time (Eq. 2.7).

$$\Delta\tau = Min\ Positive\left(\Delta\tau_{x1}, \Delta\tau_{x2}, \Delta\tau_{y1}, \Delta\tau_{y2}, \Delta\tau_{z1}, \Delta\tau_{z2}\right) \tag{2. 7}$$

Now, we know the time of flight in grid cell, its exit coordinates can be obtained by rearranging Eq. 2.6.

$$x = x_0 + u_{x0}\left(\frac{e^{c_x\Delta\tau/\phi} - 1}{c_x}\right) \tag{2. 8}$$

2.4.2 Time of Flight Sensitivity Computation

Using Darcy's law, the slowness can be written as

$$s(x) = \frac{\phi(x)}{\lambda_{rt} k(x) |\nabla P|} \tag{2. 9}$$

where λ_{rt} is total relative mobility and ∇P is pressure gradient. Because *s* is a composite quantity involving reservoir properties, its first-order variation will be given by Eq. 2.10.

$$\delta s(x) = \frac{\partial s(x)}{\partial k(x)}\delta k(x) + \frac{\partial s(x)}{\partial \phi(x)}\delta \phi(x) \tag{2. 10}$$

The partial derivatives of Eq. 2.10 are Eq. 2.11 and Eq. 2.12.

$$\frac{\partial s(x)}{\partial k(x)} \approx \frac{-\phi(x)}{\lambda_{rt}\big(k(x)\big)^2|\nabla P|} = -\frac{s(x)}{k(x)} \tag{2. 11}$$

$$\frac{\partial s(x)}{\partial \phi(x)} \approx \frac{1}{\lambda_{rt}k(x)|\nabla P|} = \frac{s(x)}{\phi(x)} \tag{2. 12}$$

The approximation in Eq. 2.11 and Eq. 2.12 is that the local perturbations in permeability and porosity generate negligible pressure changes. The implication of this assumption is that streamlines do not shift because of these small perturbations. Now, it is possible to relate the change in travel time $\delta\tau$ to the change in slowness by integration along each streamline trajectory:

$$\delta\tau = \int_{\psi} \delta s(x)dr = \int_{\psi} \left[\frac{\partial s(x)}{\partial k(x)}\delta k(x) + \frac{\partial s(x)}{\partial \phi(x)}\delta \phi(x)\right] dr \tag{2. 13}$$

The tracer travel-time sensitivity along a single streamline with respect to permeability and porosity for a particular gridblock at location *x* follows from Eq. 2.13 by simply carrying out the integral from the entry to the exit of the streamline within the gridblock,

$$\frac{\delta\tau(\psi)}{\delta k(x)} = \int \left[-\frac{s(x)}{k(x)}\right] dr = -\frac{\mathrm{s(x)}}{k(x)}\Delta r \tag{2. 14}$$

$$\frac{\delta\tau(\psi)}{\delta\phi(\boldsymbol{x})} = \int \left[\frac{s(\boldsymbol{x})}{\phi(\boldsymbol{x})}\right] dr = \frac{\mathrm{s(x)}}{\phi(\boldsymbol{x})}\Delta r \qquad (2.\ 15)$$

where Δr is the arc length of the streamline within the gridblock.

2.4.3 Sensitivity of Saturation Front Arrival Time

Consider two-phase incompressible flow of oil and water described by the Buckley-Leverett equation using the streamline TOF as the spatial coordinate (Datta-Gupta and King, 2007).

$$\frac{\partial S_w}{\partial t} + \frac{\partial f_w}{\partial \tau} = 0 \qquad (2.\ 16)$$

S_w is water saturation and f_w is fractional flow of water. The velocity of a given saturation S_w along a streamline is given by the characteristic equation.

$$\left(\frac{\partial \tau}{\partial t}\right)_{S_w} = \left(\frac{df_w}{dS_w}\right)_{S_w} \qquad (2.\ 17)$$

This equation relates the travel time of water saturation, $t(S_w, \tau; \psi)$ to the time of flight τ. We can now relate the sensitivity of the water saturation arrival time to that of the tracer time of flight.

$$\frac{\delta t(S_w, \tau; \psi)}{\delta k(\boldsymbol{x})} = \frac{\delta\tau(\psi)}{\delta k(\boldsymbol{x})} \Big/ \frac{df_w}{dS_w} \qquad (2.\ 18)$$

$$\frac{\delta t(S_w, \tau; \psi)}{\delta \phi(\boldsymbol{x})} = \frac{\delta\tau(\psi)}{\delta \phi(\boldsymbol{x})} \Big/ \frac{df_w}{dS_w} \qquad (2.\ 19)$$

2.4.4 Travel Time Inversion (TTI)

Cheng et al. (2005) have demonstrated that there are several advantages of the travel time inversion compared to the traditional amplitude inversion whereby the water-cut response is matched directly. It can be shown that the amplitude inversion is highly nonlinear when compared to the travel time inversion, which has quasilinear properties (Cheng et al., 2005). As a result, the travel time inversion is more robust and is less likely to be stuck in local minimum. Furthermore, the travel time inversion entails matching only a single data point, e.g., the breakthrough time or the arrival time of the peak response. Because of this feature, it is applicable to matching distributed water arrival time in our approach. With the advent of novel tracer technologies, water breakthrough times are now available for all completions along the length of the wellbore. Thus, we can use the travel time inversion for matching the distributed water arrival times. During history matching, we calibrate the permeability distribution to minimize the difference in water arrival time between the observed data and the simulated response for all available completions as shown in Figure 2.10.

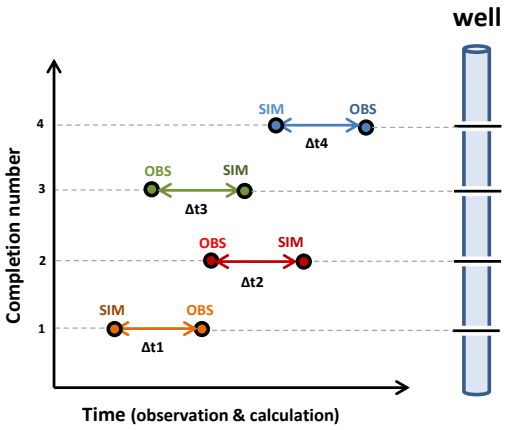

Figure 2.10 Illustration of distributed water arrival time misfit along the wellbore.

2.4.5 Generalized Travel Time Inversion (GTTI)

The GTTI is used to match the aggregated water-cut response at the well. Because of the favorable properties of travel time inversion, the GTTI poses the amplitude matching as a travel time inversion problem (He et al. 2002). Similar concepts have been effectively applied in seismic inversion, particularly for full waveform seismic inversion (Luo and Schuster 1991). In the GTTI approach, we seek an optimal time shift Δt of the data at each well so as to minimize the production data misfit at the well. This is illustrated in Figure 2.11 (left) in which the calculated water-cut response is systematically shifted in small time increments toward the observed response and the data misfit is computed for each time increment. The optimal shift will be given by the Δt that minimizes the misfit function as follows:

$$E(\Delta t) = \sum_{i=1}^{N_d} [y^{cal}(t_i + \Delta t) \; - \; y^{obs}(t_i)]^2 \tag{2.20}$$

Or, alternatively, we can maximize the coefficient of determination given by:

$$R^2(\Delta t) = 1 - \frac{\sum_{i=1}^{N_d} [y^{cal}(t_i + \Delta t) \; - \; y^{obs}(t_i)]^2}{\sum_{i=1}^{N_d} \left[y^{obs}(t_i) \; - \; \overline{y^{obs}} \; \right]^2} \tag{2.21}$$

Thus, the "generalized travel time" at well j is given by the optimal time shift, $\Delta \tilde{t}_j$ that maximizes the correlation coefficient as shown in Figure 2.11 (right).

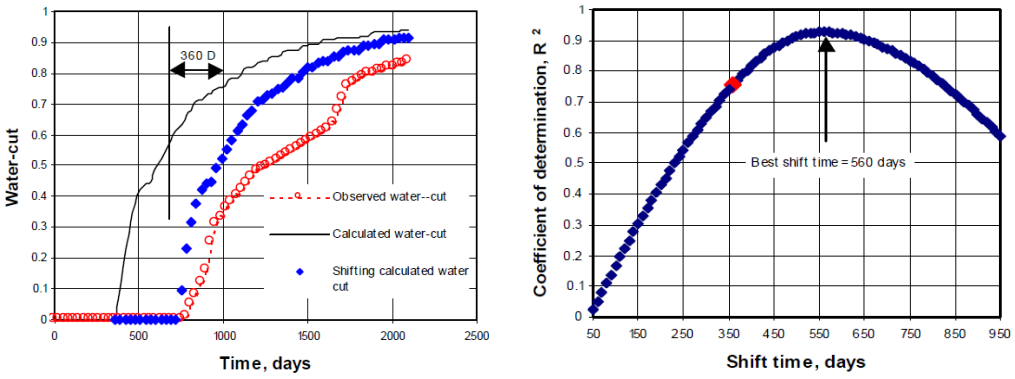

Figure 2.11 Illustration of the calculation of generalized travel time for water-cut (He et al. 2002).

2.4.6 Sensitivity of the Generalized Travel Time

In GTTI, we shift the entire observed water-cut data of each well by the optimal shift time. He et al. (2002) derived a rather simple expression for the sensitivity of the generalized travel time with respect to reservoir parameters *m*. It is given as the average of the travel time sensitivities of all data points. For example, for well j with N_d data points, the generalized travel-time sensitivity will be given as follows:

$$\frac{\partial \Delta \tilde{t}_j}{\partial m} = -\frac{\sum_{i=1}^{N_d} \left(\frac{\partial t_{i,j}}{\partial m}\right)}{N_d} \tag{2.22}$$

The negative sign in Eq. 2.22 reflects the sign convention adopted for defining the generalized travel-time shift, which is considered positive if the computed response is to the left of the observed data as shown in Figure 2.11 (left).

2.4.7 Inverse Problem

Integration of dynamic data for reservoir characterization typically requires the solution of an inverse problem for minimizing the data misfit between the computed and observed response. The mathematical formulation behind such streamline-based inverse problems has been discussed in detail elsewhere (He et al. 2002; Vasco et al. 1999). We start with a prior static model that already incorporates geologic, well logs and seismic data, and then minimize a penalized misfit function.

$$\|\delta d - S\delta R\| + \beta_1\|\delta R\| + \beta_2\|L\delta R\| \tag{2.23}$$

In Eq. 2.23, δd is the vector of the data residuals, S is the sensitivity matrix with respect to grid parameters, and δR corresponds to the change in the reservoir properties which is grid block permeability in this work. The second term, called the norm constraint, penalizes deviations from the prior model. This helps preserve geologic realism. The third term, roughness penalty, simply recognizes the fact that production data are an integrated response and are thus best suited to resolve large-scale rather than small-scale property variations. Here L defines the model roughness, a second-spatial difference operator. The minimum of Eq. 2.23 can be obtained by an iterative least-squares solution to the augmented linear system as follows:

$$\begin{pmatrix} S \\ \beta_1 I \\ \beta_2 L \end{pmatrix} \delta R = \begin{pmatrix} \delta d \\ 0 \\ 0 \end{pmatrix} \tag{2.24}$$

The weight β_1 and β_2 determine the relative strengths of the prior model and the roughness term. The selection of these weights can be somewhat subjective. In our application, the

first row in Eq. 2.24, representing the sensitivity and the data residual vector, is divided into two sections: aggregated water-cut part at each well and distributed water arrival time part at each completion.

$$S = \begin{pmatrix} S_{well} \\ S_{completion} \end{pmatrix} \tag{2.25}$$

$$\delta d = \begin{pmatrix} \delta d_{well} \\ \delta d_{completion} \end{pmatrix} \tag{2.26}$$

In Eq. 2.25, S_{well} is well based GTTI sensitivity that is average of travel time sensitivities for all data points, and $S_{completion}$ is completion travel time sensitivity that is calculated at the specific time when water breakthrough happens at individual completion. For the well data, δd_{well} in Eq. 2.26 is the optimal time shift of overall water-cut responses for a well and $\delta d_{completion}$ is arrival time misfit for each completion shown in Figure 2.10. An iterative least squares solution approach via the LSQR algorithm (Paige and Saunders, 1982) is used to solve Eq. 2.24 to obtain grid block permeability changes needed to minimize the overall data misfit.

2.5 Sensitivity Analysis for Quality and Quantity of Tracer Data

The distributed water arrival time information helps the improvement of history matching quality. However, the tracer information can have uncertainty because of packer failure, incorrect installation of tracer, or inaccurate lab analysis. In addition, it commonly has limited amount of data along the wellbore in the field. Here, we analyze the effect of the quality and quantity of the tracer information on the history matching results using simple model we have used in section 2.3.1. This analysis shows the importance of quality and quantity of tracer data in our approach.

2.5.1 Analysis of Tracer Quality

We compare three cases. Case 1 is the same as the case in section 2.3.1 using all correct tracer information. Case 2 and Case 3 add 20 percent and 50 percent of error in tracer data to check the impact of tracer data quality. The case with 20 percent error shows similar well response and water breakthrough time to the case that has all correct tracer data (Case 1) in Figure 2.12. However, when the tracer data has high uncertainty (50 percent error), the well response is impaired and the data misfit becomes bigger than the calibrated result without tracer data (Table 2.2). Although aggregated well responses are deviated by quality of tracer data, a cross plot of water arrival time in Figure 2.13 shows that the two cases with error have improvement of tracer data matching. This is because of the local permeability changes based on tracer information.

Table 2.2: Data misfit in quality analysis	
Initial model	
Well response misfit	0.436
Tracer data misfit	271.93 [days]
No tracer data (only well match)	
Well response misfit	0.117
Tracer data misfit	206.15 [days]
Case 1 (no error)	
Well response misfit	0.016
Tracer data misfit	70.83 [days]
Case 2 (20% error)	
Well response misfit	0.068
Tracer data misfit	134.34 [days]
Case 3 (50% error)	
Well response misfit	0.178
Tracer data misfit	157.22 [days]

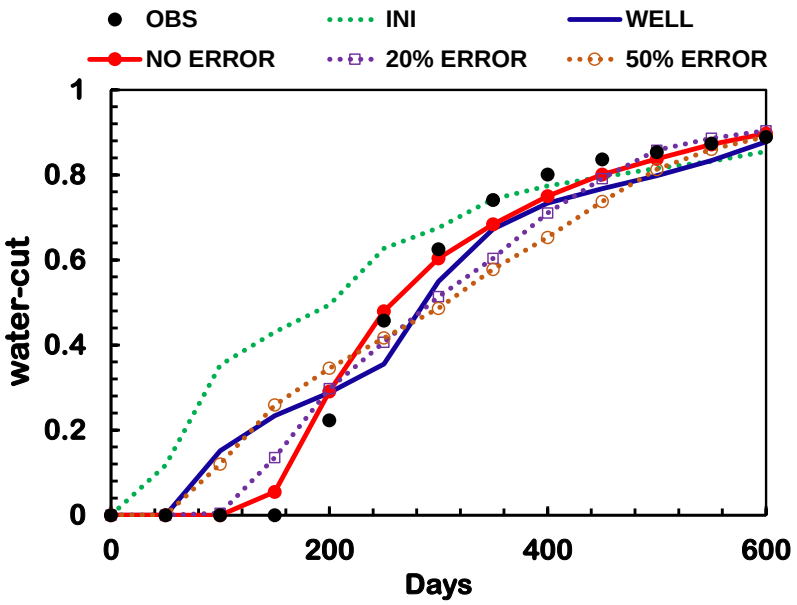

Figure 2.12 Well responses of tracer quality analysis.

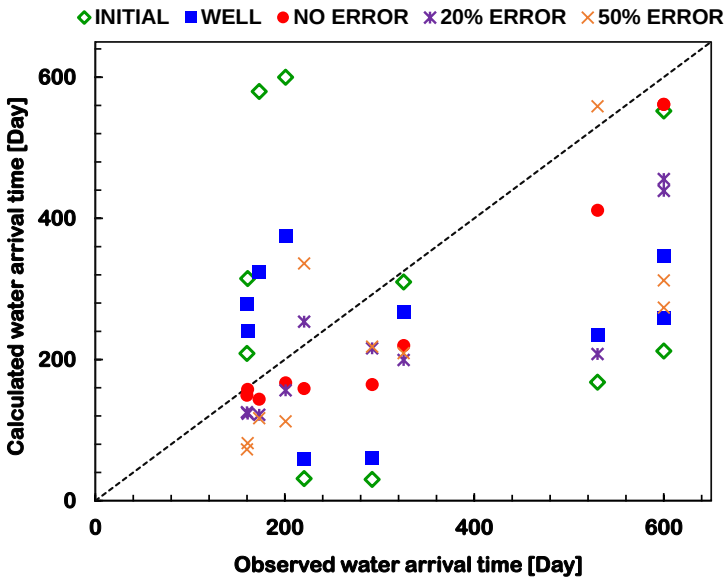

Figure 2.13 Cross plot of water arrival time of tracer quality analysis.

2.5.2 Analysis of Tracer Quantity

We analyze the quantity of tracer data by changing the number of data points, which is the location of the observed water arrival time detected along the wellbore. Case 1 has tracers at all completions. Case 2 and Case 3 have a reduced number of data, each 50 percent and 30 percent of the original tracer data, respectively. In Figure 2.14, reduced tracer data affects the well response matching. The data misfits of all cases are shown in Table 2.3. Although the well response misfits of Case 2 and Case 3 are bigger than Case 1 because of sparse data, limited amount of tracer data makes improvement of well response matching compared to the only using well data case (no tracer data). It does not worsen the result that is shown in the high uncertainty case before. The tracer data misfits (Figure 2. 15) are also reduced by adding small number of the tracer data though the magnitude is insignificant.

Table 2.3: Data misfit in quantity analysis	
Initial model	
Well response misfit	0.436
Tracer data misfit	271.93 [days]
No tracer data (only well match)	
Well response misfit	0.117
Tracer data misfit	206.15 [days]
Case 1 (100% tracer data)	
Well response misfit	0.016
Tracer data misfit	70.83 [days]
Case 2 (50% tracer data)	
Well response misfit	0.060
Tracer data misfit	173.09 [days]
Case 3 (30% tracer data)	
Well response misfit	0.107
Tracer data misfit	191.23 [days]

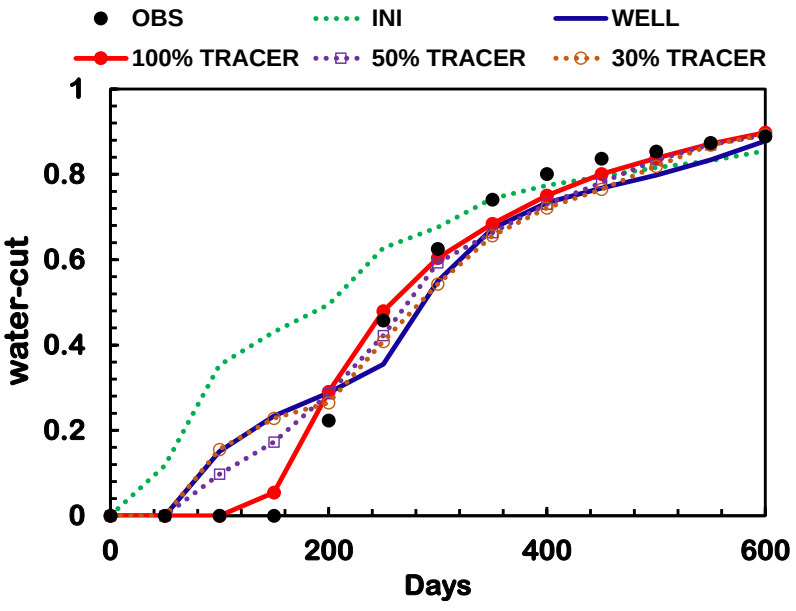

Figure 2.14 Well responses of tracer quantity analysis

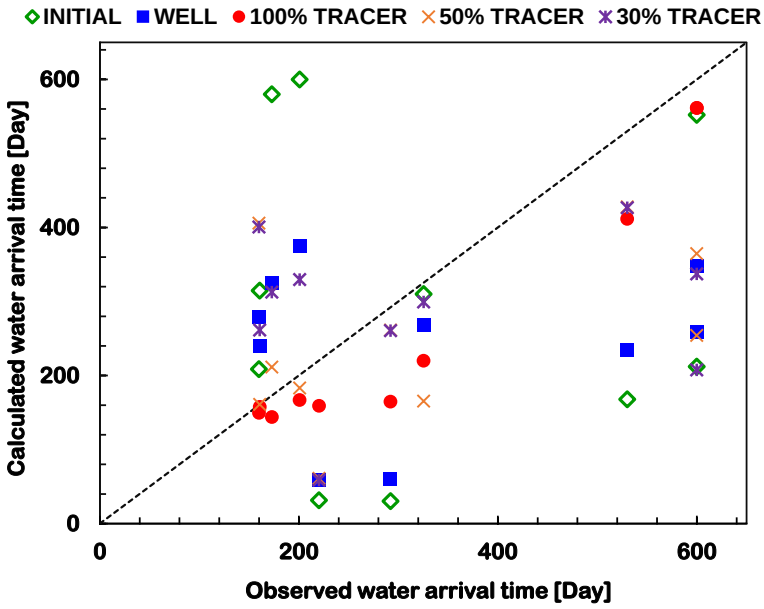

Figure 2.15 Cross plot of water arrival time of tracer quantity analysis.

This analysis demonstrates that the quality and quantity of tracer data affect the history matching result of our approach. First, despite the limited amount of data points, we can improve the well response compared to only matching the aggregated well data. Second, the poor quality of tracer data can impair the history matching results. Thus, quality control of tracer data is important.

2.6 Applications

In this section, we demonstrate the applications of our proposed approach. Total three examples are presented. The first example is the SPE Brugge benchmark model which was designed as part of a comparative study for history matching and reservoir optimization via closed loop control technology. The second case is a field tracer test at the Hill Air Force, Utah. Detailed tracer sampling with multilevel samplers was carried out to characterize a test cell to identify the location and distribution of non-aqueous phase liquid contamination. The last case is an offshore field in North America. The novel tracer technology is implemented in this offshore field to indicate the location and time of water breakthrough along the horizontal well.

2.6.1 Brugge Benchmark Model

The Brugge field model was designed for a SPE benchmark project to test the combined use of history matching and waterflooding optimization workflow (Peters et al. 2010). The structure of Brugge field consists of an east/west elongated half-dome with a large boundary fault at its northern edge and one internal fault with a modest throw at an angle of approximately 20° to the boundary fault at the northern edge (Figure 2.16). The dimensions of the field are roughly 10km x 3km. The reservoir model contains more than 40,000 active cells representing an undersaturated oil reservoir, so a two-phase simulation was sufficient. In total 30 wells are present: 20 producers located in the center of the dome and 10 water injectors around the periphery of the dome to provide pressure support in addition to the aquifer. A total of 104 realizations were generated by four classes of

geologic control parameters: (1) facies association, (2) facies modeling, (3) porosity, and (4) permeability. The detailed description of realizations of reservoir properties can be found in Peters et al. (2010).

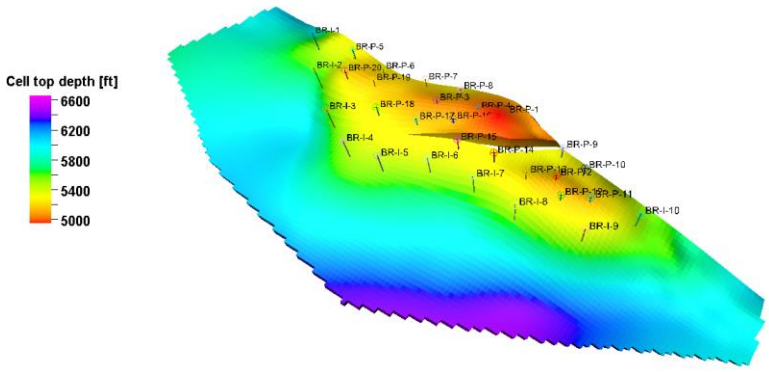

Figure 2.16 Structure of the Brugge model showing the depth and 30 wells.

We selected two models under the same parameter class among 104 realizations as the reference and prior reservoir model (Figure 2.17). Based on the reference model, we generated observed production responses such as production rate, water-cut and water arrival time at all well completions. For history matching, we will use the well liquid production rate as constraint. The prior model is used as the starting model for history matching 10 years of production data from the reference model. As before, we calibrate reservoir grid block permeability to minimize the difference between the observed and simulated well water cut and completion water arrival times.

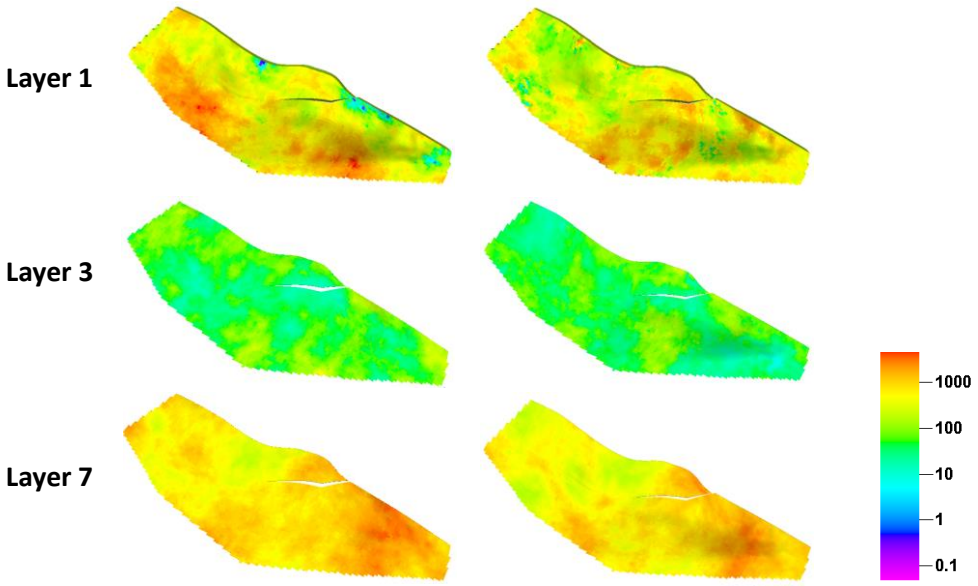

Figure 2.17 Permeability distribution of reference model (left) and prior model (right).

For the Brugge model we compare two cases for updating permeability distribution via history matching. The first case involves using aggregated well water-cut data during history matching and the second case uses distributed water arrival time in addition to the aggregated well water-cut data. From Figure 2.18 through Figure 2.21, "Final Model 1" displays the results of the first case (well GTTI) and "Final Model 2" displays the history matched responses of the second case (well GTTI + completion TTI). Compared to initial (prior) model responses, both the final models, in particular final model 2, shows significant improvements in terms of matching the observed water-cut in Figure 2.18 and the observed water arrival times in Figure 2.19. The magnitude of improvements in well by well production response is shown in Figure 2.20. Average misfit of distributed water arrival time is given as follows:

$$E_{avg.} = \frac{1}{N}\sum_{i=1}^{N}|(obs.water\ arrival\ time)_i - (cal.water\ arrival\ time)_i| \quad (2.27)$$

where *N* is number of completions along the well. Clearly, the additional information of distributed water arrival time helped further constrain the model during history matching. Finally, we compare the water saturation difference at the last simulation time step in Figure 2.21. Three cases are shown: (a) changes needed: the difference between reference model water saturation and that of the initial model, (b) changes made of model 1: water saturation of final model 1 (using aggregated water-cut) minus that of the initial model, and (c) changes made of model 2: water saturation of final model 2 (aggregated water-cut and distributed water arrival time) minus that of the initial model. As expected, the final models do not capture the saturation differences exactly; nevertheless, the changes made follow the large-scale trend of water saturation changes needed, particularly for the final model 2 (Figure 2.21c). These results clearly demonstrate the value of the distributed water arrival time information during history matching and reservoir characterization. With improved characterization, we can better assess various schemes for production optimization, identification of bypassed oil for infill targeting and EOR applications.

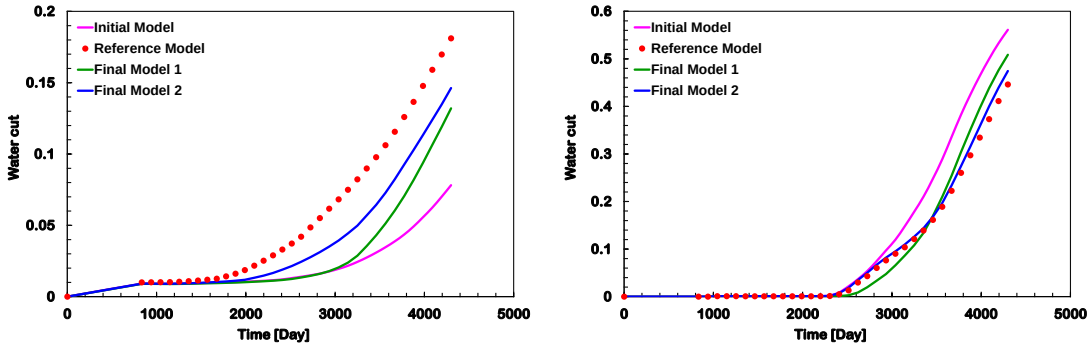

(a) P10 well **(b) P19 well**

Figure 2.18 Comparison of production data matching for the Brugge model between initial, final model 1, and final model 2.

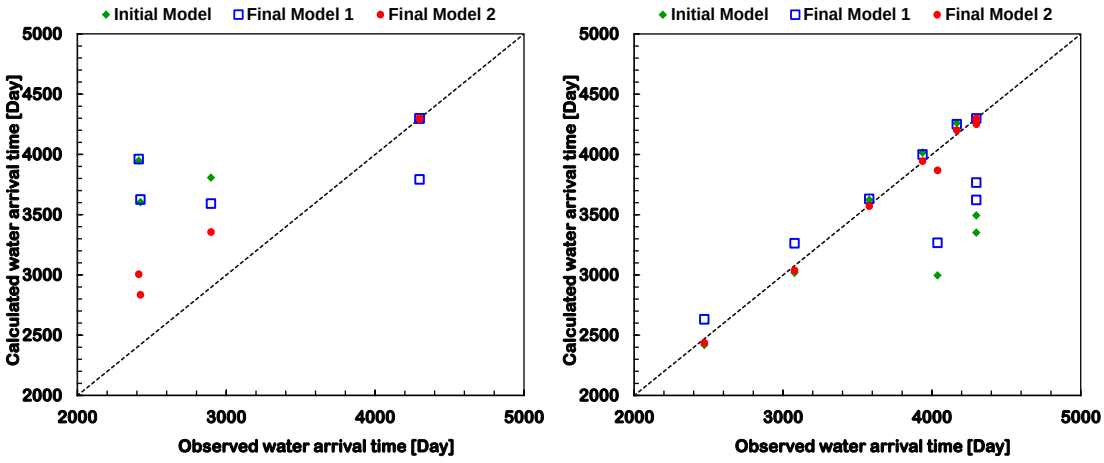

(a) P10 well **(b) P19 well**

Figure 2.19 Observed and calculated water arrival time at all completions before and after history matching for the Brugge model.

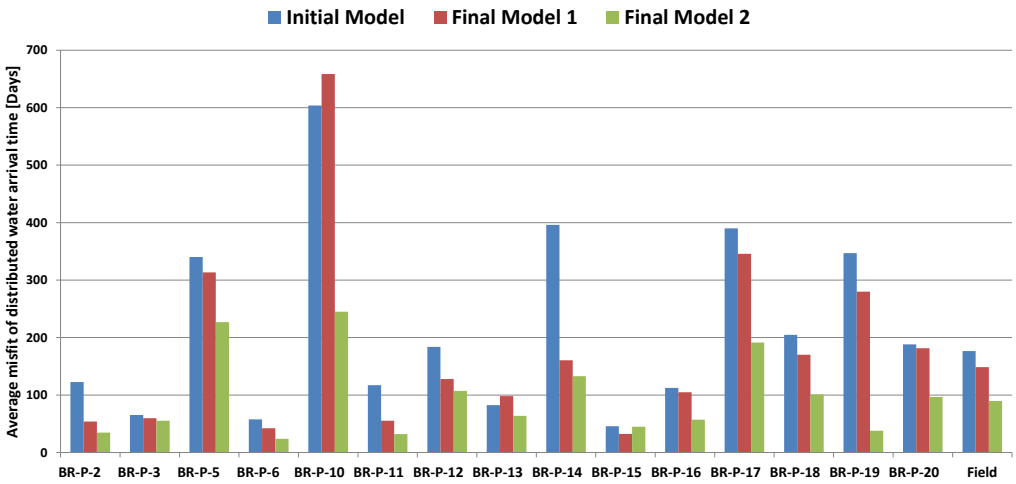

Figure 2.20 Average misfit of distributed water arrival time between the initial model and the final updated models for the Brugge model.

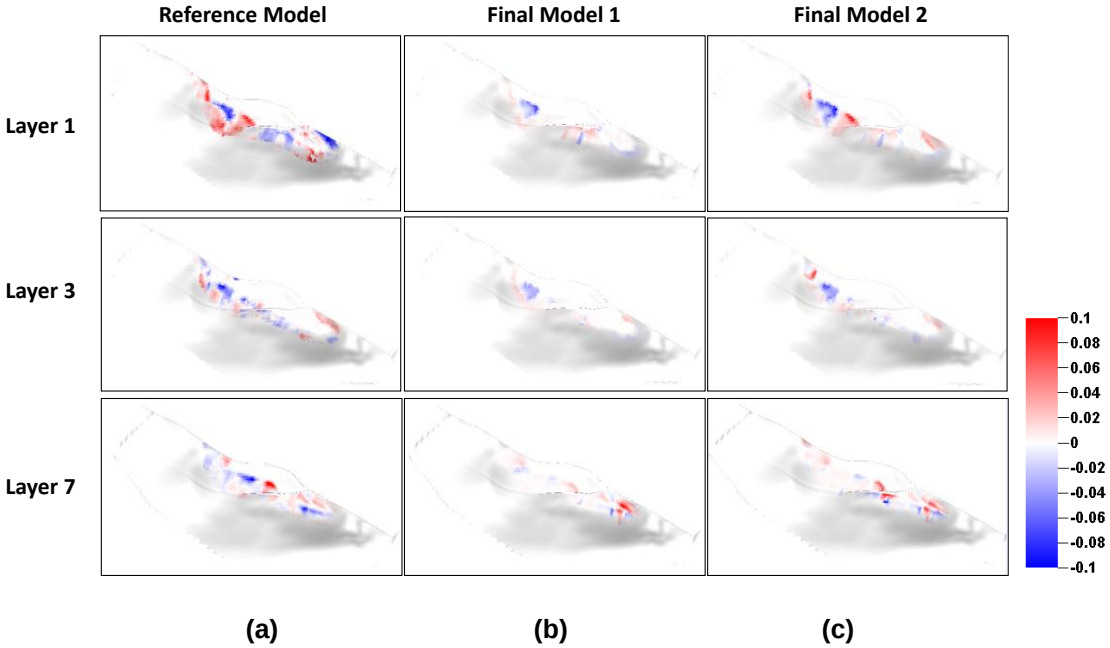

(a) (b) (c)

Figure 2.21 Comparison of water saturation difference from initial model at the last time step: (a) change needed, (b) change made 1, (c) change made 2.

2.6.2 The Hill Air Force Base Experiment

We apply our new approach to the field tracer test. The details of the tracer tests conducted at the Hill Air Force Base can be found in the work of Annable et al. (1998) and Datta-Gupta et al. (2002). Multiple tracers were injected in an isolated test cell 14.2 x 11.4 x 20 ft. in dimensions using four injection wells. Tracer responses were measured at three extraction wells at the opposite end and also at 12 multilevel samplers between the injection and extraction wells as shown in Figure 2.22. Although the test involved injection of conservative and partitioning tracers, we have history matched the conservative tracer viz. bromide for illustration of our method. We model the lower portion of the test cell using 14 x 11 x 10 grid blocks with dimensions of 1 ft. horizontally and 0.5 ft. vertically. The choice of the grid was largely dictated by the spacing of multilevel samplers to capture spatial variations between samplers both laterally and vertically.

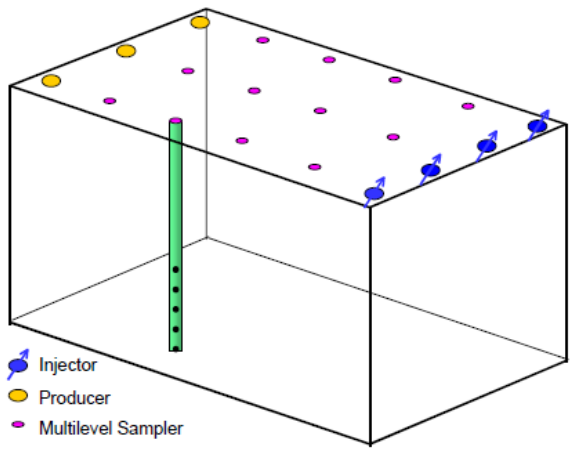

Figure 2.22 Hill Air Force Base test cell diagram (Datta-Gupta et al. 2002).

Multilevel samplers here are analogous to the novel tracer technology used in our approach and provide distributed tracer arrival times as well as concentration history. We match tracer concentration peak arrival times at each sampler using the TTI. We assume a mean of permeability of 20 Darcies based on the available data and generate the initial permeability distribution using sequential Gaussian simulation (Figure 2.23a). With the initial model we perform inverse modeling to capture the heterogeneity of the test cell using observed tracer responses at 39 multilevel sampling locations and the three producers. We assumed an effective porosity of 0.20 based on the hydraulic tests reported by Annable et al. (1998), and it was kept fixed during inversion. Final permeability field estimated from the tracer test is shown in Figure 2.23b. The TOF from each cell center reflecting tracer front movement in the final model is shown in Figure 2.23c and the streamline pattern is shown in Figure 2.24. The improvement of tracer response matching is shown in Figure 2.26 at six selected sampling locations. Although only the peak arrival times were matched during inverse modeling, we can see a substantial improvement in the overall tracer response match. In addition, cross plot of observed and calculated peak arrival time at all sampling points, again shows significant improvement compared to the initial model (Figure 2.25).

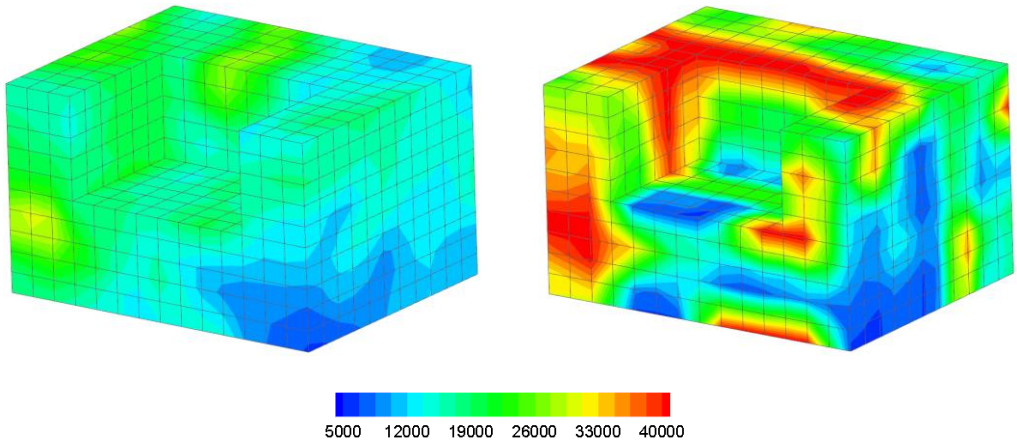

(a) Initial permeability model (md) **(b) Final permeability model (md)**

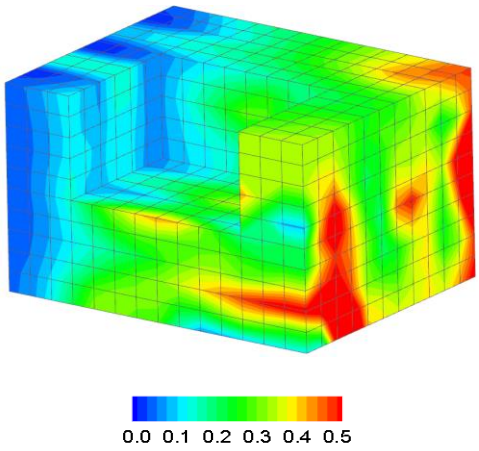

(c) Time of flight from cell center to producer based on the final model (days)

Figure 2.23 Grid properties and time of flight for the Hill Air Force model.

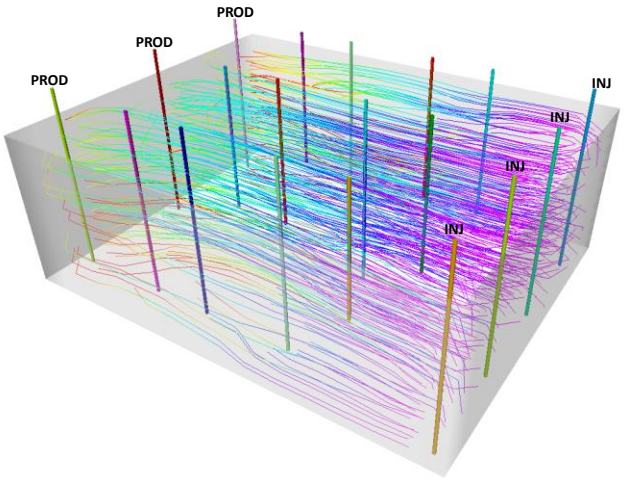

Figure 2.24 Three-dimensional streamline pattern of the final model.

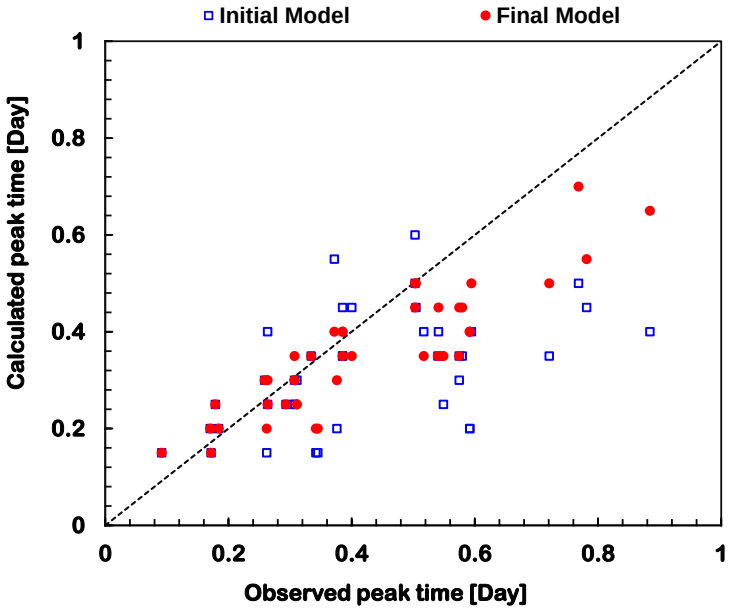

Figure 2.25 Observed and calculated tracer peak time at all sampling locations before and after inversion for the Hill Air Force model.

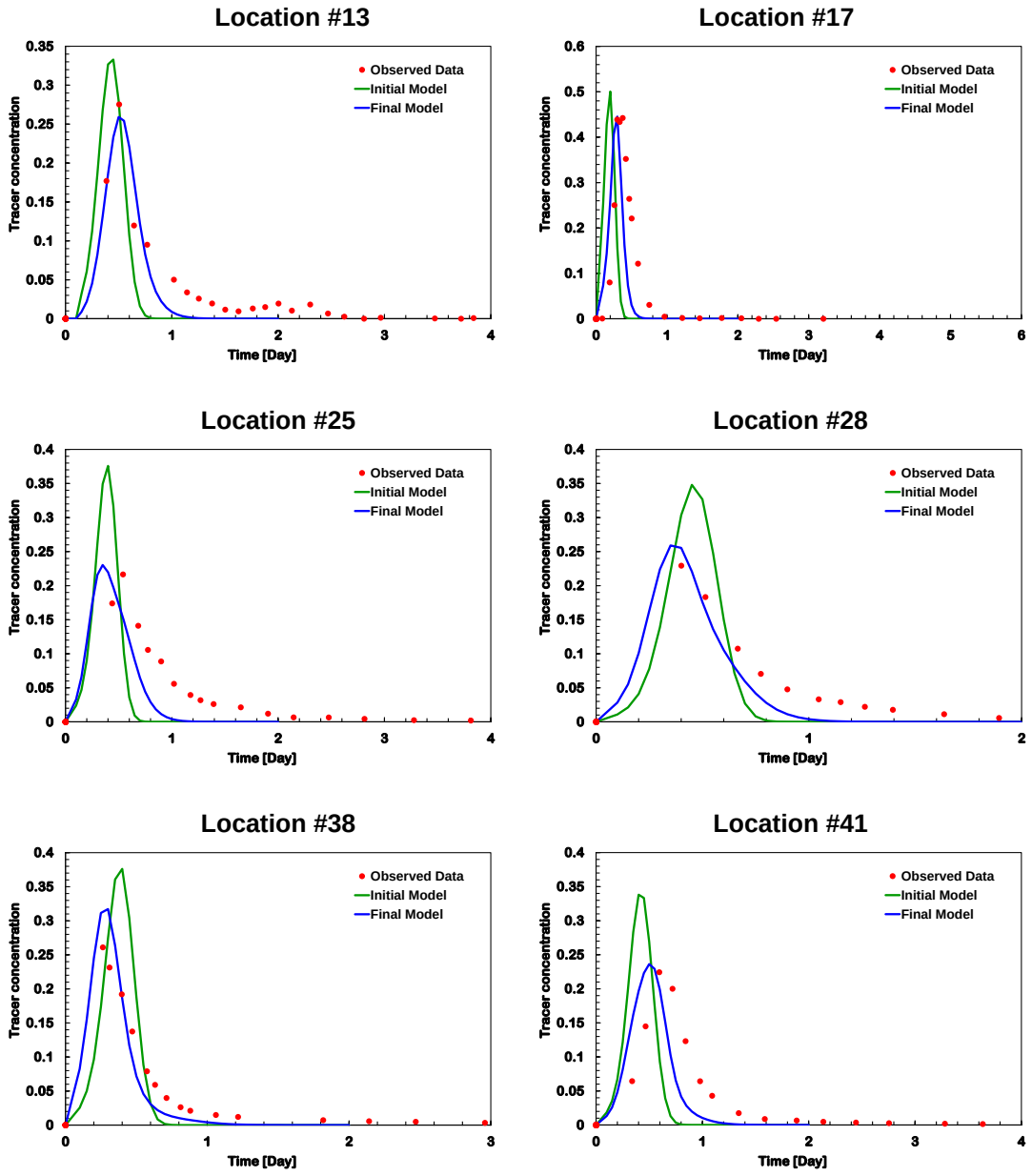

Figure 2.26 History matching of tracer responses at six selected sampling locations for the Hill Air Force model.

2.6.3 North America Offshore Field

This field was discovered in 2006 and has a relatively thin oil column (~52m) overlain by a significant gas cap and is underlain by a water leg. The fieldwide net-to-gross ratio is 90~99%, average permeability is approximately 320mD, and average porosity is approximately 22% (Montes et al. 2013). Figure 2.27 shows the field permeability distribution and well location with trajectory for four horizontal producers and four injectors. Due to the comparatively higher quality of the reservoir and the thinner oil column in this field, the risk of early water breakthrough was a major well design consideration. In order to mitigate the risk, long horizontal wells were designed with Inflow Control Device (ICD) and novel tracer technology to detect water production. The inflow tracer systems are combinations of polymers and tracer materials in the form of rods and filaments (Figure 2.28). Water tracers installed along the horizontal producers are designed to release tracer material to water. Each producer has 4 or 5 tracer sections that cover 6 to 7 percent of producing intervals.

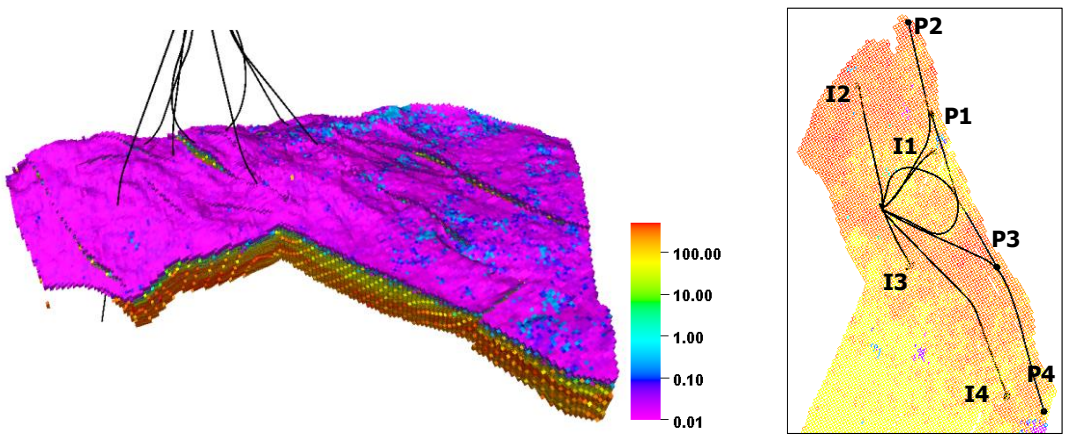

Figure 2.27 Field permeability distribution (left) and well location with trajectory (right).

Collected fluid samples at the surface were analyzed for water tracer content to detect the water breakthrough at each tracer location. Figure 2.29 and Figure 2.30 show the location of tracers along the wellbore and the tracer responses for P1 and P3 during the monitored period. Black line in Figure 2.29b and Figure 2.30b is aggregated well water-cut response and the other colored lines are tracer responses. By analyzing tracer data with water-cut, we found the water breakthrough location and time along the horizontal producers. All tracers in P1 were activated during monitoring period and 5 tracers information are integrated in inversion process. Most of tracer locations in P1 have water breakthrough when well starts to produce water. However, P3 shows only two tracer activation at the heel and toe around 640 days. To optimize the use of the tracer data, we assumed the inactivated tracers indicate no water breakthrough and the earliest possible breakthrough time is the end of monitoring period. Thus, during inversion process if calculated water breakthrough time from simulation responses at this specific location of tracer is earlier than the end of monitor period, we integrated tracer data to delay the water breakthrough until the end of monitoring time. If calculated water breakthrough is later than the end of monitoring period, we ignored the tracer information at the location.

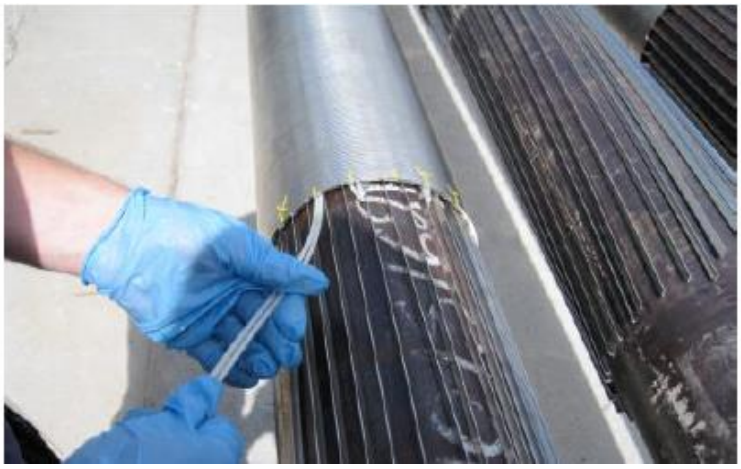

(a) Tracer filament

(b) Tracer rod

Figure 2.28 Tracer rod and filaments being installed wellbore. (http://www.resman.no)

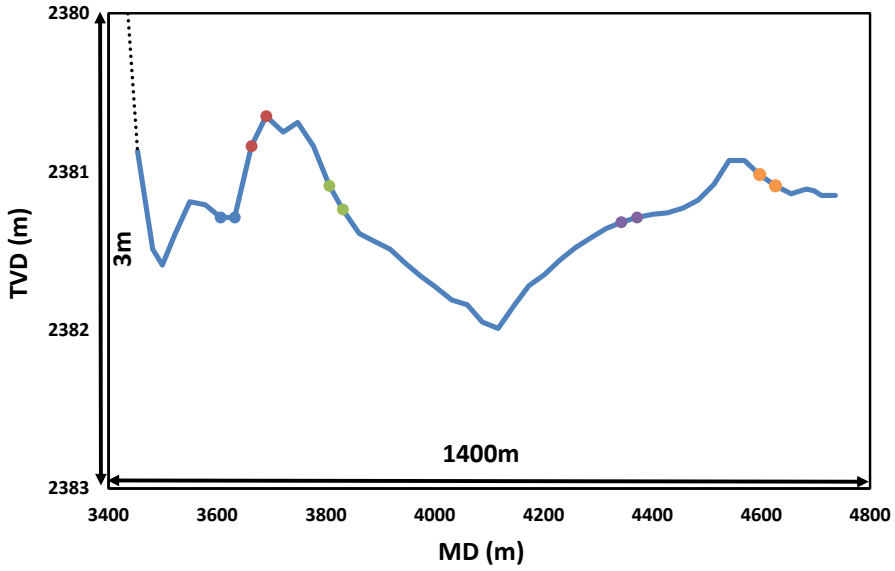

(a) Well trajectory and tracer location.

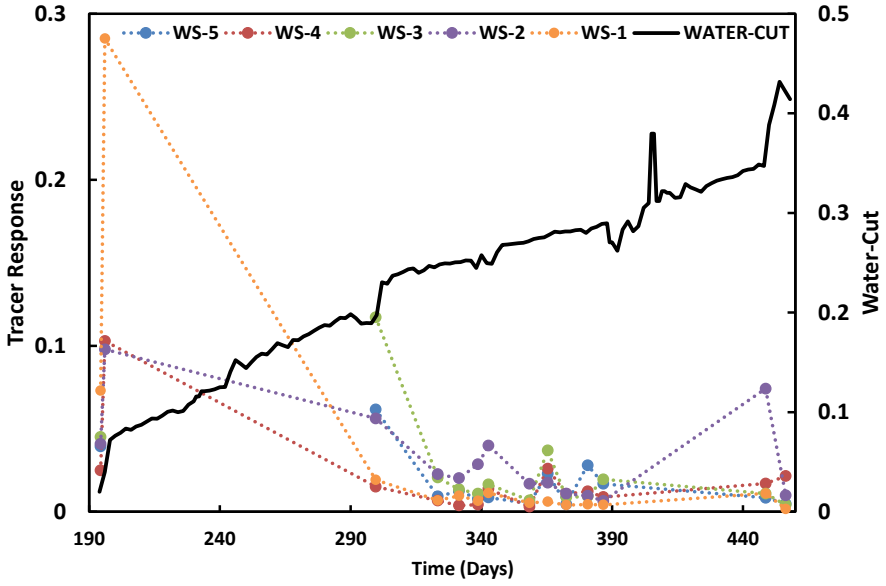

(b) water tracer responses and water-cut

Figure 2.29 P1 well tracer location and responses.

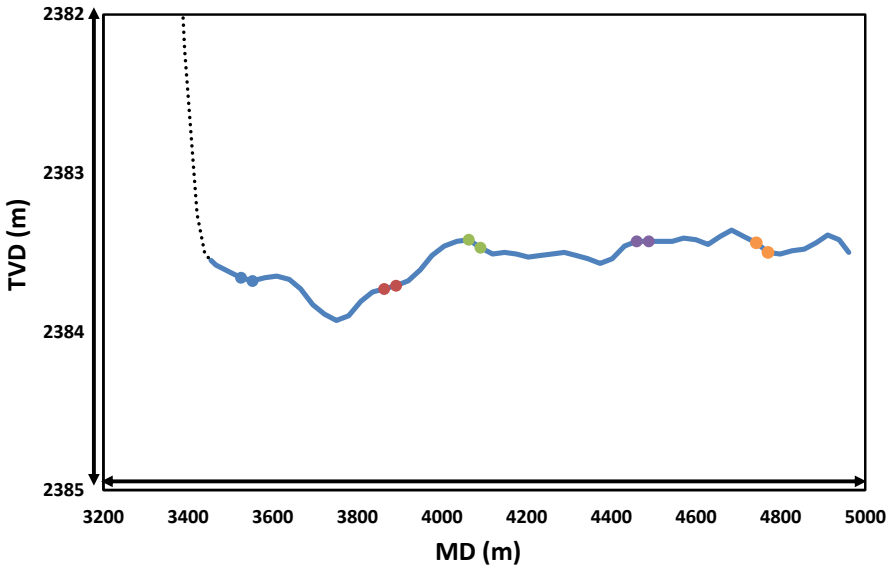

(a) Well trajectory and tracer location.

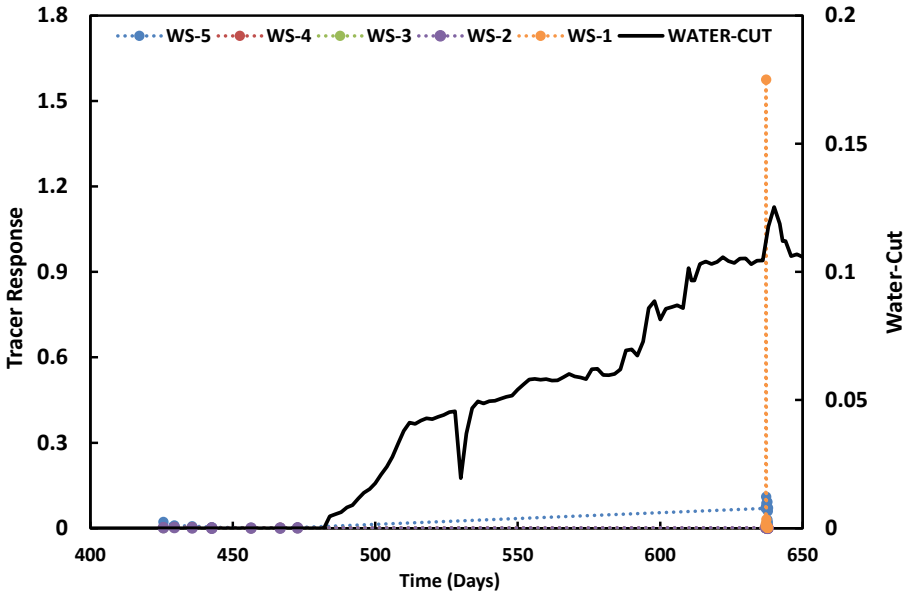

(b) water tracer responses and water-cut.

Figure 2.30 P3 well tracer location and responses.

The history matching is carried out to match four producers' well water-cut response and four producers' water breakthrough time derived from tracer analysis. Ten iterations are conducted; overall water-cut misfit convergence and cross plot of observed and calculated water arrival time after history matching are shown in Figure 2.31. Previous applications to synthetic and Brugge model have high density of tracer data because we assumed all or more than 50% of completion had tracer. As we can see in the well trajectory and tracer location (Figure 2.29a and Figure 2.30a), this field has limited tracer data. Although tracer data in this field model has covered 6~7 percent of producing interval, we see the travel time misfit and amplitude misfit of water-cut are further decreased when the distributed tracer information is included. In addition, only using the aggregated data result of cross plot does not seem to match the water breakthrough time, while using the distributed arrival time result is closer to the observed data from water tracer. RMSE of water arrival time between simulated and observed value for initial model, aggregated data only, and our new approach are 475.36 (day), 466.15 (day), and 269.86 (day), respectively. Thus, the additional tracer data in our new approach improves the results of history matching for the distributed response misfit as well as aggregated response misfit.

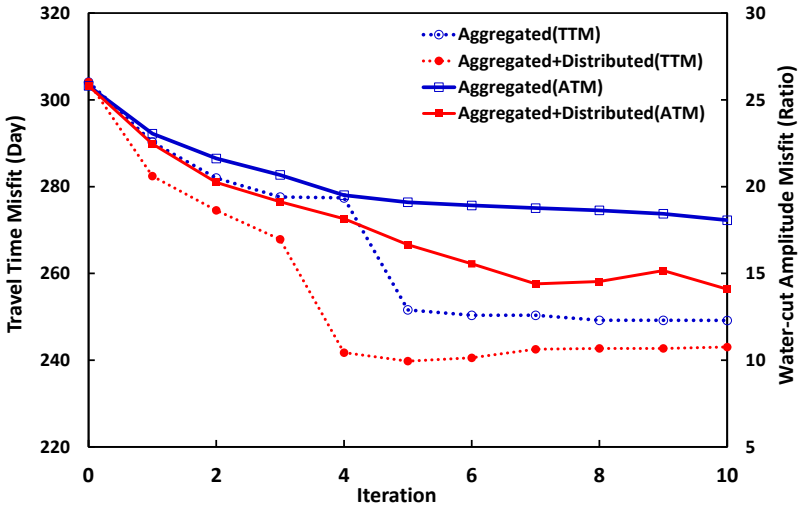

(a) Aggregated well response misfit.

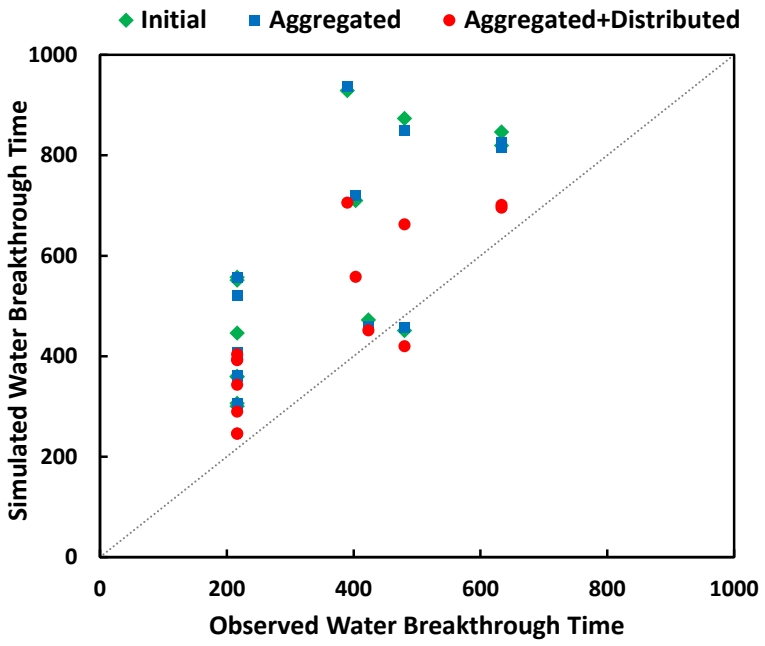

(b) Cross plot of observed and calculated water arrival time at the location of tracer installed.

Figure 2.31 History matching results for North America offshore field.

Figure 2.32 displays the difference of permeability changes after history matching for the layer 75 and the layer 90 that the producers are going through in reservoir. The red area in the Figure 2.32 shows positive change and the blue area shows negative difference between the updated model and the prior model. The calibrated model with the aggregated well response and the distributed response from tracer captures more variability, particularly around P2 and P3 (black circles) showing the difference of permeability changes compared to only using the aggregated information. The higher resolution of permeability changes made by the distributed water arrival information improves the well water-cut response that is shown in Figure 2.33. Despite the limited tracer information, all the well water-cut show closer response to the history data except P1, which was well calibrated in prior model, compared to only using aggregated well data. However, it does not make a significant improvement compared to the previous applications due to sparse tracer data. As we have shown in section 2.5, we can conclude that the quantity as well as the quality of the tracer data are important to get better matching reservoir model with our new approach.

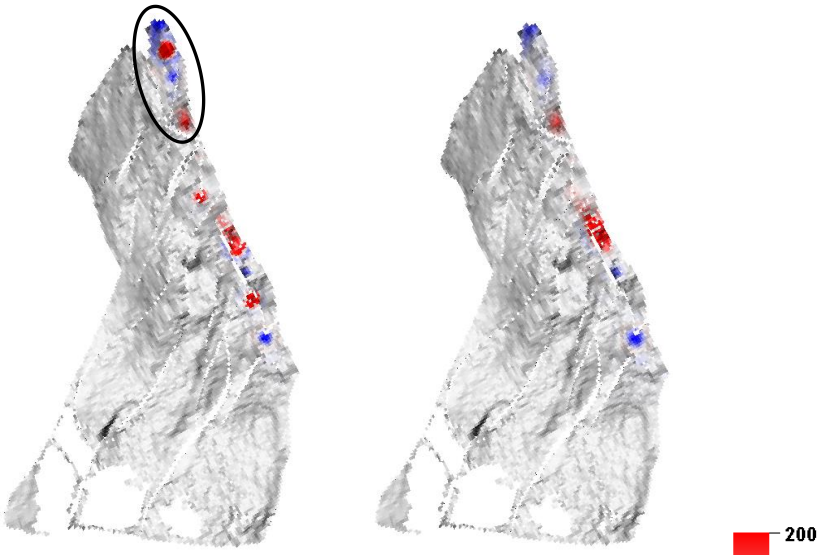

(a) Layer 75

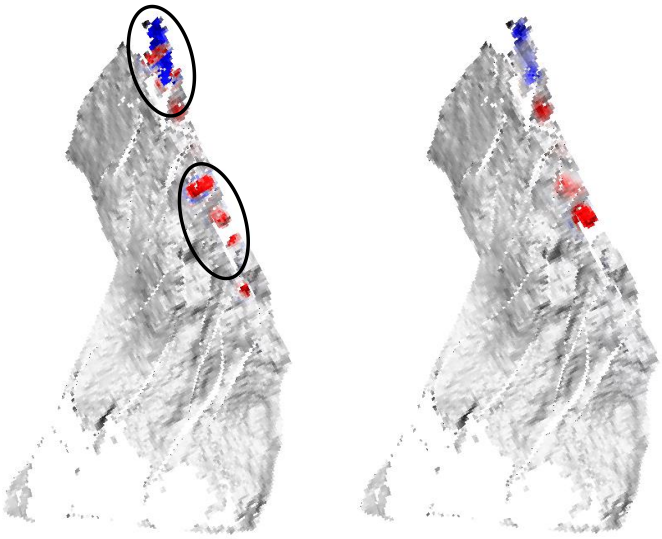

(b) Layer 90

Figure 2.32 Camparison of permeability change between using aggregated response with distributed water arrival response (left) and using aggregated response (right).

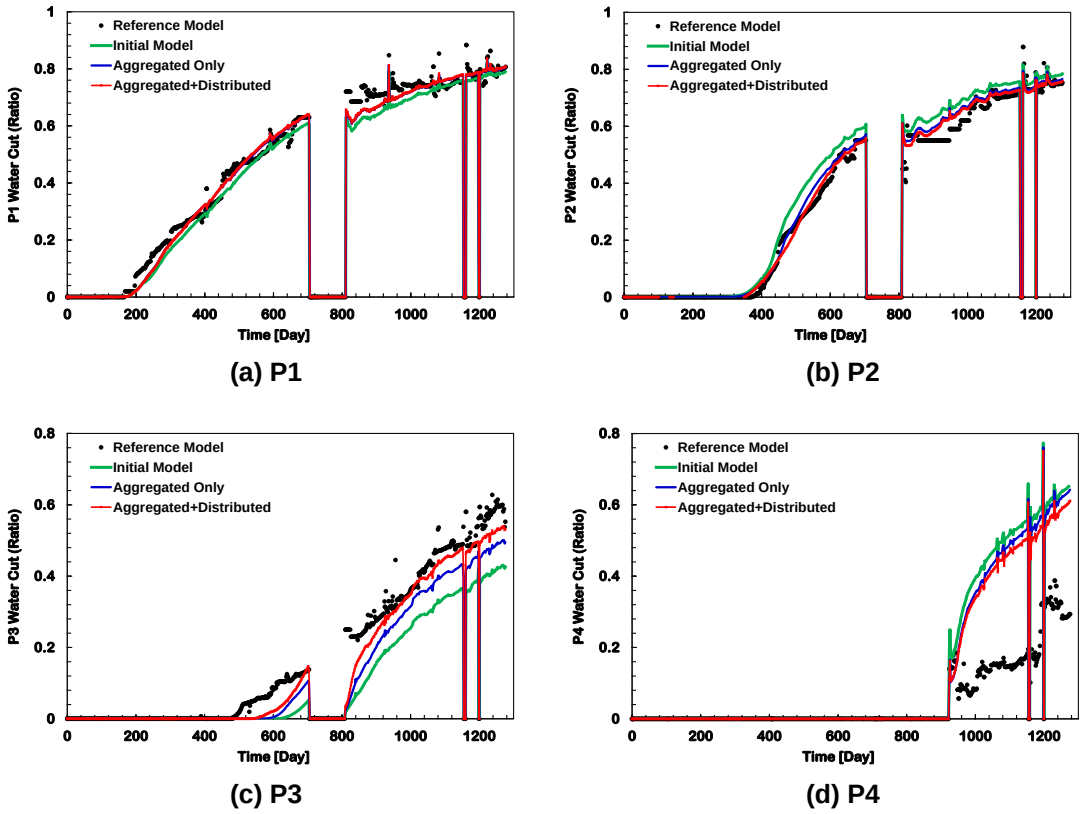

Figure 2.33 Comparison of production data matching for the offshore field case.

2.7 Chapter Conclusions

We have presented a streamline-based transport tomography for high resolution reservoir characterization using novel tracer technology that provides distributed water arrival times along the wellbore. We demonstrate the effectiveness of our proposed approach through synthetic and field applications. The major findings from this chapter are summarized below.

1. We have proposed the new approach for streamline-based history matching of distributed water arrival time made available by novel tracer technology together with the aggregated well production data. In our prior works, we matched the aggregated water-cut response over the production interval in a well using the generalized travel time inversion (GTTI). In this paper, we incorporated the distributed water arrival time along the length of wellbore using travel time inversion (TTI) in addition to the aggregated well production data by GTTI.
2. The distributed arrival time information provides significantly improved flow resolution for reservoir characterization. Comparison of history matching results using the traditional aggregated production data and our proposed approach that includes distributed arrival times clearly shows the benefits of the novel tracer technology. Specifically, the updated permeability fields are shown to reproduce the detailed flow behavior of the reference model much more closely when the distributed arrival time information is incorporated during history matching. The streamline-based approach presented here provides an efficient and practically feasible approach for such history matching.

3. We demonstrate that the quantity and the quality of tracer data affect the improvement of water-cut matching and distributed responses. Less quantity of the tracer (sparse data) reduces the effectiveness of our approach. Moreover, low quality (high uncertainty in water arrival time information) of tracer data can impair the well matching. Therefore, quality control and correct analysis of tracer data is important in the proposed approach.
4. The field application results confirm that the integration of both aggregated production data over the well interval and distributed water arrival time using novel tracer technology constrains the history matching solution effectively using our proposed approach. With improved reservoir characterization, we can better predict the future performance of the reservoir, leading to a better identification of bypassed resources for infill drilling and EOR applications.

CHAPTER III

INTEGRATING PRESSURE AND WATER-CUT DATA USING STREAMLINE-BASED METHOD WITH MULTISCALE APPROACH

3.1 Chapter Summary

Previously, the streamline based history matching was used to integrate water-cut data, assuming that pressure data was integrated with prior model and the pressure match is maintained through the streamline-based water-cut matching (Cheng et al. 2007; Yin et al. 2010). However, often times calibrating the reservoir properties with streamline-based method for production data shifts the pressure data. Thus, iterative process is required to integrate both pressure and production data simultaneously. To overcome this problem in prior works, we introduce a novel semi-analytic approach to compute the sensitivity of the bottom-hole pressure data with respect to reservoir parameters. Now, we can integrate pressure sensitivity with water-cut sensitivity for a joint inversion of production data and bottom-hole pressure without losing the computational advantages of the streamline-based approach. We also suggest the joint inversion with a multiscale approach to capture larger- and smaller-scale heterogeneity efficiently.

We verify the streamline-based pressure sensitivity by comparing with the adjoint method. Then, we apply this novel algorithm to the synthetic, Brugge benchmark model, and Norne field model with a multiscale approach. It successfully captures the large-scale permeability change and reproduces the flow behavior closer to the observed data in both pressure and water-cut.

3.2 Introduction

Streamline-based inverse modeling starts with finite-difference simulator or streamline simulator by a given prior reservoir model. If we use finite-difference simulator, we trace streamline based on velocity or flux information, calculate TOF, and compute parameter sensitivity using streamline trajectory and TOF information. Finally, we update the parameters to satisfy the objective function to be minimized (Figure 3.1). In this process, the main point of integrating the dynamic data is how to calculate the parameter sensitivity.

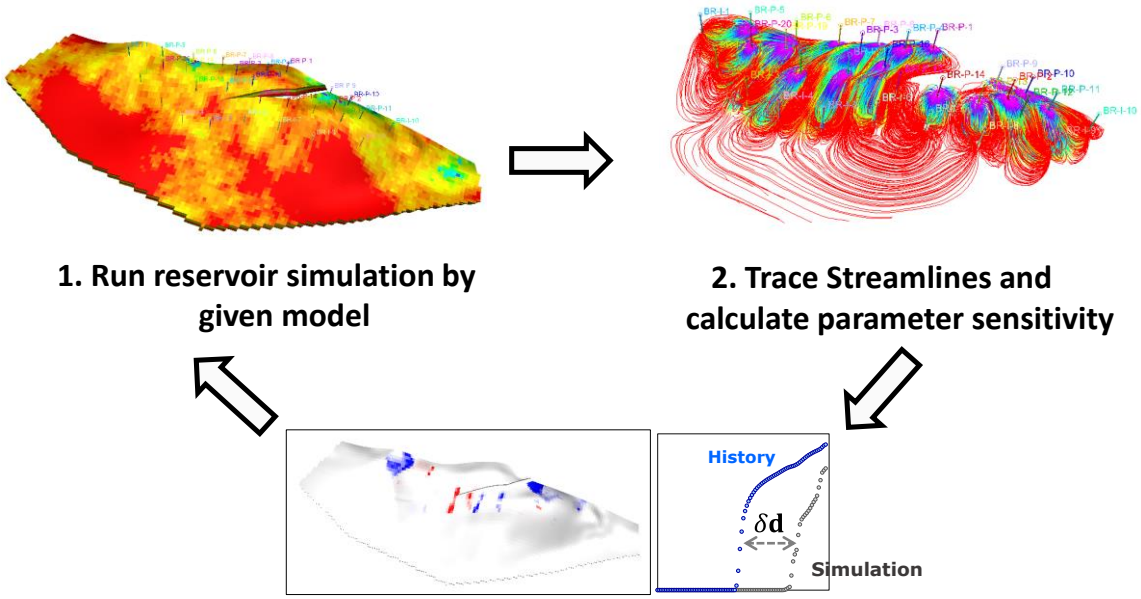

Figure 3.1 Workflow of streamline-based inverse modeling.

Previous history matching with streamline-based approach have shown great promise for integrating field-scale water-cut and tracer data into high resolution geologic models. There were several approaches for either water-cut matching or tracer data matching such as travel time inversion followed by amplitude inversion (Vasco et al. 1999) and generalized travel time inversion (Cheng et al. 2005). Cheng et al. (2005) evaluated these methods based on nonlinearity and practical implications. In chapter II, we also show the sensitivity of water front arrival time formulations and applications with novel tracer information.

However, we cannot calculate the pressure sensitivity based on streamline, to be accurate convective streamline, which is commonly used in this dissertation. In prior works, the production flow data (water-cut) and pressure data (bottom-hole pressure) were considered separately. Vasco et al. (2000) estimated reservoir properties using transient pressure data by an asymptotic formulation of the inverse problem. Kulkarni et al. (2001) introduced 'Diffusive Time of Flight' along the streamline, which represents the propagation of a front of maximum drawdown or buildup corresponding to an impulse source or sink, to integrate transient pressure data as prior process. Yin et al. (2010) matched the modular dynamic tester (MDT) pressure by calibrating pore volume multiplier and permeability multiplier using genetic algorithm followed by streamline-based water-cut matching. However, water-cut matching commonly shifts the pressure matched in pre-process. We need a joint inversion for production flow data and pressure data simultaneously. Here the new approach (Tanaka et al. 2015) is proposed to integrate

pressure data by introducing pressure drop sensitivity along the streamline with respect to reservoir property (permeability).

We know pressure data is well-suited to capture large-scale variation and saturation data captures fine-scale variation effectively (Williams et al. 1998). To account for the disparity in resolution of different type of dynamic data, we suggest a joint inversion with a multiscale approach for effective minimization of pressure and water-cut data misfit. The application of multiscale approach is getting increased attention in both forward simulation and integration of dynamic data for history matching. Yoon et al. (2001) proposed a multiscale inversion that starts with a coarse reservoir model and gradually refines the reservoir grid. Kim et al. (2010) suggested streamline-based dual scale approach with optimal coarsening. Although they ran simulations in fine grid and history matching was done at coarse scale, it showed savings in computational cost and facilitates the convergence to the global solution. Aanonsen (2008) and Stenerud and Lie (2006) also identified that a multiscale approach reduces the computational cost and improves the history matching quality compared to direct fine scale history matching.

In this chapter, we incorporate a multiscale approach for joint inversion with grid-connectivity-based transformation (GCT), a novel re-parameterization method (Bhark et al. 2011), to identify a large-scale heterogeneity of reservoir model. It is followed by the streamline-based history matching for pressure and water-cut data by calibrating fine scale (cell by cell) reservoir properties.

3.3 Bottom-hole Pressure Sensitivity

To incorporate the observed bottom-hole pressure data based on streamline, we must know the parameter sensitivity that relates the pressure change with respect to the reservoir properties (Figure 3.2). We introduce the bottom-hole pressure sensitivity and verify the analytical sensitivity calculated by the proposed method in one-dimensional and two-dimensional models by comparing with the adjoint method implemented in a commercial simulator (Schlumberger 2012b).

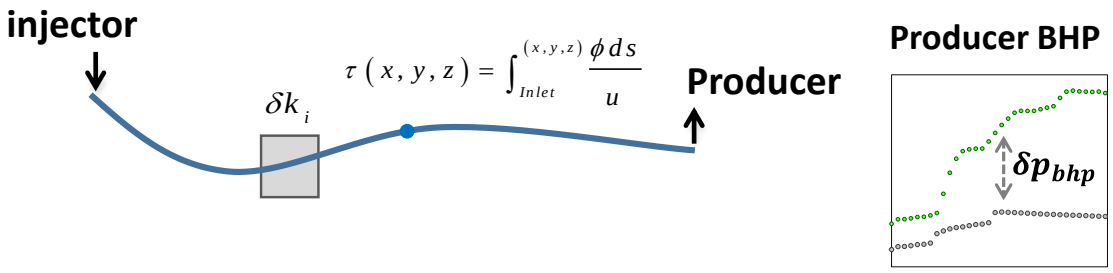

Figure 3.2 Bottom-hole pressure sensitivity along the streamline.

3.3.1 Mathematical Formulation

We construct a pressure equation along streamlines while considering the given boundary condition, and then we take a derivative with respect to the grid properties. Here, we show the pressure drop sensitivity in discretized space for practical application of history matching.

- **Pressure Drop Sensitivity**

First, the pressure drop is evaluated along streamlines between wells by summation from start to end point of the node (Eq. 3.1). The sensitivity of the pressure drop with respect to the permeability of *i*-th grid block is calculated approximately (Eq. 3.2).

$$\Delta p_{well} = \sum_{i=node} \Delta p_i \tag{3.1}$$

$$\frac{\partial \Delta p_{well}}{\partial k_i} = \frac{\partial}{\partial k_i}(\Delta p_1 + \Delta p_2 + \cdots + \Delta p_i + \cdots + \Delta p_n) \approx \frac{\partial \Delta p_i}{\partial k_i} \tag{3.2}$$

Using Darcy's equation, the pressure drop at the *i*-th grid is as follows,

$$\Delta p_i = -\frac{q}{\lambda_{t,i} k_i}\frac{L}{A} + \bar{\rho}_i g \Delta D \tag{3.3}$$

By combining Eq. 3.2 and Eq. 3.3 with an assumption that Darcy's equation can be applied along the streamline, we have the pressure drop sensitivity along the streamline.

$$\frac{\partial \Delta p_i^{sl}}{\partial k_i} = \frac{q_{sl,i}^{eff}}{\lambda_{t,i}}\frac{L_i}{A_i}\frac{1}{k_i^2} = \frac{\Delta p_i^{sl} - \bar{\rho}_i g \Delta D}{\rho_{eff}\, k_i} \tag{3.4}$$

where q_{sl}^{eff} is an effective rate along the streamline. The cross section (*A*) and distance (*L*) are given later. For compressible fluid, it is no longer constant along streamline. It is calculated by Eq. 3.5.

$$q_{sl,i}^{eff} = \frac{q_{sl,0}}{\rho_{eff}} \tag{3.5}$$

$q_{sl,0}$ is flow rate along the streamline at starting point. ρ_{eff} is 'effective density' that captures the changes in the fluid volume with pressure and can be conveniently and efficiently traced along streamlines (Cheng et al. 2006).

To get the correct sensitivity, Δp_i^{sl} is calculated using half-cell pressure drop between neighboring grid blocks. Because pressure drop is defined as differences between neighboring cells, perturbation of permeability at grid *i* will change its pressure of neighbor grids that is described in Figure 3.3. For half-cell pressure drop, Δp_i^{sl} in Eq. 3.4 is weighted by half-cell transmissibility (Eq. 3.6 and Eq. 3.7). Finally, pressure drop at *i*-th cell is summation of weighted pressure drop in sub-grids (Eq. 3.8).

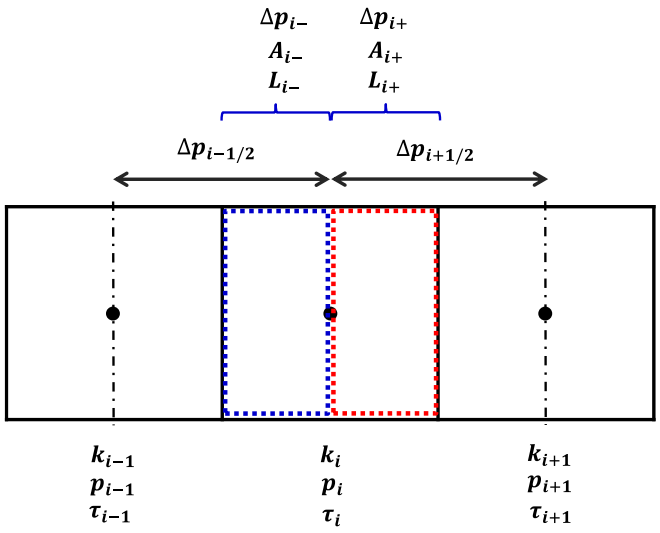

Figure 3.3 Half-cell pressure drop at *i*-th cell.

$$\Delta p_{i-}^{sl} = \Delta p_{i-1/2} \frac{\frac{L_{i-}}{k_i A_{i-}}}{\left(\frac{L_{i-}}{k_i A_{i-}} + \frac{L_{i-1+}}{k_{i-1} A_{i-1+}}\right)} \tag{3.6}$$

$$\Delta p_{i+}^{sl} = \Delta p_{i+1/2} \frac{\frac{L_{i+}}{k_i A_{i+}}}{\left(\frac{L_{i+}}{k_i A_{i+}} + \frac{L_{i+1-}}{k_{i+1} A_{i+1-}}\right)} \tag{3.7}$$

$$\Delta p_i^{sl} = \Delta p_{i-}^{sl} + \Delta p_{i+}^{sl} \tag{3.8}$$

where *A* (area) and *L* (length) can be calculated using streamline information (Eq. 3.9 and Eq. 3.10). It is described in Figure 3.4.

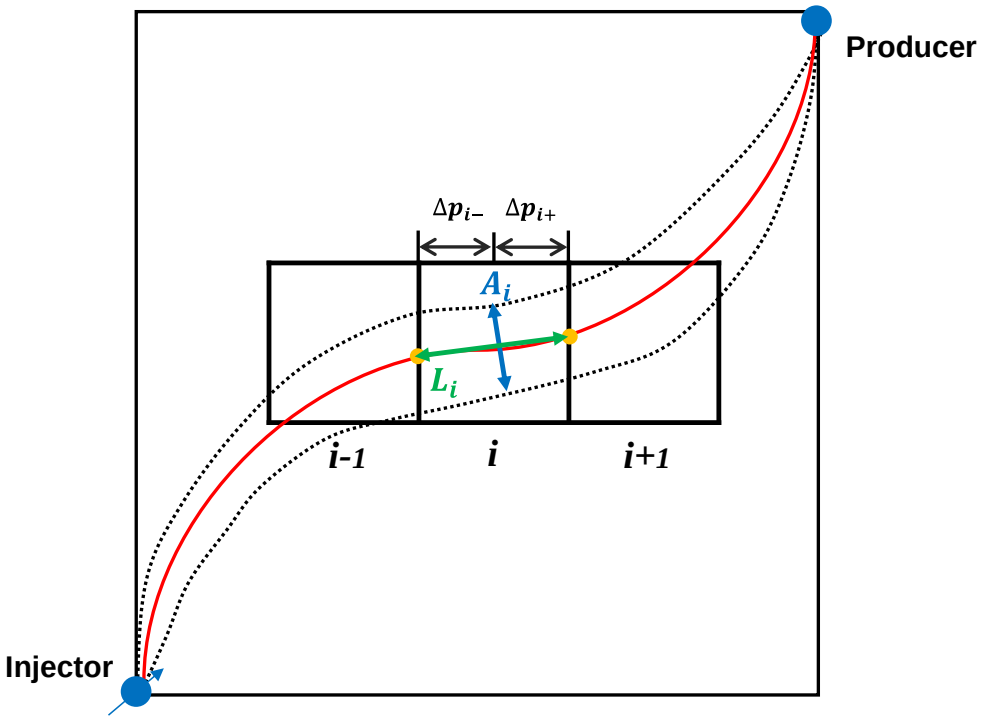

Figure 3.4 Area and length along the streamline: red line is a streamline and black dotted lines show a streamtube.

$$A_i = \frac{q_{sl,i}\Delta\tau_i}{\phi_i L_i} \tag{3.9}$$

$$L_i = \sqrt{\Delta x_i^2 + \Delta y_i^2 + \Delta z_i^2} \tag{3.10}$$

Eq. 3.4 is the sensitivity along the streamline. To solve the inverse problem by calibrating cell properties such as permeability or porosity, we need the sensitivity on the grid. When we calculate the grid sensitivity, we consider all streamline that are reached at well *p*. Then, the sensitivity at each grid is a summation of all the sensitivities weighted by the flux ratio based on the streamlines passing through the *i*-th grid (Eq. 3.11).

$$\frac{\partial \Delta p_{i,p}}{\partial k_i} = \sum_{k=1}^{\substack{all\ sl\ pass\ through \\ i-th\ grid,p}} \left(\frac{q_{along\ the\ single\ sl,k}}{\sum_{j=all\ sl\ to\ the\ well\ p} q_{sl,j}} \frac{\partial \Delta p_i^{sl}}{\partial k_i} \right) \tag{3.11}$$

- **Bottom-hole Pressure Sensitivity**

The Eq. 3.2 is applicable if one of well constraints is constant pressure. In this case, the pressure drop sensitivity is equivalent with bottom-hole pressure sensitivity. For example, if injector is constrained by pressure, we can get the bottom-hole pressure sensitivity at producer using Eq. 3.12.

$$\frac{\partial \Delta p_{well}}{\partial k_i} = \frac{\partial \left(p_{bhp}^{inj}\right)_{rate} - \partial \left(p_{bhp}^{prod}\right)_{press}}{\partial k_i} = -\frac{\partial p_{bhp}^{prod}}{\partial k_i} \approx \frac{\partial \Delta p_i}{\partial k_i} \tag{3.12}$$

However, when both wells connected by streamline are constrained by rate, the Eq. 3.2 is not applicable. For the rate-rate constraint case, we use the Eq. 3.13 which computes the

bottom-hole pressure sensitivity by weighting the rate-pressure constraint sensitivity based on the time of flight ratio.

$$\left.\frac{\partial\left(p_{bhp}^{prod}\right)}{\partial k_i}\right|_{\substack{rate \\ \leftrightarrow rate}} = \left.\frac{\partial\left(p_{bhp}^{prod}\right)}{\partial k_i}\right|_{\substack{press \\ \leftrightarrow rate}} \frac{\tau_i}{\tau_{total}} \tag{3.13}$$

where τ_{total} is total time of flight between injector or aquifer (boundary) and producer. τ_i is the time of flight from injector to the *i*-th grid. At this point, we do not have a mathematical derivation for this. However, intuitively we think that as we approach the producer the sensitivity should increase. This is the rationale behind the weighting factor τ_i/τ_{total}. We will compare the sensitivities with adjoint method later in the chapter.

Now, we can construct sensitivity matrix for bottom-hole pressure and solve it like Eq. 2.23. However, we have two misfit terms that have different units and magnitude. We normalize it by inverse of standard deviation of measurement error as α_1 and α_2 (Eq. 3.14).

$$\alpha_1\|\delta d_{wct} - S_{wct}\delta R\| + \alpha_2\left\|\delta d_{bhp} - S_{bhp}\delta R\right\| + \beta_1\|\delta R\| + \beta_2\|L\delta R\| \tag{3.14}$$

The data misfit of pressure term in the matrix is the difference between simulated pressure and observation data, which are averaged over all the data points. This is a similar way of GTTI that makes one equation for each well data to reduce the size of the minimization matrix. It makes it possible to run inverse problems of high resolution reservoir model.

3.3.2 One-dimensional Sensitivity Verification

We verify the proposed analytic pressure sensitivity using a simple 1D heterogeneous model with 100 grids in Figure 3.5. The permeability ranges from 1 to 100 md, and the porosity is constant at 0.4. The initial condition is 1,550 psi.

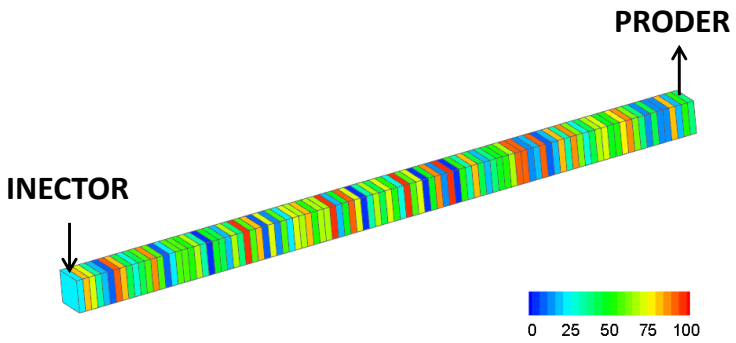

Figure 3.5 Permeability distribution used for 1D pressure sensitivity verification.

Analytic sensitivity is compared to the adjoint based method implemented in a commercial simulator (E300, Schlumberger 2012b). We test two models; the first case is rate-pressure constraint, and the second one is rate-rate constraint.

- Case 1 – injector: 2,898 psi, producer: 0.4 stb/day
- Case 2 – injector: 0.5 stb/day, producer: 0.49 stb/day

Case 1 uses Eq. 3.12 and Case 2 uses Eq. 3.13 to calculate the pressure sensitivity. As shown in Figure 3.6 and Figure 3.7, the sensitivity of producer bottom-hole pressure shows positive values. Because increasing the permeability between well pairs decreases the pressure drop, which results in pressure increase at the producer. They show good agreement with adjoint sensitivity. Therefore, we can apply the proposed pressure

sensitivity to the inversion process to capture the heterogeneity in a reservoir based on bottom-hole pressure history data.

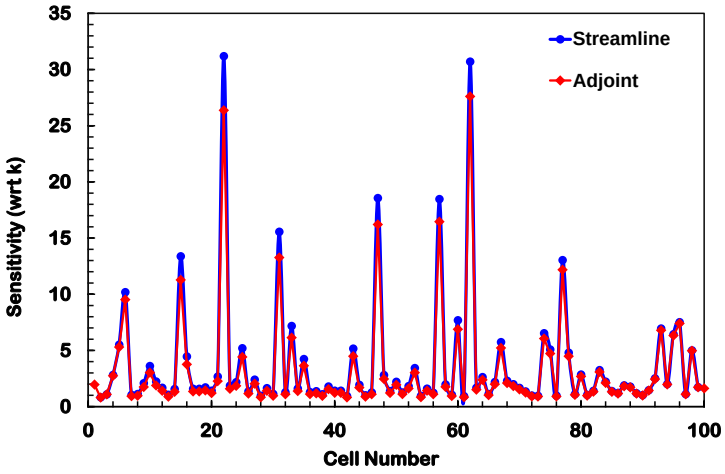

Figure 3.6 Bottom-hole pressure sensitivity between injector and producer (Case 1)

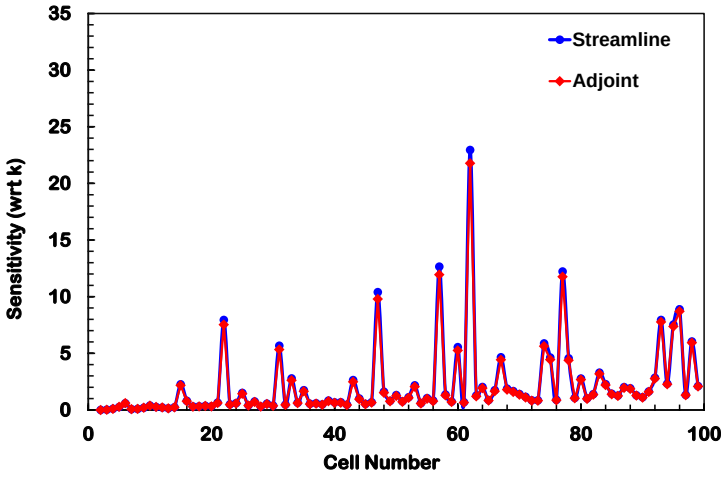

Figure 3.7 Bottom-hole pressure sensitivity between injector and producer (Case 2)

3.3.3 Two-dimensional Sensitivity Verification

The model we use for 2D verification is a 50 by 50, 5-spot heterogeneous model (Figure 3.8). Producers are constrained by a rate of 500 stb/day, and an injector is constrained by 5,900 psi. The initial condition is 5,863 psi with zero water saturation. The simulation time is 0.5 days.

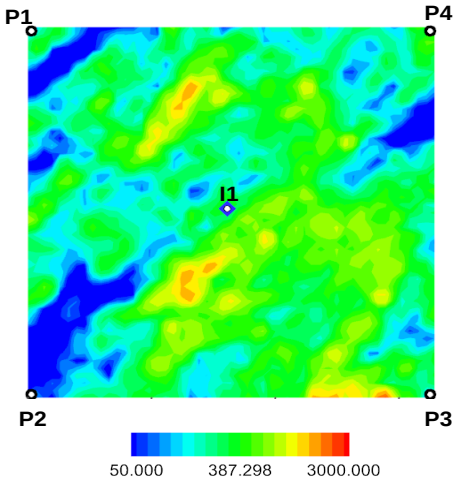

Figure 3.8 Premeability distribution for 2D sensitivity verification.

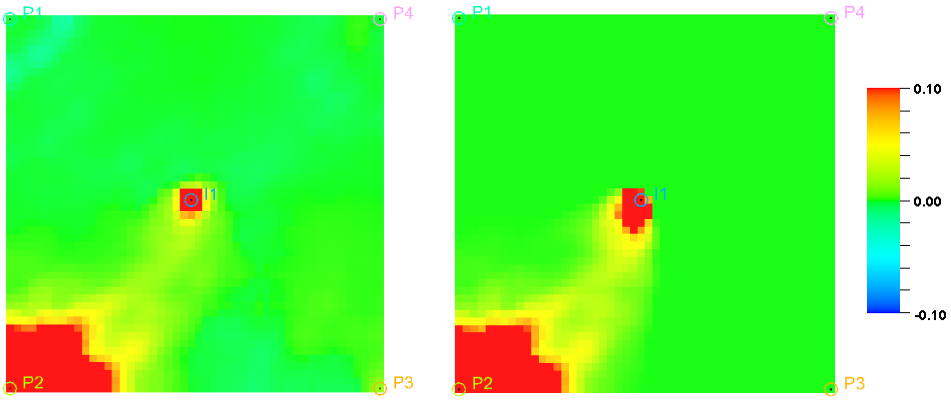

(a) Adjoint method **(b) Streamline-based approach**

Figure 3.9 Bottom-hole pressure sensitivity of P2 well compared with the adjoint method.

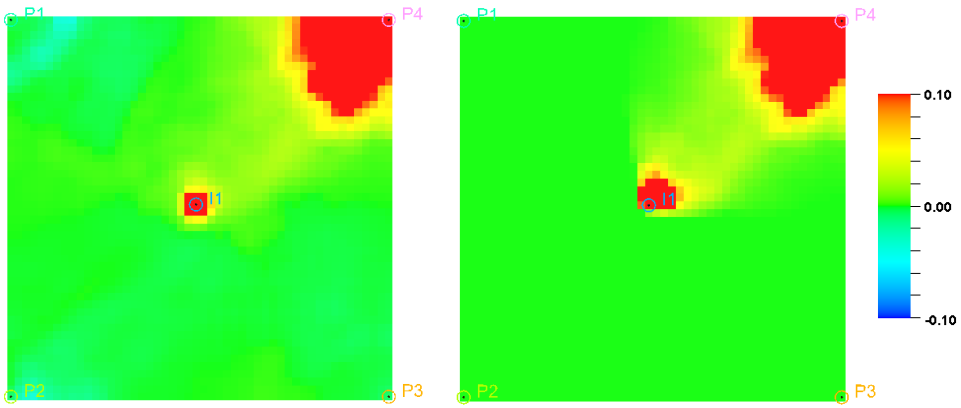

(a) Adjoint method **(b) Streamline based approach**

Figure 3.10 Bottom-hole pressure sensitivity of P4 well compared with the adjoint method.

Figure 3.9 and Figure 3.10 are the sensitivity of P2 and P4 producer using adjoint method (left) and streamline based method (right). They show very good agreement in the main trend between the injector and producer. The difference is observed around the other producers' area, which has negative value based on adjoint sensitivity. However, the streamline-based method has no sensitivity value there because our approach calculates along the streamline between specific well pairs to be evaluated. Thus, the negative values nearby other producers are not included in the proposed method. This 2D model will be used for application of the inversion problem in section 3.4.

3.4 Application of History Matching

With bottom-hole pressure sensitivity we have shown in section 3.3, we start history matching for water-cut and bottom-hole pressure simultaneously. Here, we use same model in section 3.3.3 for 2D sensitivity verification and will show the field-scale application with a multiscale approach in section 3.5.

Initial permeability is shown in Figure 3.8 and reference permeability for making history data is shown in Figure 3.11. It has south-west to north-east trend of low and high permeability distribution. Two permeability distributions are generated by sequential Gaussian simulation but with different geostatistical parameters. The detail model description is in Table 3.1 and Figure 3.12. The objective function of this problem is to minimize the water-cut and bottom-hole pressure data misfit of four producers by calibrating an initial permeability model.

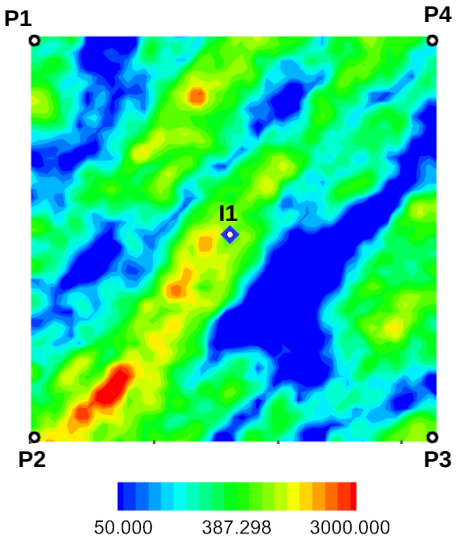

Figure 3.11 Reference permeability model for joint inversion with 2D synthetic model.

Table 3.1: General parameters for 2D five spot model for joint inversion	
Parameters	Input Values
Grid number	(nx,ny,nz) = (50,50,1)
DX	32.8 [ft]
DY	32.8 [ft]
DZ	32.8 [ft]
Porosity	0.25
Rock compressibility	8.1 E-06 [1/psi]
Oil density	52.1 [lb/cf]
Water density	63.29 [lb/cf]
Oil viscosity	0.29 [cp]
Water viscosity	0.31 [cp]
Oil formation volume factor	1.305 [rb/stb]
Water formation volume factor	1.04 [rb/stb]
Total simulation time	2080 [days]
Time step size	260 [days]

***PVT values for oil are at the reference pressure of 2897.1 psi**
***Values for water and rock are at the reference pressure of 5863.8 psi**
***Density is surface condition (14.7 psi)**

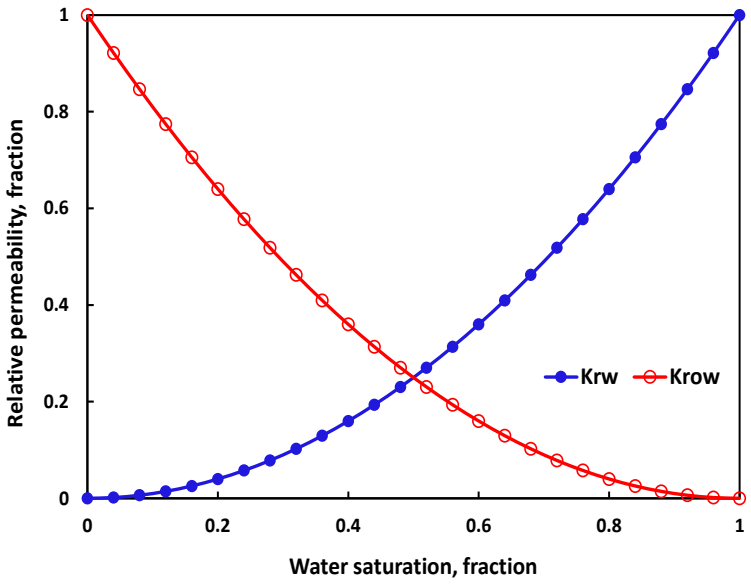

Figure 3.12 Oil-water relative permeability data for 2D five spot synthtic model.

To show the effectiveness of joint inversion, we compare the two cases;

- 1st case: only water cut matching.
- 2nd case: joint inversion for water-cut and bottom-hole pressure simultaneously.

Figure 3.13 shows the convergence of data misfit. Two cases after 10 iterations have the same convergence for water-cut data misfit (around 50% reduced). However, bottom-hole pressure data misfit clearly explains the impact of pressure data integration. Only water-cut matching (blue line) reduces 30% of pressure misfit, but proposed joint inversion (red line) decreases 80% of initial data misfit.

The well responses of water-cut and bottom-hole pressure are shown in Figure 3.14. As we have seen in the misfit convergence, the water-cut response is well matched with reference data, and two cases have very comparable results. However, joint inversion makes much closer bottom-hole pressure response to the reference data. This application confirms the necessity of integrating pressure data. For example, updated pressure data of P3 and P4 has been impaired when only water-cut data is considered during history matching. Permeability needs to be increased for early water breakthrough of P4 water-cut, whereas, reduction of permeability is required to decrease pressure response. They appear conflicting, but our joint inversion with proposed pressure sensitivity successfully matches the two objectives simultaneously.

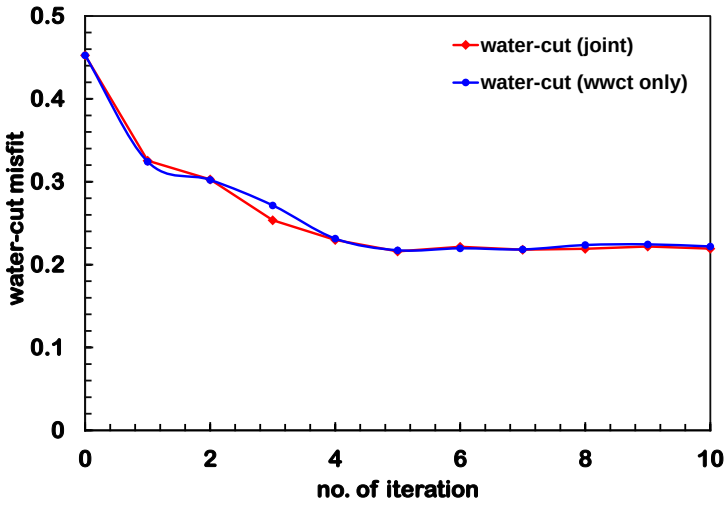

(a) Convergence of water-cut data misfit.

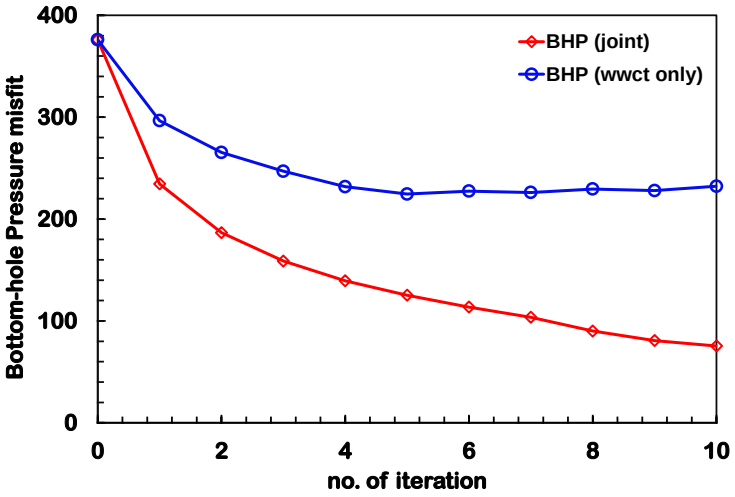

(b) Convergence of bottom-hole pressure data misfit.

Figure 3.13 Convergence of the objective function through iteration.

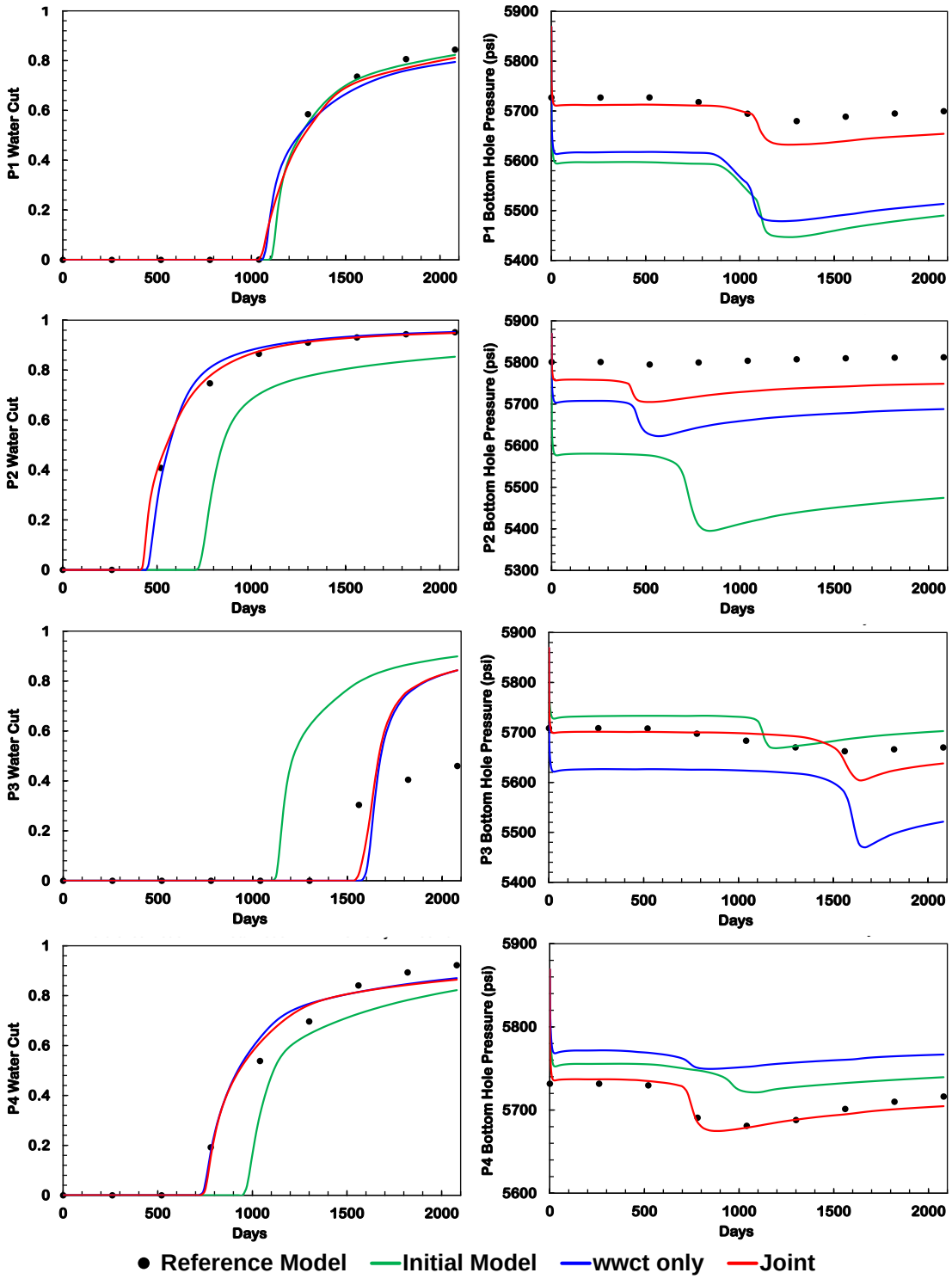

Figure 3.14 Final well responses of water-cut (left) and bottom-hole pressure (right) for 4 producers.

The final permeability model made by integrating two objectives is displayed in Figure 3.15. In Figure 3.16, left side is the permeability change needed (reference model – initial model) and right side is the permeability change made (final model – initial model). Although initial model does not have high and low permeability trend, inversion process captures the trend of reservoir property and reproduces well responses to be consistent with the reference model. Thus, after history matching, final model has a high permeability between P2, P4 and I1. In addition, it captures low permeability at south-east area.

Although integration of pressure data provides more information compared to the conventional streamline-based approach that is only matching the water-cut data, we need additional information such as seismic data to generate more consistent permeability distribution with reference model.

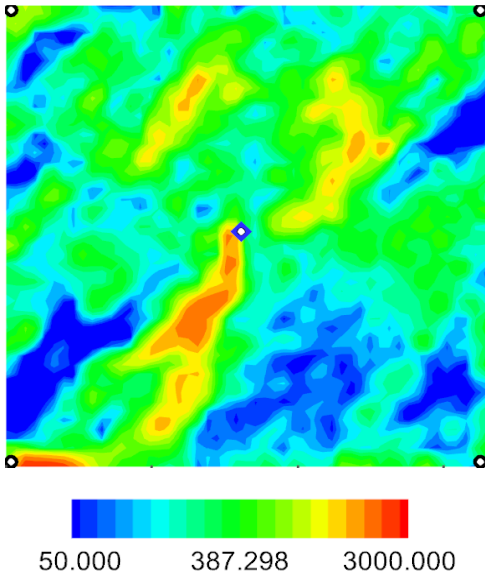

Figure 3.15 Final permeabiltiy distributioution after joint inversion.

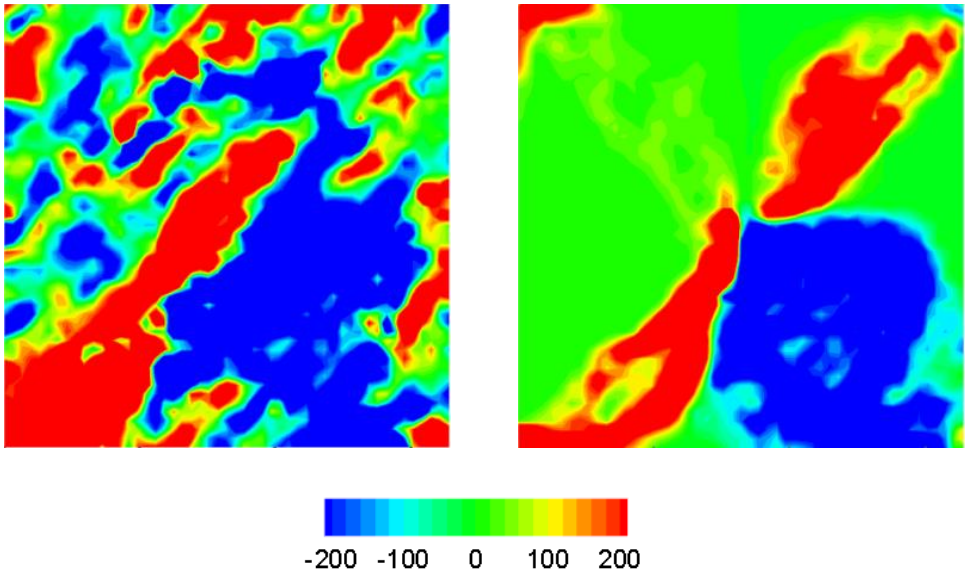

Figure 3.16 Change needed (left) and change made (right) during history matching.

3.5 Applications of Joint Inversion with Multiscale Approach

The joint inversion for water-cut and bottom-hole pressure in section 3.4 reconciles two different types of data. As we know, pressure data is well-suited to capture a large-scale variation of heterogeneity, and saturation data is good for reproducing a small-scale variation. Williams et al. (1998) have presented a structured approach that sequentially adjusts from global (fieldwide), then to flow units, followed by local changes in model parameters. They first matched the pressure to correctly distribute fluids, followed by saturation matching to mimic the movement of water and free gas in the reservoir. Cheng et al. (2008) showed a similar structured approach for assisted probabilistic history matching. Here, we suggest the multiscale approach based on streamline for joint inversion to account for the disparity in resolution of different types of data.

3.5.1 Methodology of Multiscale Approach

The multiscale approach has two stages as displayed in Figure 3.17. For the large-scale update, the geological model is parameterized using a Grid Connectivity Transform (GCT) basis (Bhark et al. 2011), and then the inversion problem is solved using streamline-based sensitivity to update coefficients in spectral domain. The second stage for the fine-scale update is the same as a joint inversion by calibrating grid properties in section 3.4.

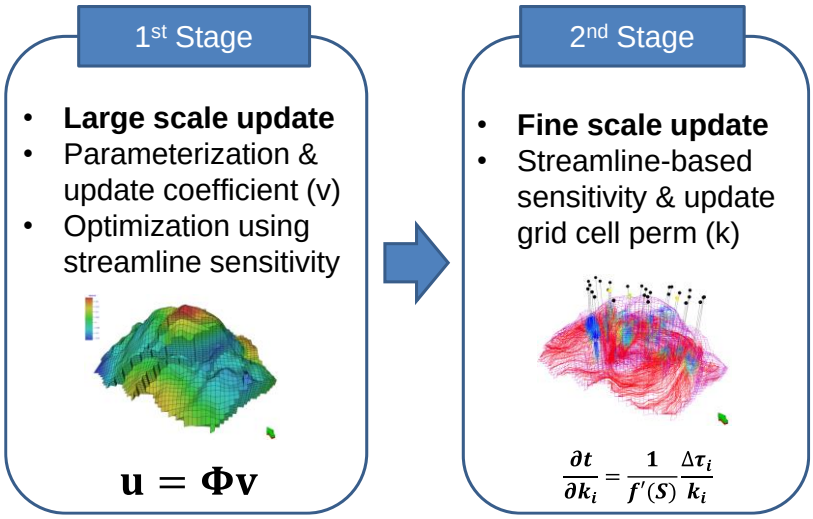

Figure 3.17 Multiscale approch with two stage workflow.

Grid Connectivity Transform (GCT)

GCT is a linear transformation that is characterized by the spectral modes of the reservoir model grid system. A multiplication of the grid properties with the GCT basis, which is constructed from the eigenvectors of a grid Laplacian, performs the transformation from the spatial to spectral domain. Bhark et al. (2012) described how to construct grid

Laplacian based on grid connectivity well. These eigenvectors can be generalized as the "natural vibration modes" and corresponding eigenvalues can be generalized as the "associated natural frequencies." This parameterization method is efficient for the estimation of reservoir parameters by reducing the dimensionality and the enforcement of spatial continuity or smoothness in the process of calibration.

Using orthogonal basis, a discrete spatial field (**u**) is mapped to the transform domain (**v**) as

$$\mathbf{v} = \mathbf{\Phi}^{\boldsymbol{T}}\mathbf{u} \;\Leftrightarrow\; \mathbf{u} = \mathbf{\Phi v} \tag{3.15}$$

where **u** has $N\times1$ dimension (N is the discretization of the estimable property field such as permeability or porosity). The column vector **v** is M-length of the parameter set in the transform domain. $\mathbf{\Phi}$ is a ($N\times M$) matrix containing M-columns that defines the discrete basis functions of each length N. It is well displayed in Figure 3.18. Because most of the energy is compressed in the fewest coefficients, M is much smaller than N, typically less than one percent of the original dimension in the spatial domain (Kang et al. 2014).

For model calibration in history matching, a spatial multiplier field instead of a permeability field itself has been applied like Eq. 3.16.

$$\mathbf{u} = \mathbf{u_0} \circ \mathbf{\Phi v} \tag{3.16}$$

where $\mathbf{u_0}$ is the prior (initial) property and $\mathbf{\Phi v}$ defines the multiplier field in the spatial domain. A multiplication operator ($\circ$) is the element-wise product (Schur product).

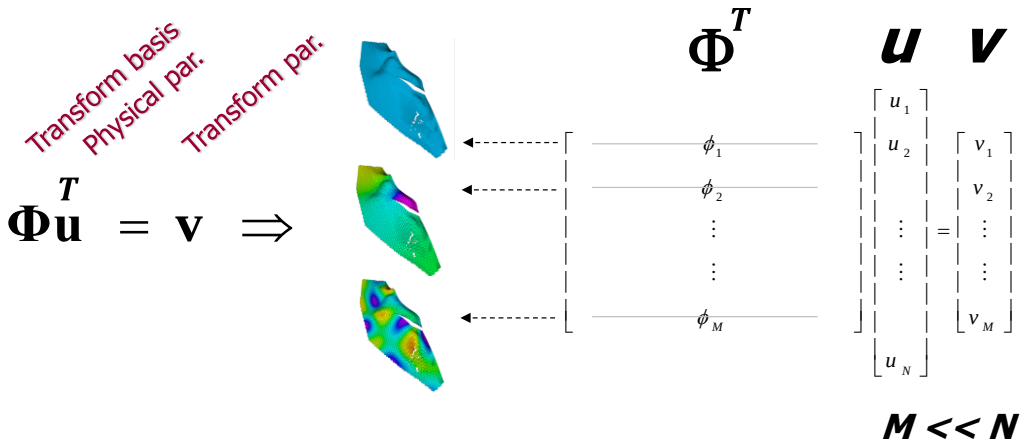

Figure 3.18 Transformation between spatial domain (*u*) and spectral domain (*v*).

Large-scale update workflow

The suggested large scale history matching workflow is presented in Figure 3.19. As we mentioned, a permeability multiplier is used instead of a cell property itself. The multiplier at each cell is assigned an initial value of unity, and it is parameterized and adjusted in the large-scale update. The parameterization is accomplished by projecting the spatial field onto basis functions. The linear transform results in a set of spectral coefficients, which will be updated by streamline-based sensitivity. After updating coefficients in the spectral domain, it back-transforms to the multiplier in the spatial domain by multiplication of the coefficient vector with GCT basis. Finally, the multiplier field is applied to the prior model to check the data misfit between simulation data and historical data. This whole process works iteratively until the maximum number of iterations or data misfit is less than tolerance we set.

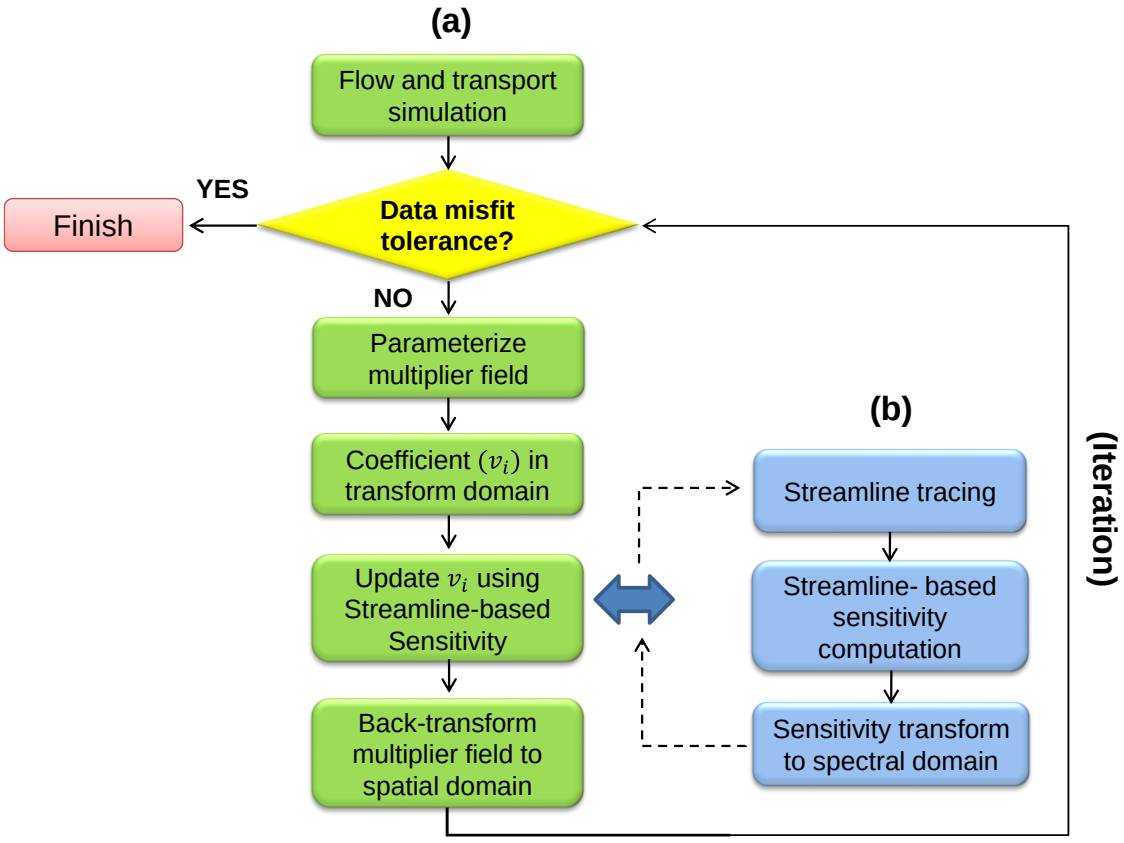

Figure 3.19 1st stage workflow including (a) large-scale update using GCT basis for calibrating coefficient in spectral domain and (b) streamline-based coefficient sensitivity calculation.

Transform parameter sensitivity

Here, we explain the Figure 3.18b that is a calculation of streamline-based sensitivity with respect to the coefficient in a spectral domain and LSQR minimization we used in Chapter II. Bhark et al. (2011) used a gradient-based method for updating coefficients. Although this problem is parameterized and a less ill-posed inverse problem, formulation of the sensitivity matrix is still computationally expensive. Kang et al. (2014) used streamline-derived coefficient sensitivity for water-cut matching. Here, we apply this approach to the

joint inversion of pressure and water-cut. To calibrate coefficients, we need to calculate partial derivatives to relate well response to the coefficient (v) as follows,

$$\frac{\partial A}{\partial \mathrm{v}_i} = \frac{\partial A}{\partial \mathrm{u}} \frac{\partial \mathrm{u}}{\partial \mathrm{v}_i} \tag{3.17}$$

where *A* is a well response that can be travel time for water-cut matching and bottom-hole pressure difference for pressure matching in our approach. In RHS of Eq. 3.17, we know how to calculate $\frac{\partial A}{\partial \mathrm{u}}$, sensitivity of well response (bottom-hole pressure and water-cut travel time) with respect to the reservoir properties. The model parameter u is a linear combination of coefficients weighted by basis function. Thus, we can calculate $\frac{\partial \mathrm{u}}{\partial \mathrm{v}_i}$ using Eq. 3.15.

$$\frac{\partial \mathrm{u}}{\partial \mathrm{v}_i} = \frac{\partial (\Phi \mathrm{v})}{\partial \mathrm{v}_i} = \Phi_i \tag{3.18}$$

If we use a multiplier field instead of a reservoir property itself, Eq. 3.18 can be

$$\frac{\partial \mathrm{u}}{\partial \mathrm{v}_i} = \frac{\partial (\mathrm{u}_0 \circ \Phi \mathrm{v})}{\partial \mathrm{v}_i} = \mathrm{u}_0 \circ \Phi_i \tag{3.19}$$

Finally, we can calculate the coefficient sensitivity by combining Eq. 3.17 with Eq. 3.18 or Eq. 3.19.

$$\frac{\partial A}{\partial \mathrm{v}_i} = \frac{\partial A}{\partial \mathrm{u}} \Phi_i \tag{3.20}$$

$$\text{or,} \qquad \frac{\partial A}{\partial \mathrm{v}_i} = \frac{\partial A}{\partial \mathrm{u}} (\mathrm{u}_0 \circ \Phi_i) \tag{3.21}$$

dAs we have mentioned before, $(\circ)$ is the element wise multiplication and the other one is dot product. Therefore, Eq. 3.20 and 3.21 make a single value (*1×1*) for each corresponding coefficient. After calculation of the coefficient sensitivity, we minimize the penalized misfit function (Eq. 3.14) to update parameters in a spectral domain.

$$o(\delta v) = \alpha_1 \|\delta d_{wct} - S_{wct}\delta \mathrm{v}\| + \alpha_2 \left\|\delta d_{bhp} - S_{bhp}\delta \mathrm{v}\right\| + \beta_1 \|\delta \mathrm{v}\| \qquad (3.\ 22)$$

However, we do not have the 'smoothness' term in the objective function (Eq. 3.22). The parameterization with GCT basis captures the large-scale geologic continuity and makes the smoothness of reservoir properties during the history matching.

3.5.2 Brugge Benchmark Model

Joint inversion with the multiscale approach is tested in the Brugge benchmark model in section 2.6. The information of this model is described in the previous chapter. It has a total of 104 realizations and we selected three of them (1, 67 and 92) to account for the uncertainty of the prior model. Figure 3.20 shows the permeability distribution of three initial models. They also have different porosity and net-to-gross ratio.

We start with a large-scale update using GCT basis to update coefficient in spectral domain. It uses the permeability multiplier that has a value of unity for all cells initially in this application. When data misfit does not decrease, we move to the second stage. Our objective is matching water-cut and bottom-hole pressure for 20 producers.

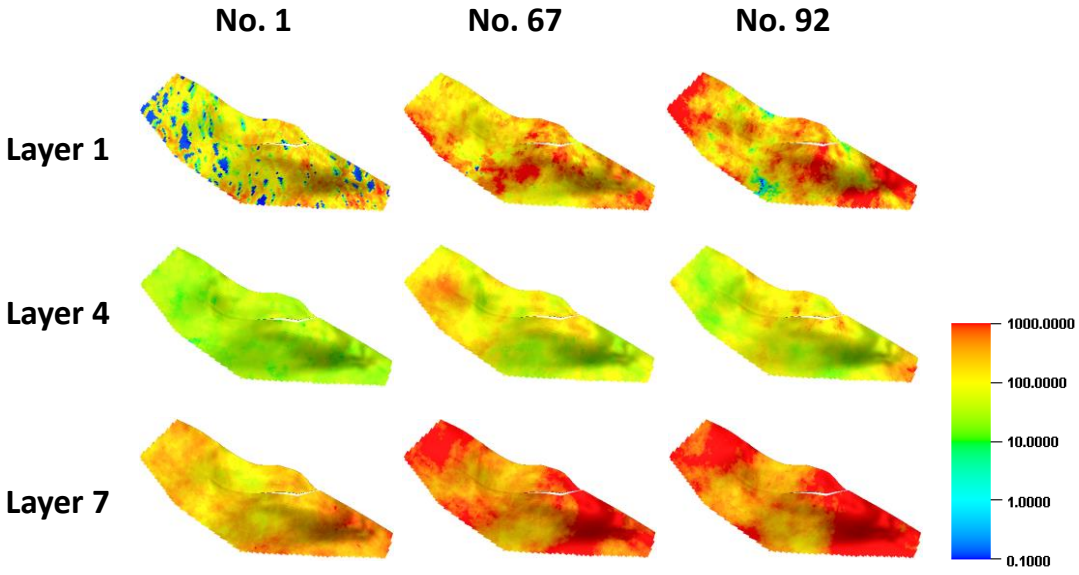

Figure 3.20 Permeability distribution of three layers (by row) for three initial models (column).

In spectral domain, the permeability multiplier field is a linear combination of bases and coefficients like in Figure 3.21. It clearly illustrates the Eq. 3.16. In this problem, we use 100 basis vectors which is much less than one percent of the total grid number.

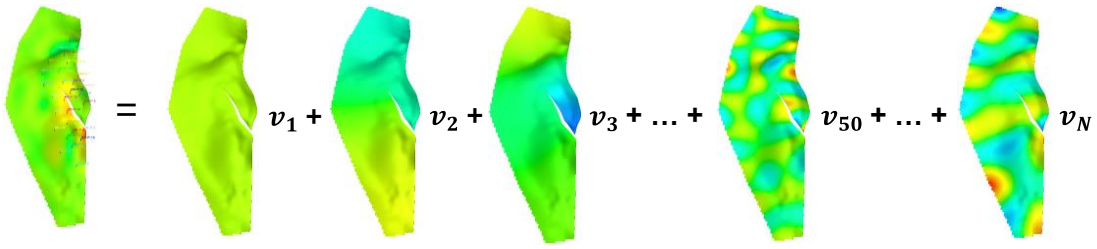

Figure 3.21 Parameterization of the permeability multiplier field as the weighted linear combination of GCT basis vectors.

The history matching is conducted with two different scenarios to validate the effectiveness of the multiscale approach in joint inversion. The first scenario is the multiscale approach that updates the large-scale permeability field followed by the fine scale updating, and the second one is direct fine scale updating. Figure 3.22 shows the convergence of water-cut and pressure data misfit through 10 iterations of the Brugge model. The black dot line in the middle of the figure is the starting point of the second stage history matching. All three models with the multiscale approach show the better convergence of objective functions compared to the fine scale only results. The result of the multiscale approach has 50% decrease in water-cut and 50% to 70% of pressure misfit reduction. However, the fine scale only makes 30% to 40% reduction in water-cut and 10% to 30% reduction of pressure misfit. Particularly, the no.1 model with the multiscale shows much smaller pressure misfit and most of the improvement happens in the first stage. This is because realization no.1 has a different trend of permeability distribution and a huge misfit of bottom-hole pressure data exists initially. It also shows the large-scale updating reproduces the pressure response effectively, and water-cut is well matched by both multiscale and fine-scale approaches. The other two models also have smaller data misfit for both water-cut and bottom-hole pressure when we apply the proposed joint inversion with the multiscale approach. These results support the importance of updating larger- before smaller-scale heterogeneity.

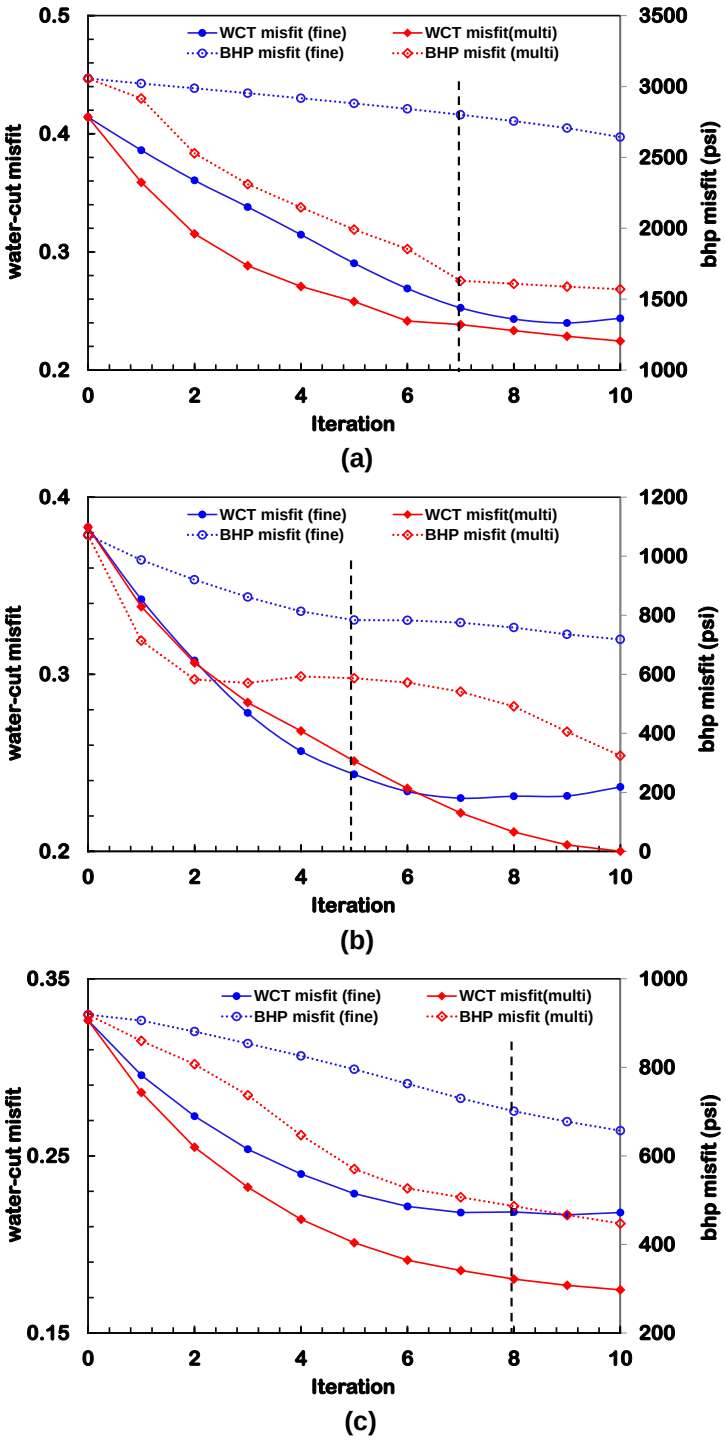

Figure 3.22 Convergence of objective function for three prior model (a) No. 1, (b) No. 67, and (c) No. 92 realization.

Figure 3.23 is the final permeability distribution after 10 iterations with large- and fine-scale calibration. There is no unrealistic permeability change that is seen occasionally when we match pressure data by calibrating the fine-scale model directly. The result of the permeability change is shown in Figure 3.24. Fine-scale only shows the permeability change along the streamline. However, the multiscale approach makes a smoother change of reservoir parameters and captures the large-scale permeability change. Therefore, it has a smaller data misfit in Figure 3. 22 and, particularly, better pressure matching of well responses in Figure 3.25.

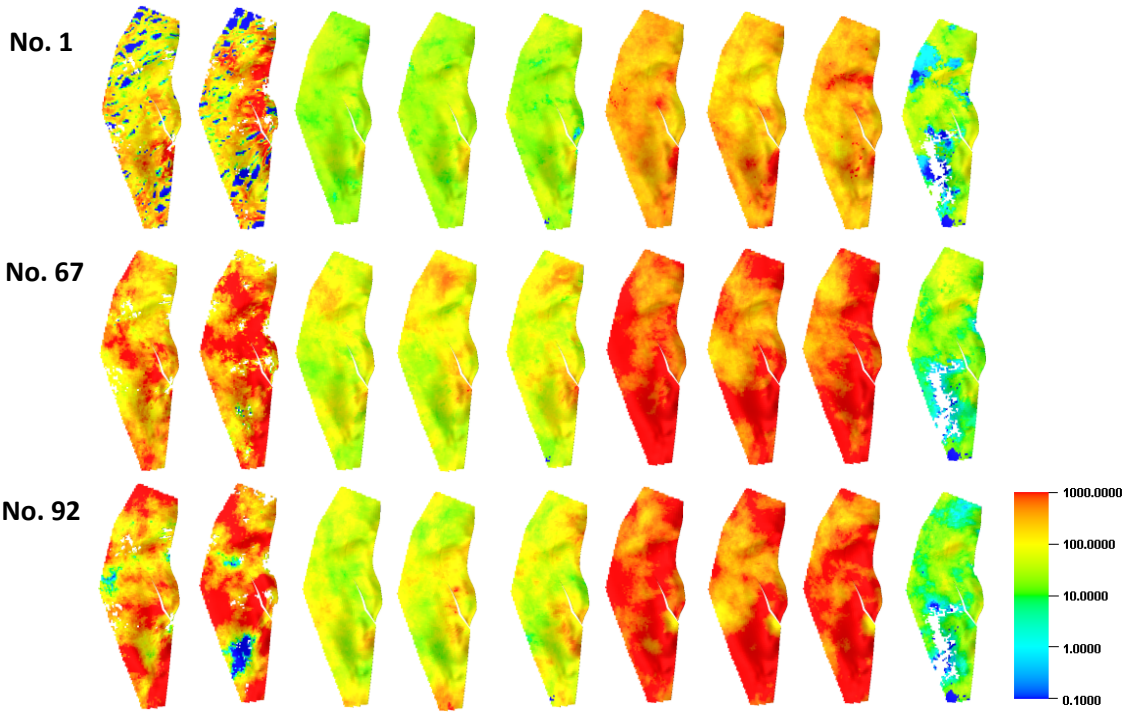

Figure 3.23 Three final updated permeability models (by row) for all 9 layers (column) by multiscale approach.

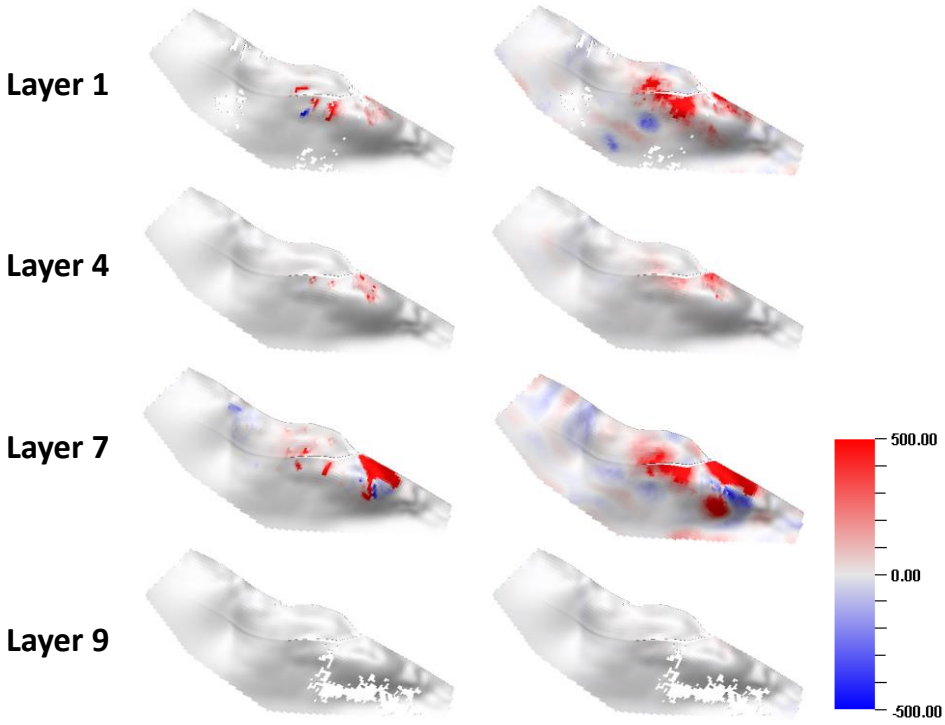

Figure 3.24 The change of permeability (updated model – initial model) after only fine scale history matching (left column) and multiscale history matching (right column) with realization No. 67.

Last, in Figure 3.25 bottom-hole pressure and water-cut well responses are shown, respectively, for selected 16 wells that have a water breakthrough. Although a few wells have small changes (P-12, P-13, P-19, and P-20), most of the wells show improvement. P1 is one of the wells with no water breakthrough and it has only pressure term in the objective function. Again, Figure 3.24 supports the effectiveness of the multiscale approach in the proposed joint inversion for bottom-hole pressure and water-cut matching.

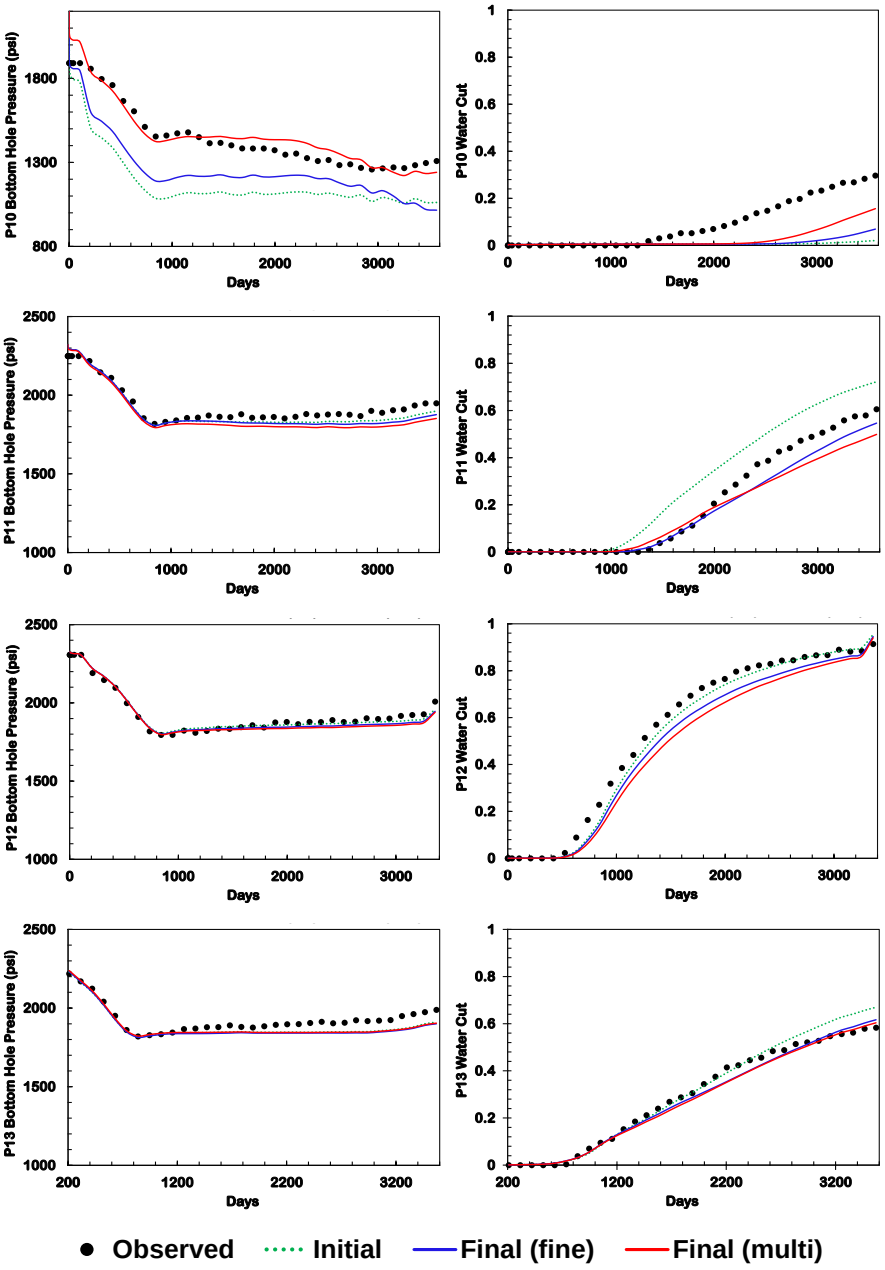

Figure 3.25 Bottom-hole pressure (left column) and water-cut (right column) responses at each production well corresponding to the reference, initial, and calibrated Brugge model of realization No. 67 by fine scale only and multiscale approach.

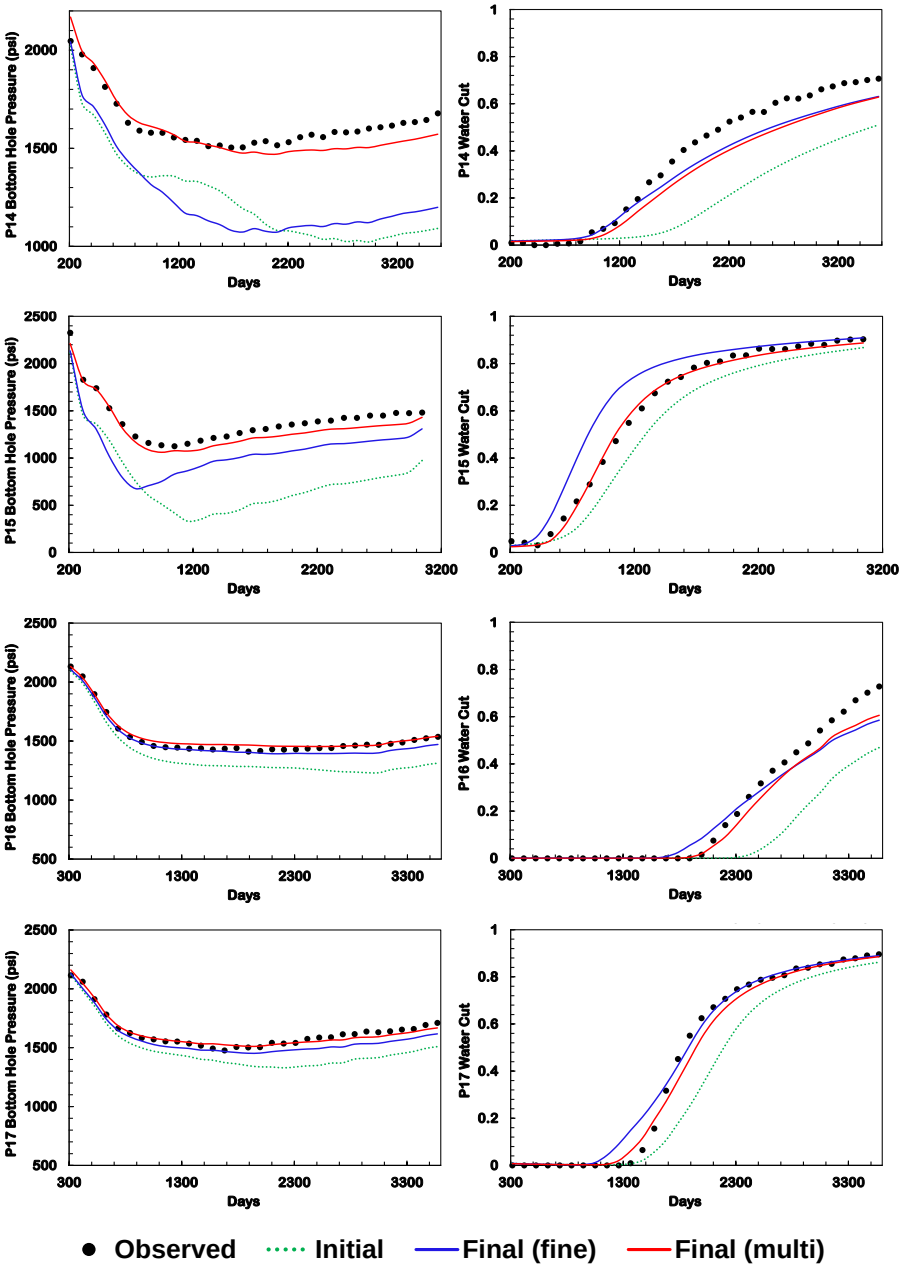

Figure 3.25 continued.

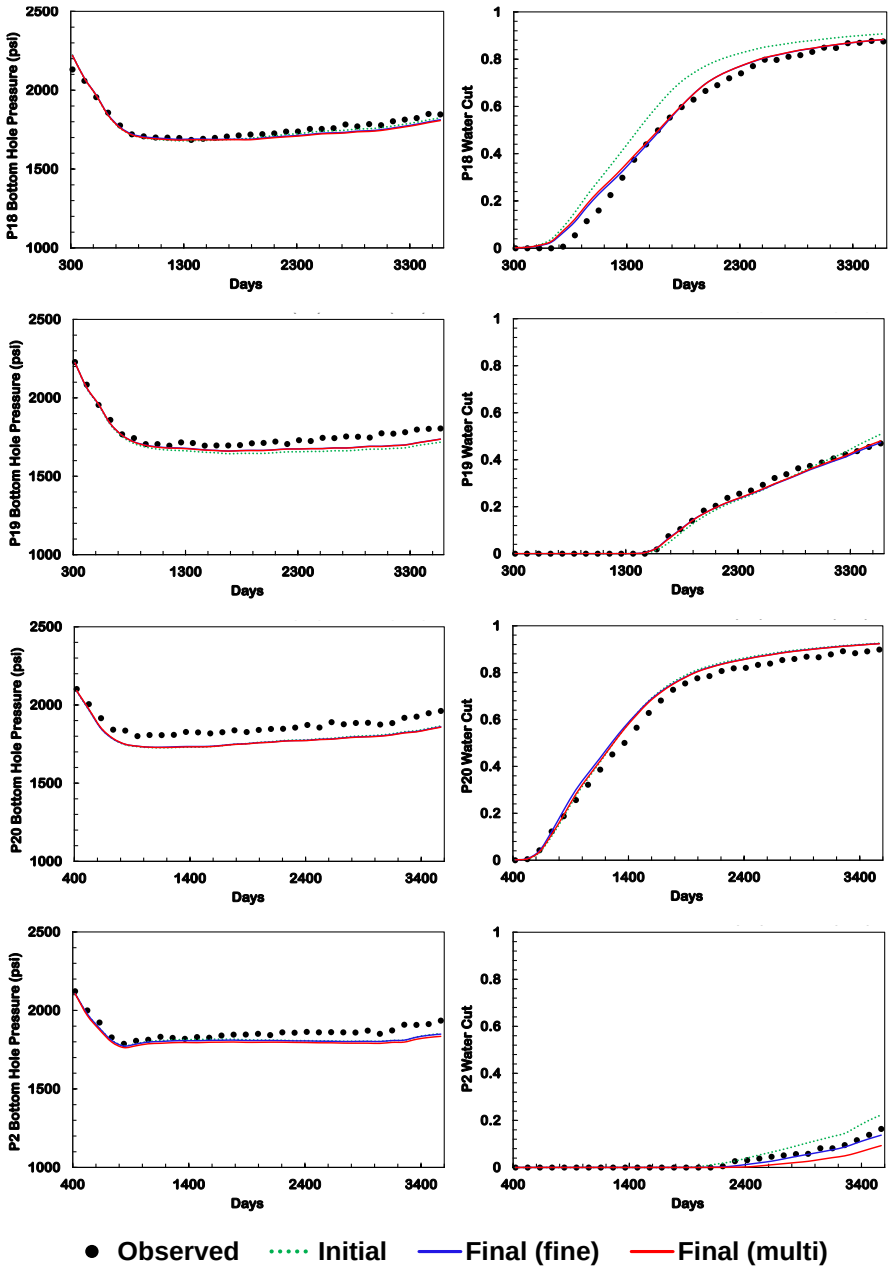

Figure 3.25 continued.

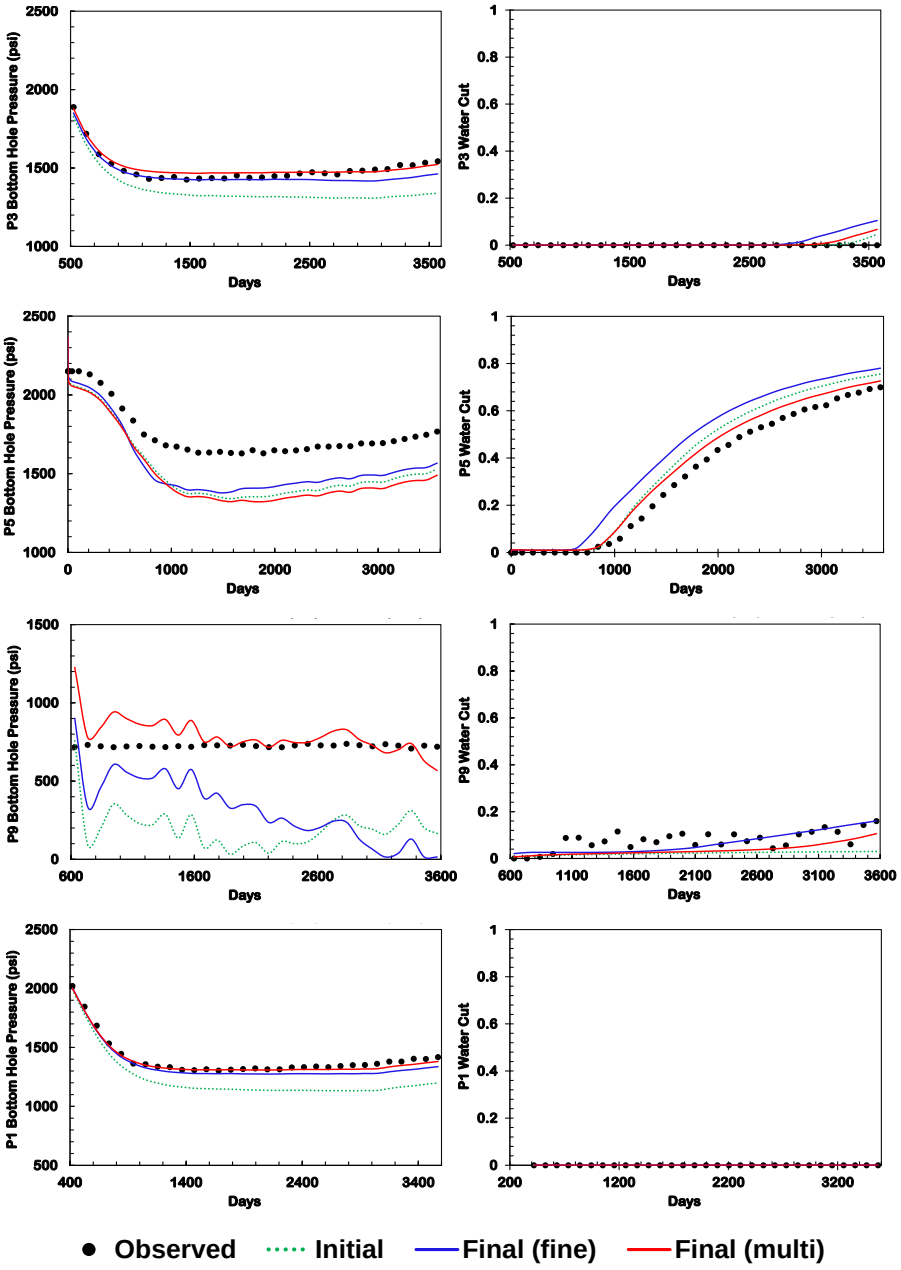

Figure 3.25 continued.

An example of the streamlines connected to P-14 explains the improvement of well responses after history matching. Based on the initial well response of P-14, higher bottom-hole pressure and early water breakthrough are required during the inversion process. By comparing the streamlines of initial and updated models in Figure 3.26, the calibration of permeability field makes additional support from I-1 and aquifer to P-14 and a new connection between I-8 and P-14 (circle with solid line). It results in increasing bottom-hole pressure. Based on the time-of-flight, we identify that the water flows faster to the producer after history matching (circle with dotted line). It results in accelerating the water-cut response.

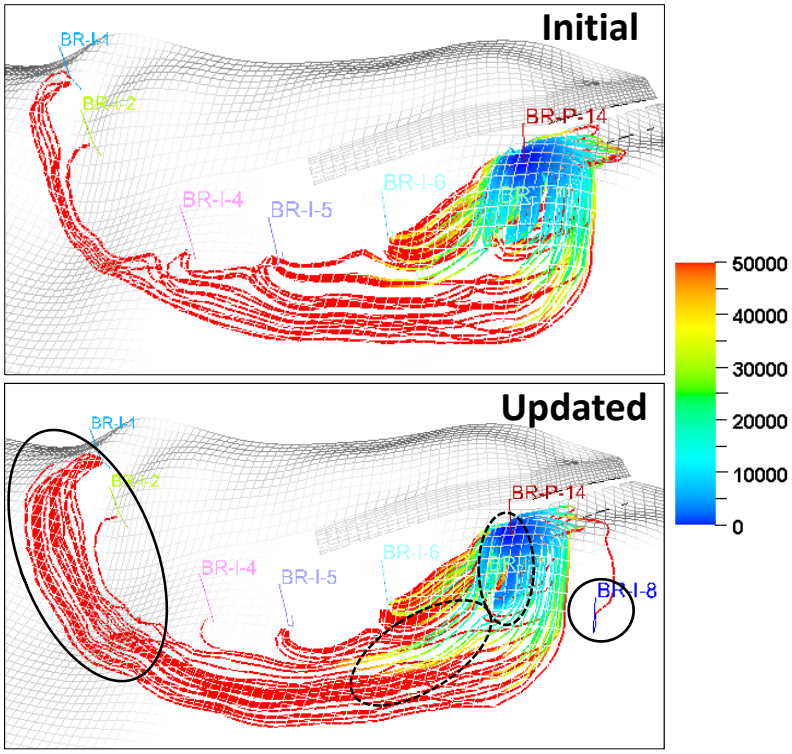

Figure 3.26 Streamlines connected to the P-14 at initial (top) and after multiscale history matching (bottom) (The colour means the time-of-flight from the producer).

Analysis of convergence of multiscale approach

We analyze the effect of the multiscale approach on pressure and water-cut matching. Here, coarse scale basis functions, corresponding to low modal frequencies, are applied first to enable adjusting of the large-scale heterogeneity. Then, we increase the number of parameters by adding higher modal frequencies to capture the smaller-scale spatial details. Figure 3.27 shows the convergence of our objectives. It indicates that the large-scale updating with the smaller number of basis decreases the pressure data misfit drastically. The small-scale updating with the large number of basis and the fine-scale updating (cell by cell) successfully reduces the water-cut data misfit with maintaining the pressure matched in the large-scale process. Thus, it demonstrates the importance of the multiscale approach for pressure and water-cut matching and confirms that the large-scale approach matches the pressure well and the small-scale approach achieves the water-cut improvement.

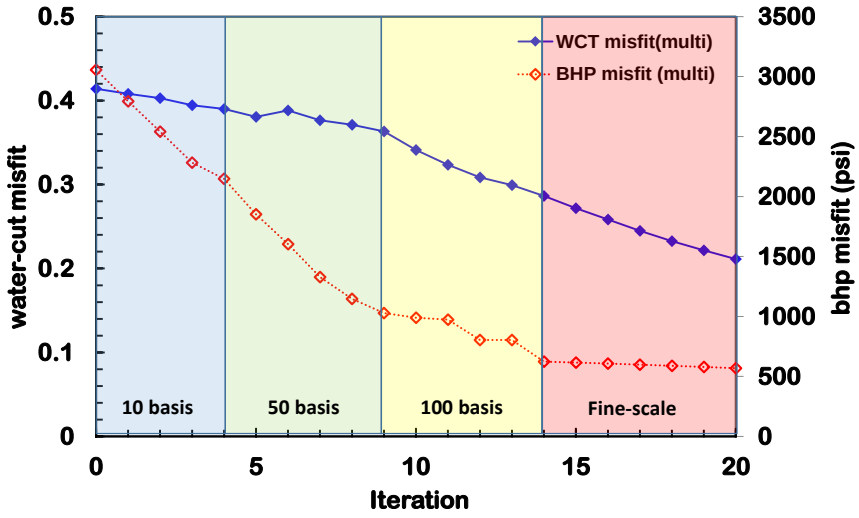

Figure 3.27 Analysis of multiscale approach.

3.5.3 Norne Field

We demonstrate the practical feasibility of our proposed joint inversion with a multiscale approach through the history matching of Norne field. The field was discovered in 1991 and it started production in November 1997. It is located on the Norwegian continental shelf approximately 200 kilometers offshore of central Norway. The geologic model consists of five zones: Garn, Not, Ile, Tofte and Tilje. Oil is mainly found in the Ile and Tofte formations, and gas is found in the Garn formation. The sandstone are buried at a depth of 2500-2700m. The porosity is in the rage of 25-30%, while permeability varies from 20 to 2500mD (Steffensen and Karstadt, 1996; Osdal et al. 2006). The reservoir model has 113,334 grid cells (44,927 of active cells) and contains 36 wells (9 injectors and 27 producers) as shown in Figure 3.28. We consider the production period from 1997 to 2006 for the history matching of water-cut and bottom-hole pressure data. The actual simulation model, containing all grid information and properties, and historical production data were provided by the operator. The details of the data set is described in Rwechugura et al. (2012).

Watanabe et al. (2013) matched history data with acoustic impedance using a combination of stochastic and streamline based approach. The objective of history matching is different with our application because it incorporates the seismic data (related with pressure and saturation effect) first and matches well water-cut sequentially. Thus, it still has the issue we mentioned that the water-cut matching shifts the pressure data matched before.

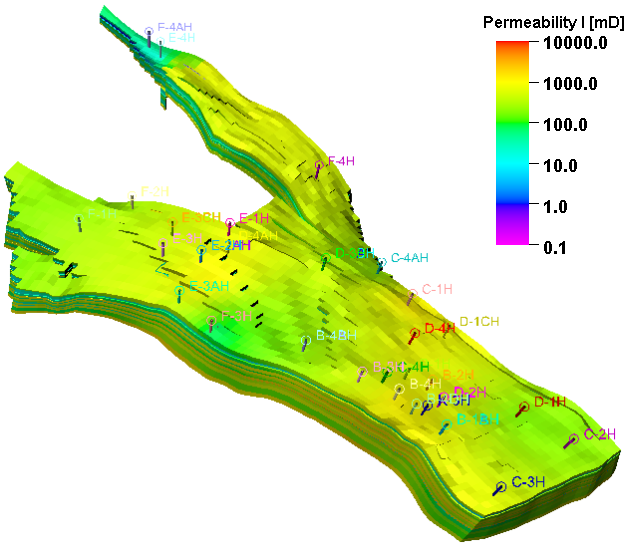

Figure 3.28 Structure and well location of Norne field (colour shows permeability distribution.)

History matching results

The history matching workflow is the same as the application in the Brugge model (Figure 3.17 and Figure 3.19). As discussed before, we start with the large-scale update using GCT basis, followed by the streamline-based fine-scale update. First, we adjust the WOC for E-3AH based on the previous work (Rwechungura et al. 2012). Second, we apply our proposed approach to the model. We have a much smaller number of unknown values when we parameterize the permeability field. Thus, we can match the pressure amplitude instead of the average misfit of pressure data applied in the Brugge model. In the Norne field model, most of the calculated pressure responses are similar with history data because this field was already calibrated to match the reservoir energy (regional pressure by pore volume multipliers). Therefore, after 13 iterations, bottom-hole pressure shows less

improvement compared to water-cut matching (Figure 3.29). Figure 3.30 shows the well response after history matching. Most of the wells show closer well responses to the history data and maintain the initial responses if it was already well calibrated. Although water-cut matching of E-4AH is deteriorated, pressure matching shows significant improvement (we do not include E-4AH for the misfit calculation in Figure 3.29). This phenomenon might have happened because of a potential conflict between two objectives. We will explain this issue in more detail in chapter IV. The final updated model is shown in Figure 3.31. The permeability change in the large-scale update and the fine-scale update are compared in Figure 3.32. As we expected, the 1st stage with GCT parameterization captures the large-scale heterogeneity and the 2nd stage adjusts the small-scale permeability change to match our objectives.

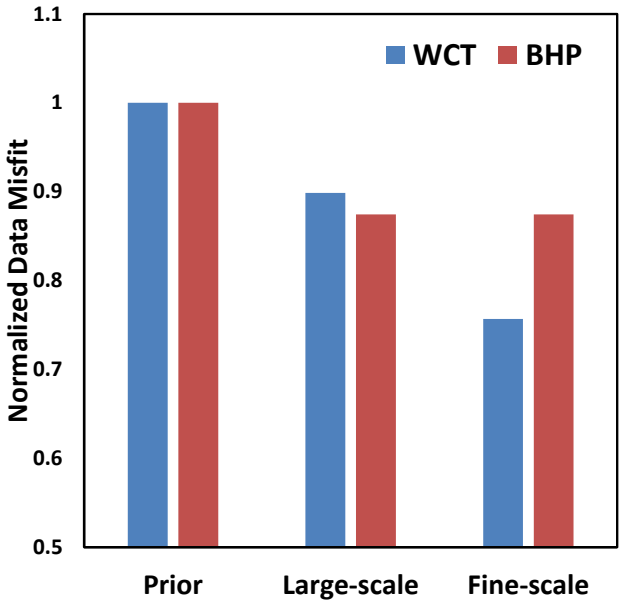

Figure 3. 29 The comparison of the nomalized objective function for water-cut and bottom-hole pressure among prior (after WOC calibration), large-scale matching, and fine-scale matching.

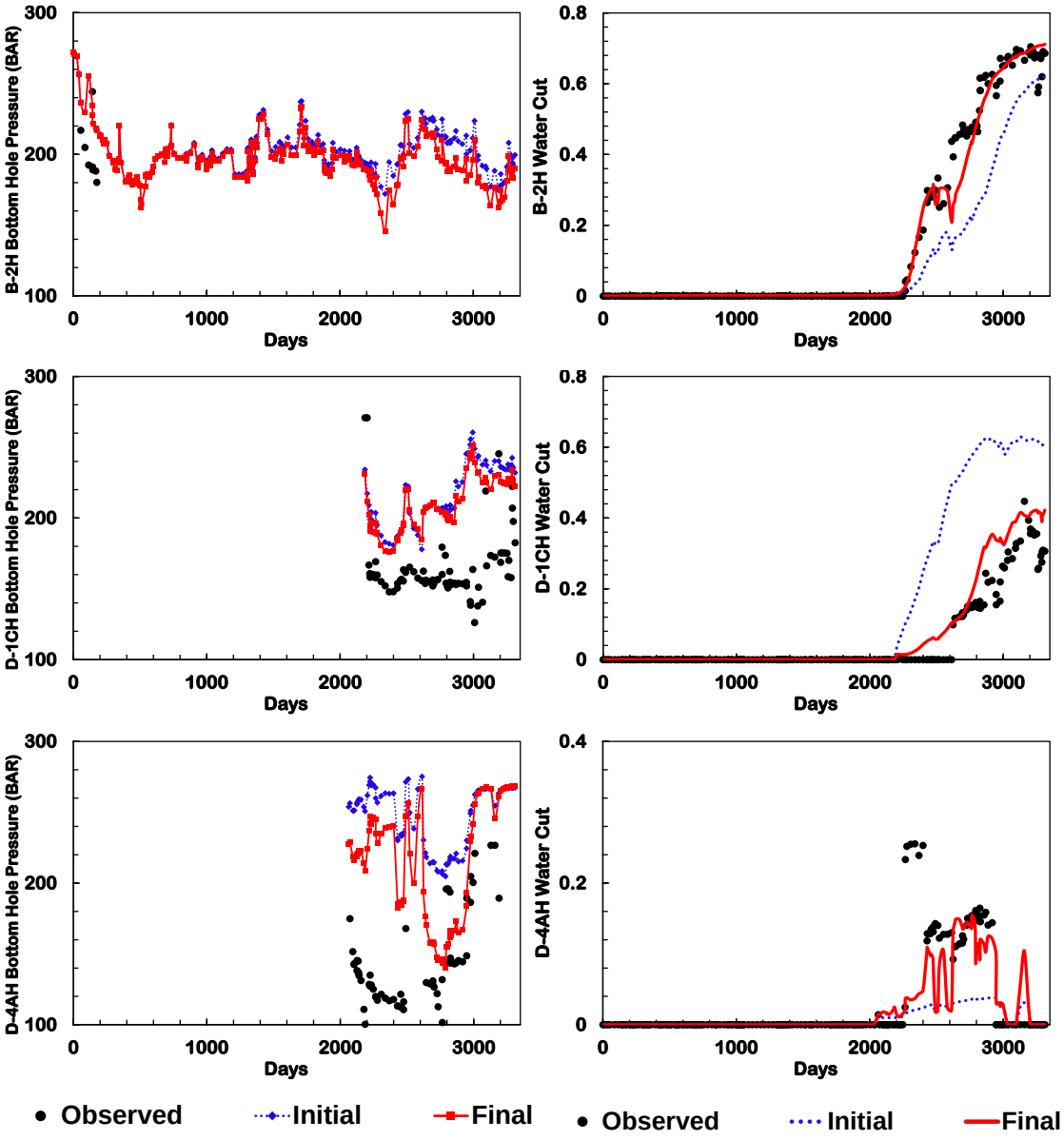

Figure 3.30 Bottom-hole pressure (left column) and water-cut (right column) at each production well corresponding to the reference, initial, and calibrated Norne field model by joint inversion with multiscale approach.

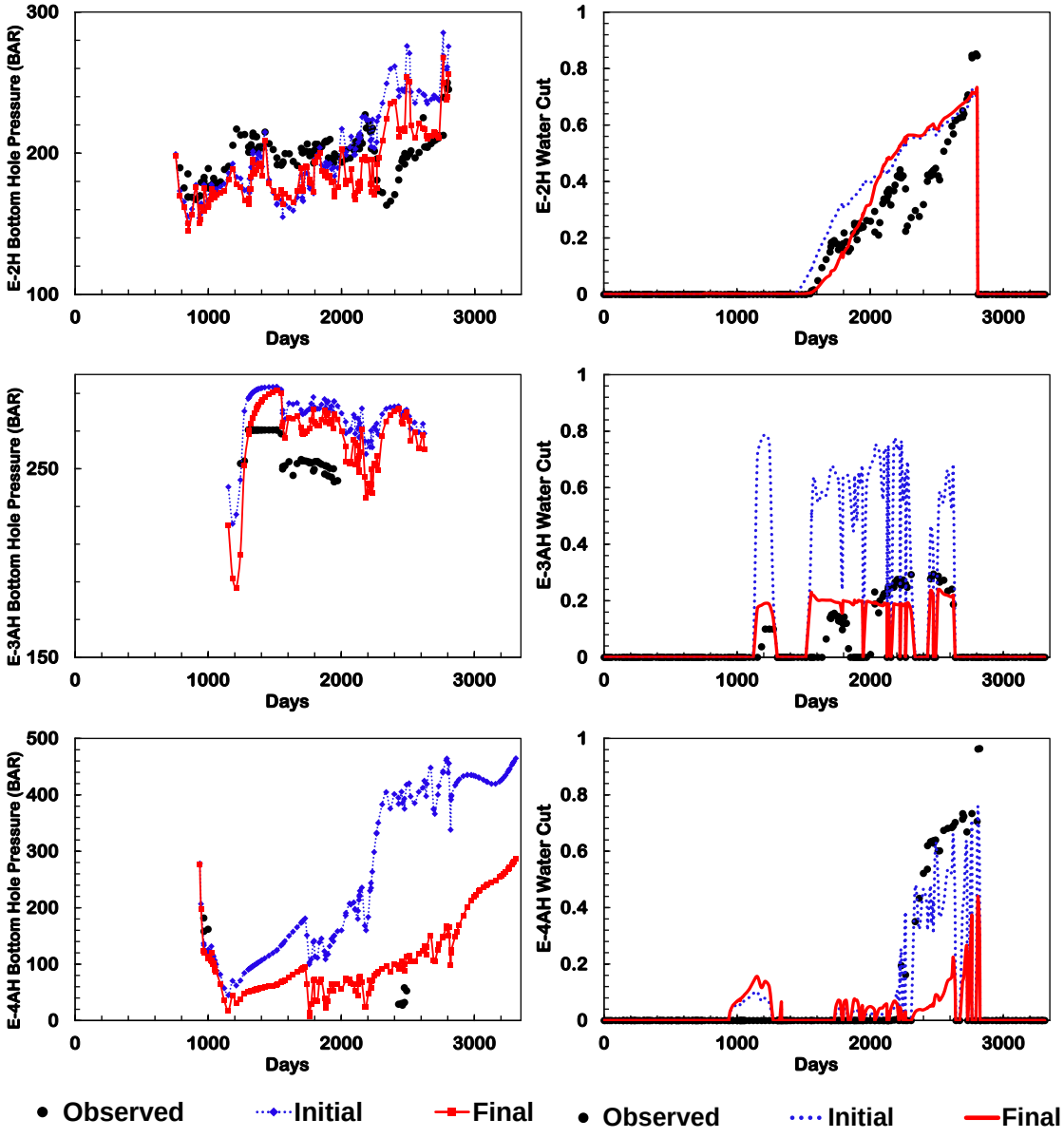

Figure 3.30 continued.

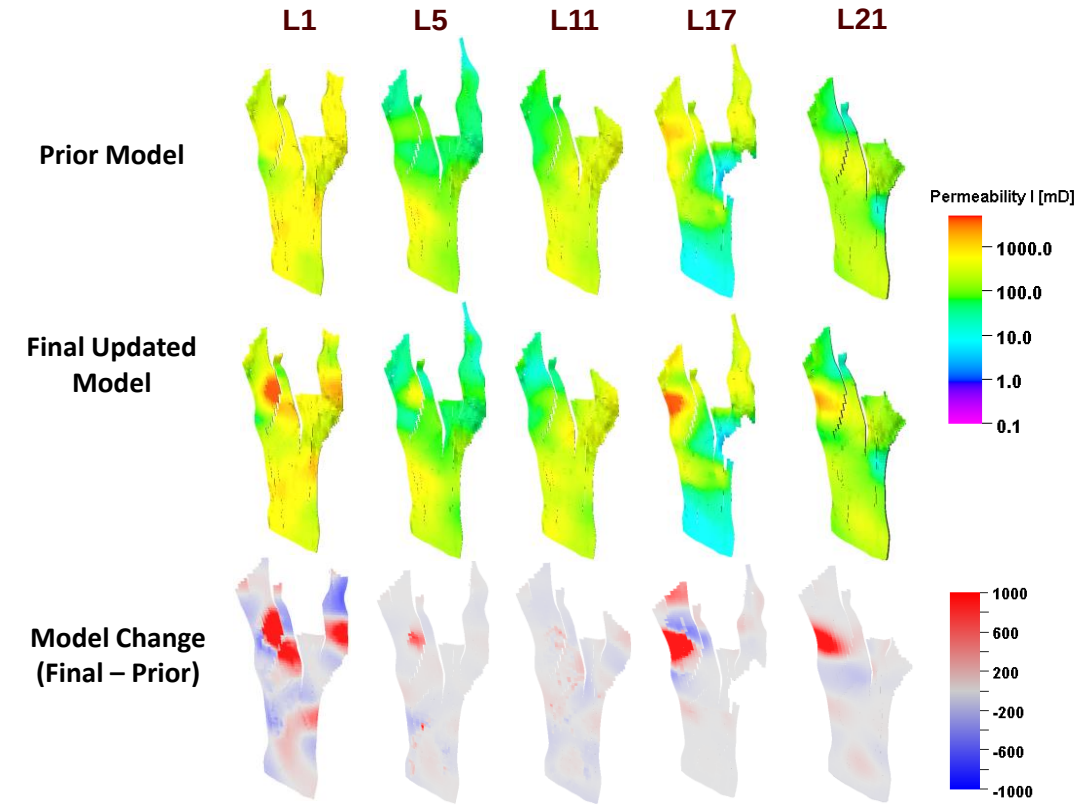

Figure 3.31 Five selected layers (each column) of the prior, updated permeability, and permeability change (by each row).

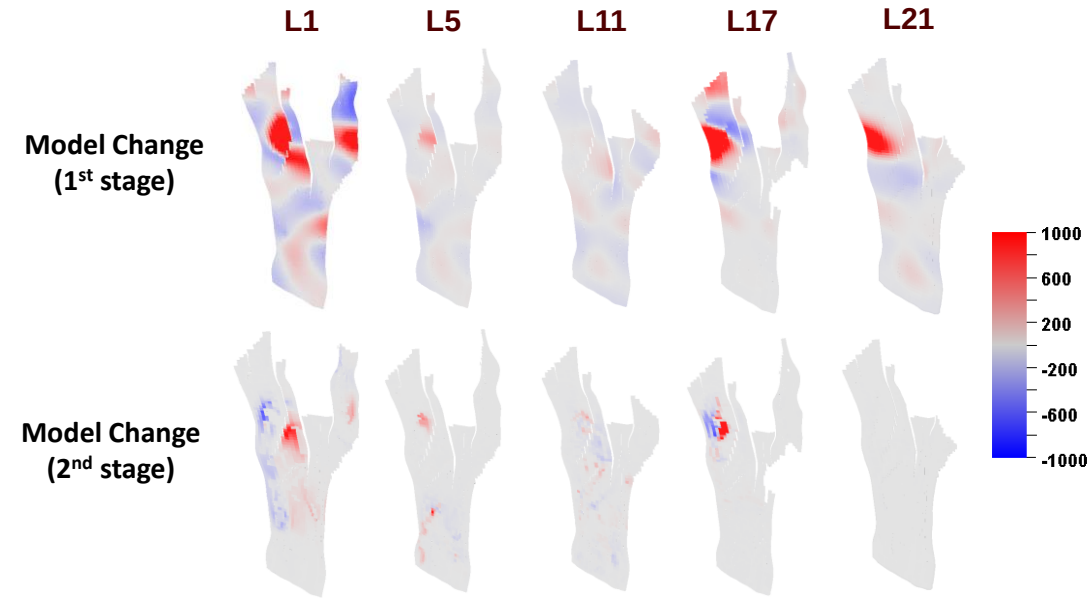

Figure 3.32 Permeability change in 1st and 2nd stage for the selected five layers.

3.6 Chapter Conclusions

We have presented a new approach to calculate pressure sensitivity based on streamline. Using this analytical sensitivity, we propose a streamline-based joint inversion with a multiscale approach. We demonstrate the effectiveness of the joint inversion through a synthetic model and showed the importance of multiscale approach for the joint inversion through the Brugge benchmark model and Norne field application. The major findings from this chapter are summarized below.

1. We have proposed a new methodology for the streamline-based analytic approach to calculate sensitivity of bottom-hole pressure with respect to the reservoir permeability. We validated the bottom-hole pressure sensitivity by comparison with the adjoint method.
2. We apply the joint inversion for bottom-hole pressure and water-cut matching simultaneously to the synthetic model and compare with the only water-cut matching case. Adding pressure data makes significant improvement in inversion. We can avoid the problem in the sequential process, matching pressure data followed by water-cut history matching that was used in prior works, by introducing the pressure sensitivity calculation based on streamline.
3. We suggested the joint inversion with a multiscale approach. Brugge benchmark application with the multiscale approach shows better convergence and improves well response matching compared to the only fine-scale history matching. The multiscale approach with GCT captures the large-scale heterogeneity and makes a smooth change of permeability. In addition, we show the importance of updating

larger- before smaller-scale heterogeneity by analysis of the convergence of data misfit in the multiscale approach; large-scale matches the pressure and small-scale achieves the water-cut improvement.

4. The Norne field application results confirm that the joint inversion with the multiscale approach constrains the history matching solution effectively and reproduces the well responses through the large and fine scale inversion.

CHAPTER IV

STREAMLINE-BASED THREE-PHASE HISTORY MATCHING AND FIELD APPLICATION

4.1 Chapter Summary

It is well known that integration of pressure data is essential for the history matching in the three-phase system because the gas phase is sensitive to pressure. The prior works matched the pressure data, followed by integration of water-cut and gas-oil ratio (Cheng et al. 2005, Oyerinde et al. 2009). As the pressure sensitivity based on streamline was derived in chapter III, now we can integrate the pressure data and the three-phase production data simultaneously. In this chapter, we present the calibration of reservoir properties for the three-phase reservoir model using the sensitivities for bottom-hole pressure, water-cut, and gas-oil ratio, all based on streamlines.

By applying our approach to synthetic models with water injector or gas injector, we demonstrate the improvement of gas phase matching by incorporating pressure data and production data (water-cut and gas-oil ratio) in the three-phase reservoir. We show the practical applications using the field cases and validate the utility of our approach. Finally, we test the Norne reservoir model again for the three-phase history matching by a combination of the evolutionary algorithm and the streamline-based method.

4.2 Introduction

Reconciling reservoir model with a variety of data is one of the most demanding tasks in reservoir characterization. The streamline-based history matching started from the two-phase system, and previous researchers were trying to apply it to the three-phase problem. Recently, streamline simulation was extended to the three-phase flow model. Cheng et al. (2006) generalized streamline model to compressible flow by introducing the concept of "effective density" that captures the changes in the fluid volume with pressure for compressible flow. This density term can be conveniently and efficiently traced along streamlines. Cheng et al. (2007) proposed an approach to the history matching of three-phase flow using a novel compressible streamline formulation and streamline-derived analytic sensitivities. They assumed the pressure is matched before, or they first matched the bottom-hole pressure manually, followed by a joint inversion of water-cut and gas-oil ratio. It had an issue we mentioned in chapter III that joint inversion shifts the pressure matching done in the pre-processing. Oyerinde et al. (2009) applied the previous approach with pressure data. However, it required the pressure matching before the gas-oil ratio matching. They carried out the pressure matching in the frequency domain by taking a Fourier transform of the pressure data following the procedure outlined by Vasco and Karasaki (2006). Now, we know how to calculate the pressure sensitivity based on streamline which is explained in chapter III. Therefore, three-phase flow production data and pressure data can be matched simultaneously using streamlines.

Multi-objective problems such as minimizing water-cut, bottom-hole pressure, and gas-oil ratio etc. that we are considering can be potentially conflicting because the data

comes from different sources, collected from different measurements, and has different level of uncertainties. For example, minimizing the water-cut misfit can increase the bottom-hole pressure error, and vice versa. To consider the objectives separately, multi-objective optimization evolutionary algorithm (MOEA) is designed. It searches solutions in the Pareto optimal front (Deb et al. 2002). Park et al. (2013) applied MOEA with GCT coefficient as parameter to the history matching of production and seismic data. Watanabe et al. (2013) matched production history data with acoustic impedance (AI) using MOEA with the streamline-based approach. Here, we also consider the evolutionary algorithm to avoid relative weighting issues in the streamline-based joint inversion. This proposed approach will be explained in detail later.

The outline of this chapter is as follows. To start with, we analyze the gas-oil ratio sensitivity formulation and show the applicability to history matching. We then illustrate the three-phase history matching with a synthetic model that has a water injector or gas injector. We demonstrate our approach using field-scale models (SPE9 and modified Brugge benchmark model) to show the effectiveness of adding gas-oil ratio information in the inverse modeling. Lastly, the Norne reservoir model is tested with the multiscale approach that is a combination of Pareto-based method and streamline-based approach.

4.3 Gas-oil Ratio Sensitivity

Before going into the application of history matching, we discuss the gas-oil ratio arrival time sensitivity. A main advantage of streamline model is that the sensitivities with respect to the reservoir parameters can be computed analytically using a single flow simulation. This benefit is also applicable to the gas-oil ratio sensitivity.

4.3.1 Mathematical Formulation

Cheng et al. (2007) proposed an approach for the history matching of three-phase flow based on streamline. To compute the gas-oil ratio arrival time sensitivity, the gas saturation equation along streamlines can be obtained starting with the mass conservation equation for the gas.

$$\phi \frac{\partial}{\partial t}\left(\frac{S_g}{B_g}+\frac{S_o R_s}{B_o}\right)+\nabla\cdot\left(\overrightarrow{u_t}\frac{f_g}{B_g}+\overrightarrow{u_t}\frac{f_o R_s}{B_o}\right)=0 \qquad (4.\ 1)$$

By transformation to the streamline time of flight coordinate using operator identity (Eq. 4.2) and noting $\nabla\cdot\vec{u}=c$, we have the Eq. 4.3.

$$u\cdot\nabla = \phi\frac{\partial}{\partial\tau} \qquad (4.\ 2)$$

$$\frac{\partial}{\partial t}\left(\frac{S_g}{B_g}+\frac{S_o R_s}{B_o}\right)+\frac{\partial}{\partial\tau}\left(\frac{f_g}{B_g}+\frac{f_o R_s}{B_o}\right)=-\left(\frac{f_g}{B_g}+\frac{f_o R_s}{B_o}\right)\frac{c}{\phi} \qquad (4.\ 3)$$

From the rules of an implicit function derivative,

$$\frac{\partial t}{\partial m} = -\frac{\frac{\partial S_g'}{\partial \tau}\frac{\partial \tau}{\partial m}}{\frac{\partial S_g'}{\partial t}} \tag{4. 4}$$

Here, S_g' represents the quantity $\frac{S_g}{B_g} + \frac{S_o R_s}{B_o}$. Finally, we combine the Eq. 4.3 and Eq. 4.4 in order to obtain the arrival-time sensitivity of S_g',

$$\frac{\partial t}{\partial m} = \frac{\frac{\partial}{\partial \tau}\left(\frac{S_g}{B_g} + \frac{S_o R_s}{B_o}\right)\frac{\partial \tau}{\partial m}}{\frac{\partial}{\partial \tau}\left(\frac{f_g}{B_g} + \frac{f_o R_s}{B_o}\right) + \left(\frac{f_g}{B_g} + \frac{f_o R_s}{B_o}\right)\frac{c}{\phi}} \tag{4. 5}$$

This equation consists of the time of flight sensitivity and a pre-factor that is a function of saturation and pressure. All terms in Eq. 4.5 are readily available along the streamlines.

4.3.2 Gas-oil Ratio Sensitivity Analysis

Now, we analyze the sensitivity with various boundary conditions. At first, we test with the 1D homogeneous model by comparing the analytical sensitivity with numerical sensitivity. The detail properties of the model are described in Table 4.1 and fluid properties are shown in Figure 4.1. The initial pressure is 4,477 psi and the bubble point pressure is 4,400 psi. The gas phase exists in the reservoir after production starts. Oyerinde et al. (2009) verified that the divergence of flux term in Eq. 4.5 tend to dominate at early times and the fractional flow term dominates when the flow is fully developed. Here, we test the cases after water breakthrough. Additional analyses are conducted in Appendix A.

Table 4.1: General parameters of 1D model for GOR sensitivity analysis	
Parameters	Input Values
Grid number	(nx,ny,nz) = (100,1,1)
DX	10 [ft]
DY	10 [ft]
DZ	10 [ft]
Porosity	0.3
Permeability	50 [md]
Rock compressibility	3.6 E-06 [1/psi]
Oil density	32.0 [lb/cf]
Water density	60.11 [lb/cf]
Gas density	0.1062 [lb/cf]
Water viscosity	0.65 [cp]
Water formation volume factor	1.04 [rb/stb]
Injector location	(1,1,1)
Producer location	(100,1,1)

***Values for water and rock are at the reference pressure of 1990.3 psi**
***Density is surface condition (14.7 psi)**

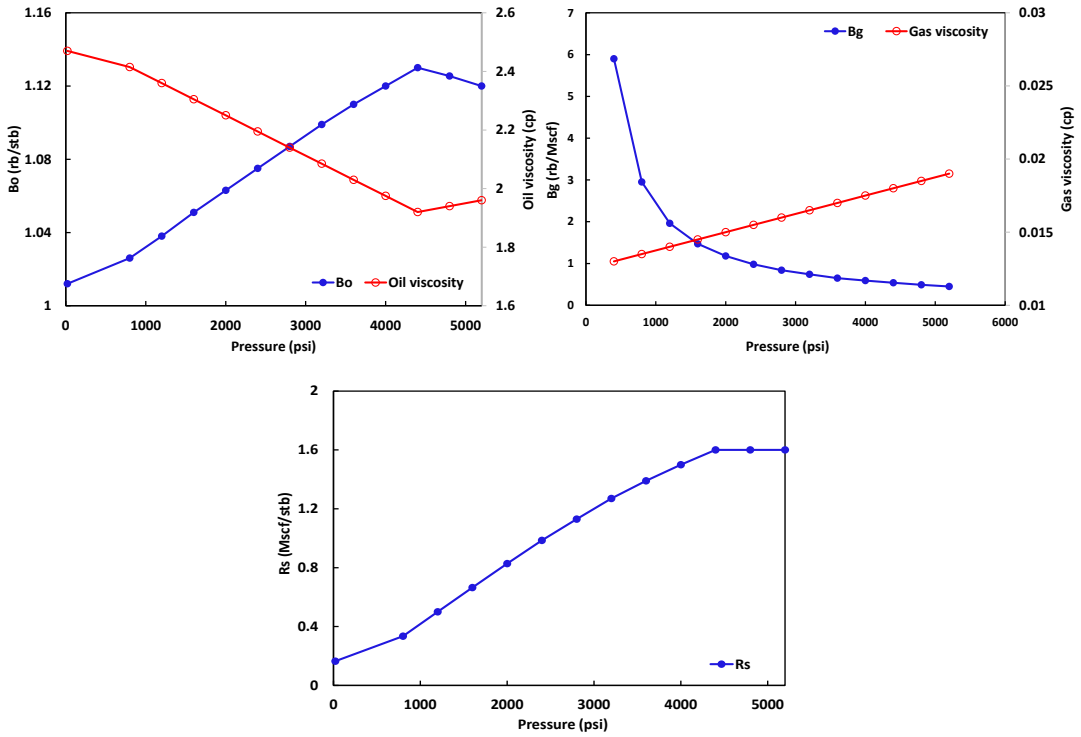

Figure 4.1 Fluid properties for 1D GOR sensitivity analysis.

The numerical perturbation method is calculated by 3 steps. First, we run a simulation with an original permeability and measure the time of the specific GOR (2.0 Mscf/stb for example). Second, we change the permeability by 5% at each cell and measure the arrival time of GOR at 2.0. Because the production response is discontinuous by time step size, we interpolate linearly between the data points to find the exact time. Finally, we calculate the sensitivity of dt/dk and then continue this whole process to the entire grid blocks.

1D: BHP-BHP constraint

The first case is both wells have pressure constraints. The injector is constrained at 5,000 psi and the producer is controlled at 3,800 psi. Figure 4.2 shows the sensitivity of numerical perturbation and the analytical sensitivity based on streamline. As gas phase is released around grid 78, sensitivities have small fluctuation. They show good agreement in this boundary condition.

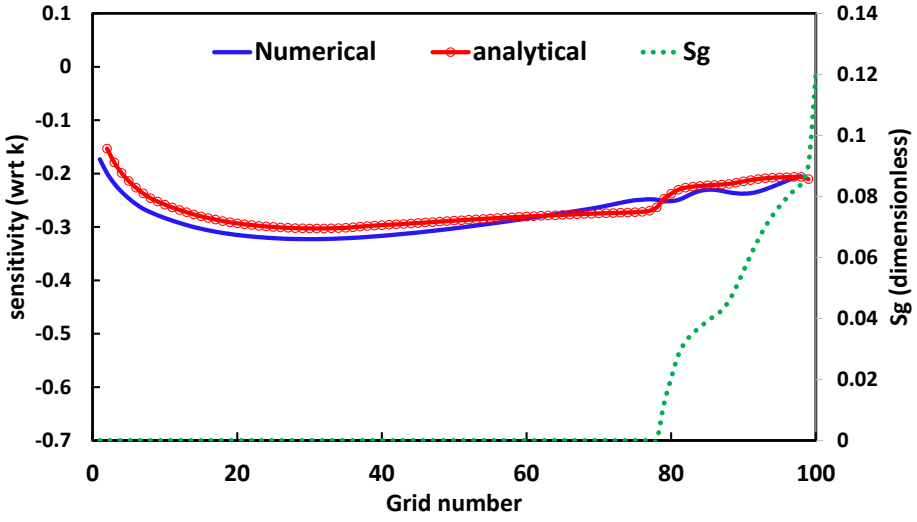

Figure 4.2 GOR sensitivity comparison between numerical and analytical in BHP-BHP constraint case.

1D: BHP-Rate constraint

The well constraints are changed in this case. The injector has a pressure constraint (4800 psi) but the producer is constrained by rate (3.0 rb/day). Although the magnitude of sensitivity is different, numerical and analytical values show a similar trend in Figure 4.3. Particularly, the cells where the gas phase exists ($p_{cell} < p_{bhp}$) have a difference. The reason of the difference in this condition might be that the sensitivity formulation does not explicitly include the pressure term, though it is considered implicitly by the pre-factor in the formulation. However, we will show in the applications later that this approximation of sensitivity may be adequate to the practical history matching.

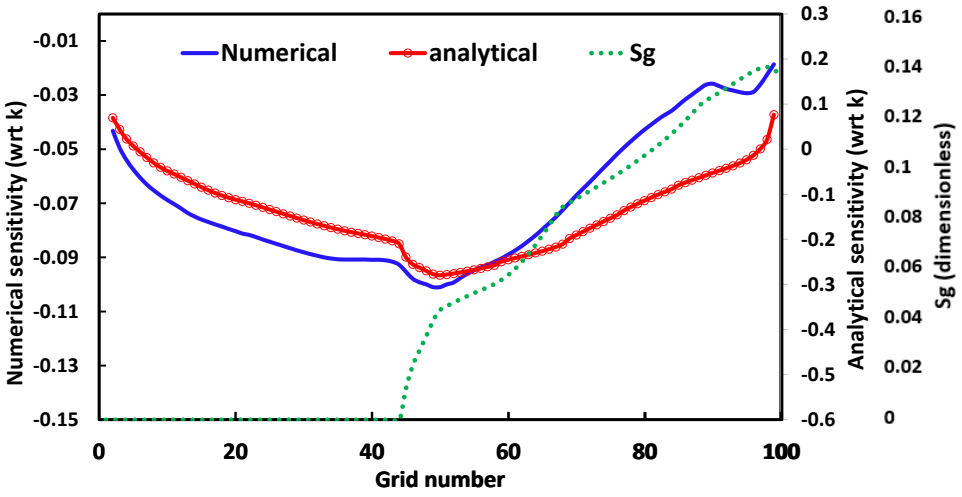

Figure 4.3 GOR sensitivity comparison between numerical and analytical in BHP-Rate constraint case.

2D: Rate-Rate constraint

Now, we test using a 2D homogeneous model with rate constraints for both wells. We simulate a water injection case in a quarter five-spot pattern. The detailed reservoir information is described in Table 4.2 and Figure 4.4. It starts with bubble-point pressure. As the pressure drops, solution gas comes out from the oil phase. We perturb 5% of permeability at each grid block and compute the partial derivative of the arrival time of a fixed gas-oil ratio value.

Table 4.2: General parameters of 2D model for GOR sensitivity analysis

Parameters	Input Values
Grid number	(nx,ny,nz) = (21,21,1)
DX	52.86 [ft]
DY	52.86 [ft]
DZ	37 [ft]
Porosity	0.1
Permeability	81.2 [md]
Rock compressibility	3.8 E-06 [1/psi]
Oil density	49.1 [lb/cf]
Water density	64.79 [lb/cf]
Gas density	0.065 [lb/cf]
Water viscosity	1.0 [cp]
Water formation volume factor	1.0 [rb/stb]
Initial reservoir pressure	3000 [psi]
Injector location	(21,21,1)
Producer location	(1,1,1)
Injection rate	500 [rb/day]
Production rate	625 [rb/day]

***Values for water and rock are at the reference pressure of 2200 psi**
***Density is surface condition (14.7 psi)**

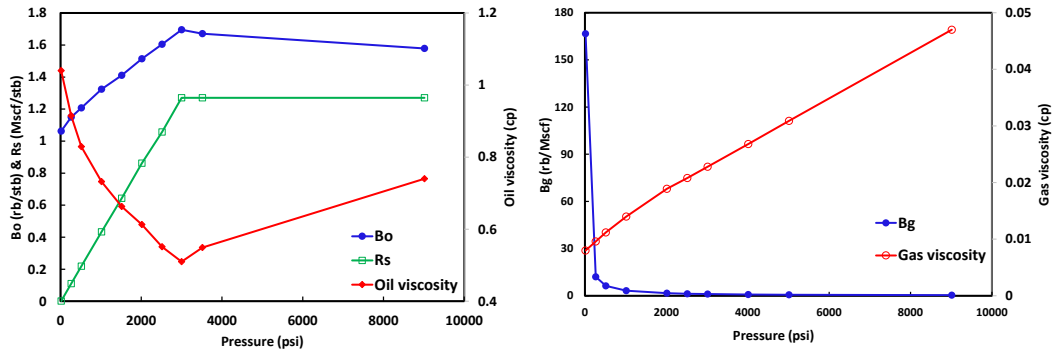

(a) Oil and gas PVT properties

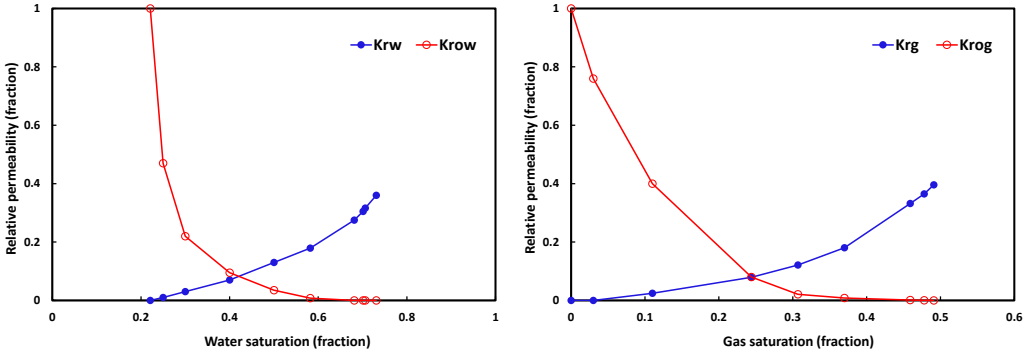

(b) Three-phase relative permeability data

Figure 4.4 Fluid properties (a) and relative permeability data (b) of 2D model for GOR sensitivity analysis.

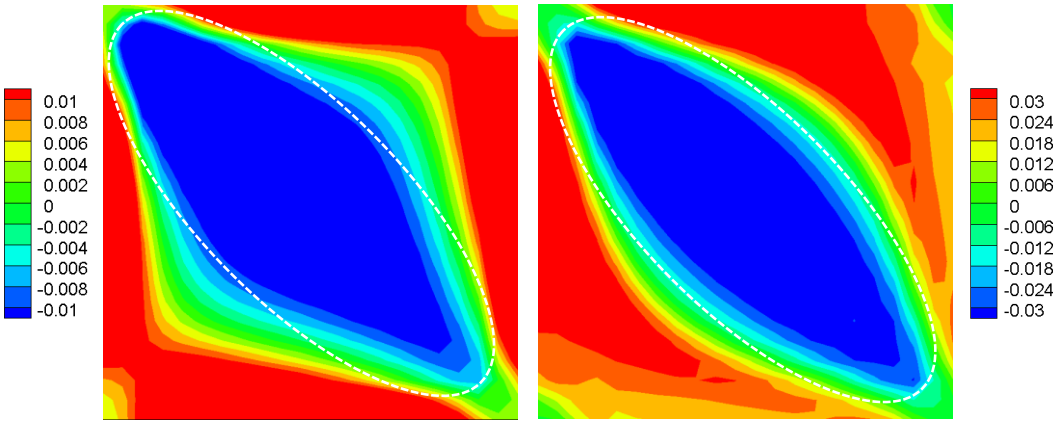

Figure 4.5 Comparison of numerical (left) and analytical sensitivity (right) in a quarter-five spot pattern.

Figure 4.5 shows the numerical (left) and the analytical (right) gas-oil ratio sensitivity. We obtain good agreement between numerical and analytical arrival time sensitivity using Eq. 4.5. The location and area of the negative and positive sensitivities are also in close agreement. The shape is slightly different since the analytical sensitivity is calculated along the streamlines. Thus, the shape of the analytical sensitivity is in accordance with streamline trajectory. The other reason of this differences is because of the inherent approximations in the analytical computation, particularly the assumption of streamline-based sensitivity that the streamlines do not shift because of small perturbation in grid properties. In spite of the approximations, the overall size of the main negative part (blue) inside of the white dotted line is similar. The gas-oil ratio sensitivity at the injector area is slightly different from the producer area (non-symmetric). The analytical sensitivity also captures the differences.

4.4 Application for History Matching

We will show several applications from synthetic to the field model that have a water injector or gas injector. These confirm the applicability of our approach to the three-phase history matching. In addition, by comparing two cases that are with and without a gas-oil ratio term in the objective function, we verify the effectiveness of our approach on the three phase flow model.

4.4.1 Two-dimensional Synthetic Model

The synthetic case is a two-dimensional three-phase reservoir model with a five spot pattern. The model of initial and reference permeability is the same as the one we used in chapter III (Figure 3.7 and Figure 3.10). PVT properties are in Figure 4.4. Due to BHP-Rate constraints, the reservoir has a continual pressure drop and more free gas in the reservoir in the vicinity of the producers.

Table 4.3: General parameters of 2D model for history matching

Parameters	Input Values
Grid number	(nx,ny,nz) = (50,50,1)
DX	30 [ft]
DY	30 [ft]
DZ	10 [ft]
Porosity	0.15
Rock compressibility	3.8 E-06 [1/psi]
Oil density	49.1 [lb/cf]
Water density	64.79 [lb/cf]
Gas density	0.065 [lb/cf]
Water viscosity	1.0 [cp]
Water formation volume factor	1.0 [rb/stb]
Initial reservoir pressure	3000 [psi]
Injection constrain	3200 [psi]
Production constrain	200 [rb/day]

***Values for water and rock are at the reference pressure of 3000 psi**
***Density is surface condition (14.7 psi)**

Case 1: Three-phase model with water injector

The previous approach by Cheng et al. (2007) and Oyerine et al. (2009) for the three-phase flow model matches water-cut and gas-oil ratio with an assumption that pressure data was matched reasonably by a pre-processing. However, the primary objective in our approach is reproducing the water-cut, gas-oil ratio, and bottom-hole pressure responses simultaneously by calibrating the permeability field.

The first case has a water injector at the center of reservoir, and only dissolved gas exists initially. Figure 4.6 shows the reduction of data misfit through 15 iterations. Three objectives are decreased simultaneously. Although the gas-oil ratio sensitivity is an approximation, it works properly for the three-phase history matching.

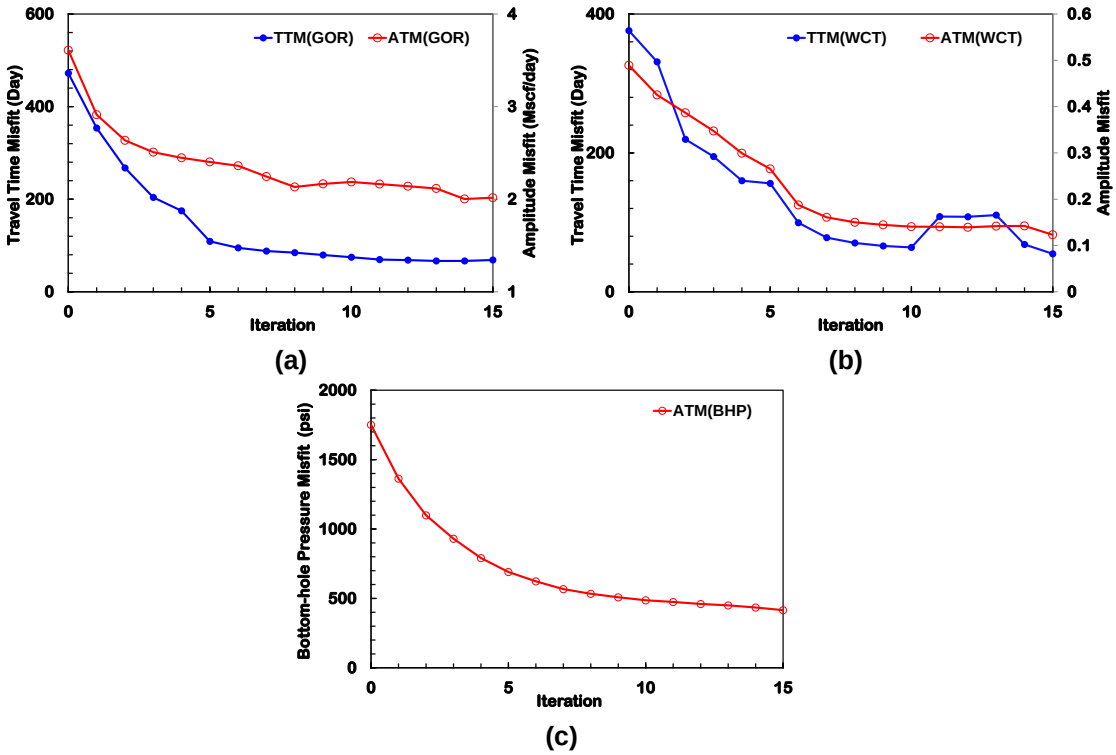

Figure 4.6 Convergence of the objective function for (a) GOR, (b) WCT, and (c) BHP for water injection case.

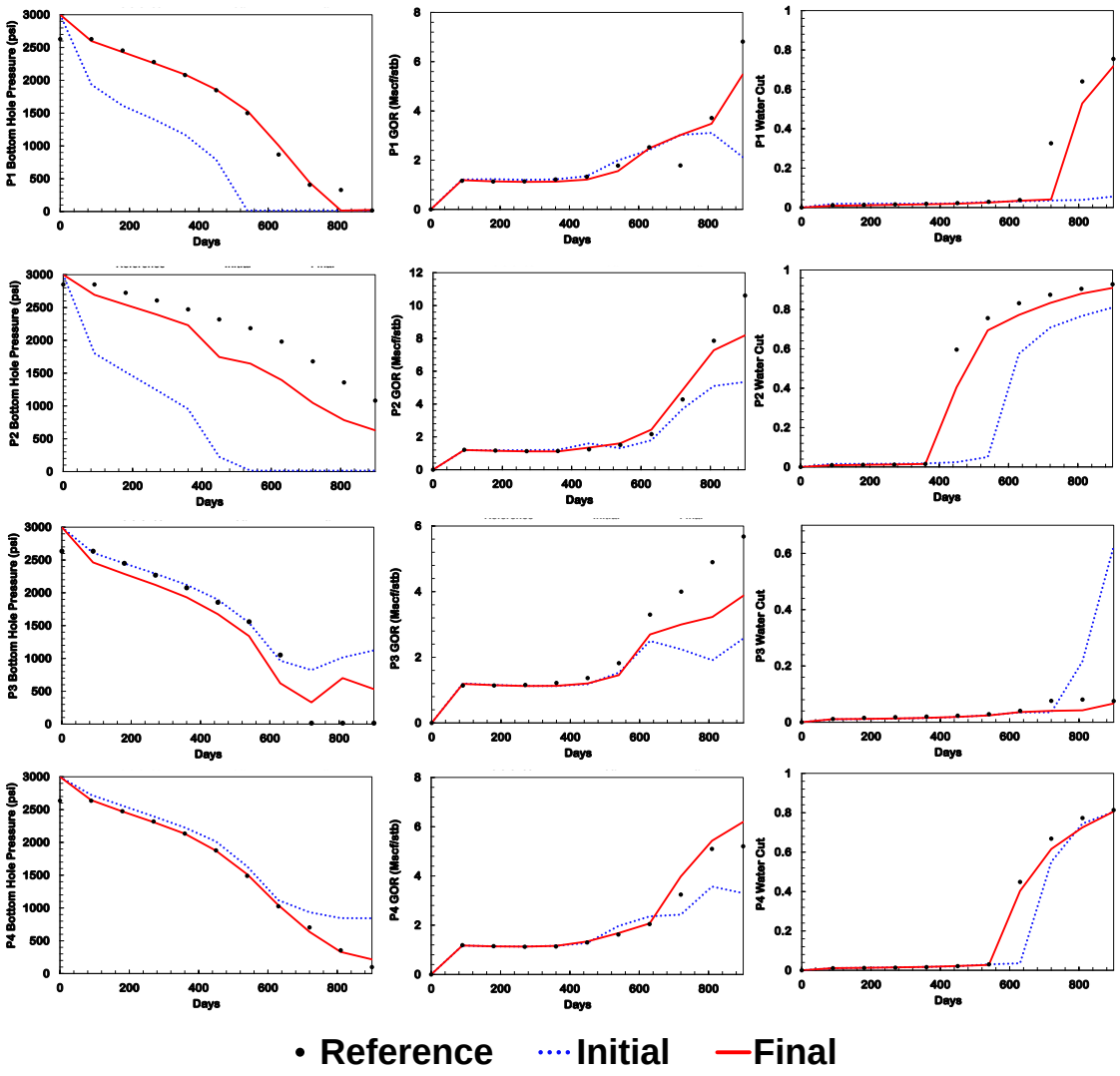

Figure 4.7 BHP (1st column), GOR (2nd column), and WCT (3rd column) of four procuers (by each row) corresponding to the reference, initial and calibrated model.

Figure 4.7 shows well responses of four producers. Water phase has weak dependence on the pressure; water-cut was usually well matched in previous applications. However, gas phase properties (solution gas-oil ratio, gas formation volume factor) are very sensitive to the pressure. Thus, integration of pressure and gas phase flow data should be considered

simultaneously. Our approach here seems to successfully reproduce the three-phase flow well responses.

Case 2: Three-phase model with gas injector

In this case, we use the same model but replace the water injector with a gas injector. The reservoir has not only dissolved gas, but also free gas from a gas injector. This case has very limited water production which is not considered; our objective is matching gas-oil ratio and pressure together. Figure 4.8 shows the convergence of 10 iterations. As we expected, the data misfits are continually reduced, and the final misfit is less than 20% of initial one. Well responses after history matching (Figure 4.9) show good agreement with the historical data. Therefore, the Eq. 4.5 is also applicable to the gas injection case.

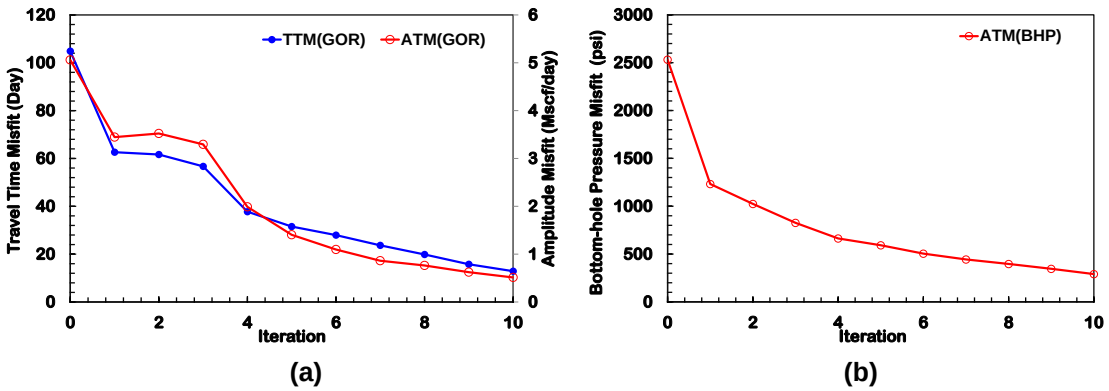

Figure 4.8 Convergence of the objective function for (a) GOR and (b) BHP for gas injection case.

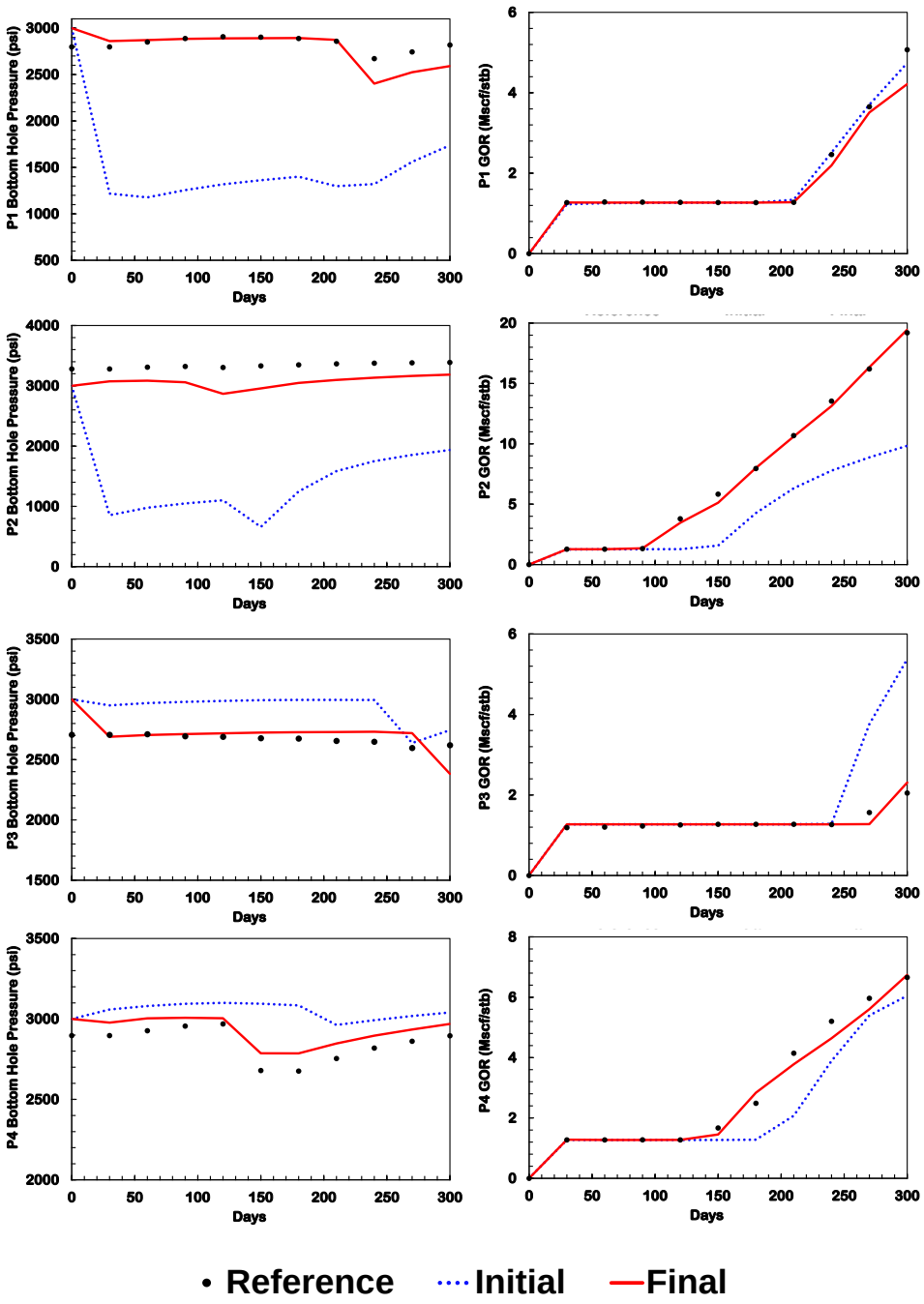

Figure 4.9 BHP (1st column) and GOR (2nd column) of four procuers (by each row) corresponding to the reference, initial, and calibrated model in gas injection case.

4.4.2 Three-dimensional Three-phase Field Scale Model

In this section, we demonstrate the feasibility of our approach for field studies by application to the three-dimensional three-phase field-scale models (SPE9 and modified Brugge benchmark model).

Case 1: SPE 9

The first field-scale model is a slightly modified version of the SPE 9 comparative study (Killough et al. 1995). This study investigates a waterflood in a dipping reservoir with natural water support from an aquifer at a bottom part. The reservoir has 24x25x15 mesh with rectangular coordinates (Figure 4.10). The grid blocks in both X and Y directions are 300 feet and cell (1,1,1) is at a depth of 900 feet subsea. The remaining cells dip in the X direction at an angle of 10 degrees. The detailed reservoir properties such as porosity and permeability can be found in the paper by Killough (1995).

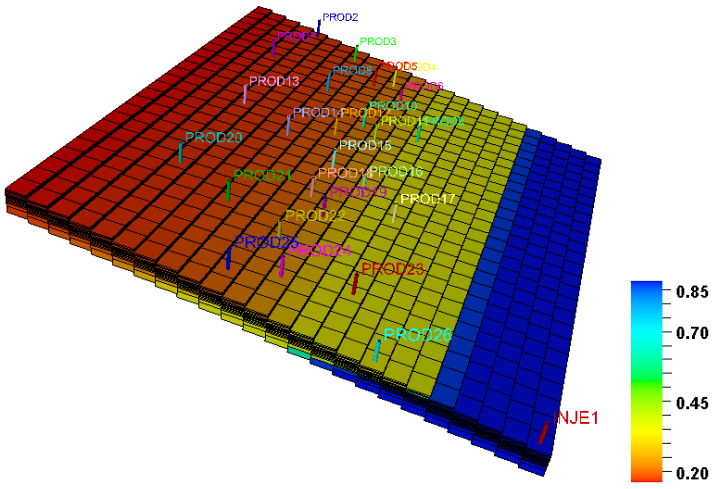

Figure 4.10 Modified SPE9 model with water saturation at 900 days.

The solution gas-oil ratio, gas and oil formation volume factors, and relative permeabilities are the same as those provided for the comparative study. The initial pressure at 9,035 feet is 3,600 psi and there is no free gas initially. The oil/water contact is 9,950 feet. After 900 days of production, there is considerable free-gas saturation in the reservoir. Figure 4.11 is the gas phase streamline at three different time steps. It clearly shows the gas phase comes out from the right top area (the farthest point from the injector) as pressure depleted. After 900 days production, most of the area has the gas phase except for an aquifer part under 9,950 feet.

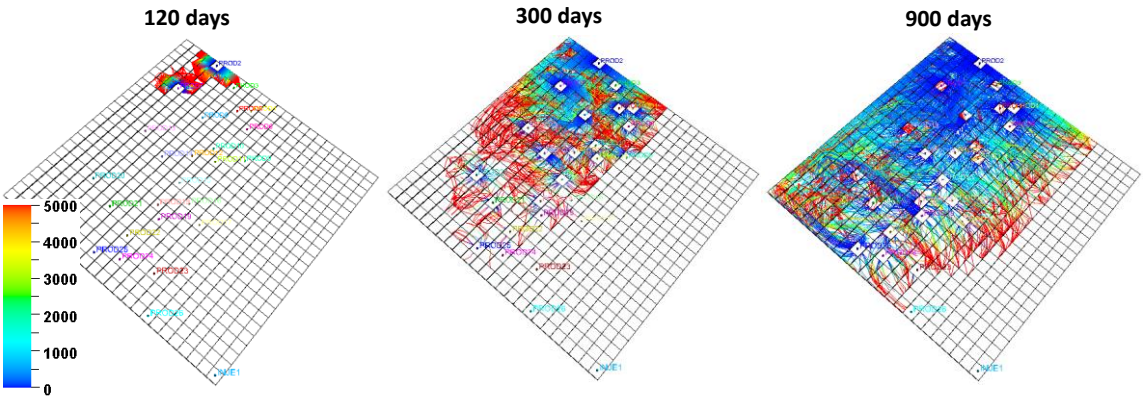

Figure 4.11 Gas phase streamlines at three time steps with TOF from producer along the streamlines.

In this application, the original permeability of the comparative study is used for a reference permeability model to generate production histories (flow rate and pressure data). An initial permeability distribution, the starting point of history matching, is generated geostatistically as random realization of a sequential Gaussian simulation using

the value at the well locations of original model. There are 25 producers and one injector as shown in Figure 4.10. The injector has completions from layer 1 through 11. Most of the producers except for 9, 17, 23, and 26 are completed from layer 1 to 13. The producers 9, 17, 23, and 26 are completed from layer 1 through 5 to avoid completions in the water leg.

In the previous section, we have analyzed the gas-oil ratio sensitivity. Although it has assumptions and approximates the sensitivity, it captures the overall trend of the numerical sensitivity. With the synthetic model, we have shown the applicability of the sensitivity to the three-phase inversion problem. Here, we verify the effectiveness of adding the gas-oil ratio term in the history matching by comparing two cases.

- The 1st case is matching the water-cut and bottom-hole pressure data that we did in chapter III. Because the gas phase is sensitive to the pressure, this case shows the impact of pressure matching to the gas-oil ratio matching (blue line in Figure 4.12).
- The 2nd case is matching the water-cut, bottom-hole pressure, and gas-oil ratio together. It can show the effectiveness of gas-oil ratio sensitivity in a history matching process (red line in Figure 4.12).

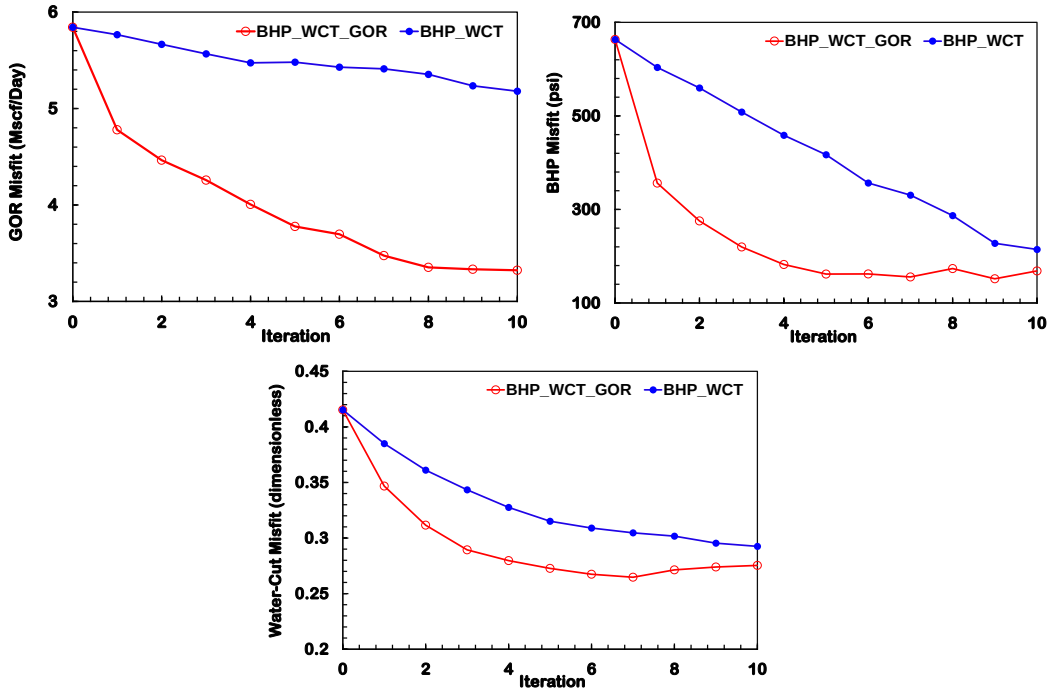

Figure 4.12 Convergence of the objective function of two cases for GOR, BHP, and WCT in SPE 9 model.

The data misfit convergence demonstrates significant improvement of the gas-oil ratio matching when we add the gas phase sensitivity (Figure 4.12). Although the first case shows a reduction of data misfits, the second case has a much smaller gas-oil ratio misfit as well as additional reductions of bottom-hole pressure and water-cut data misfit compared to the first case. The calibrated model in the 2nd case can be closer to the true solution when adding the gas phase term. Thus, all objectives have a smaller value and show a faster convergence. Figure 4.13 shows well responses of two cases after history matching. Most well responses show better matching when we add the gas-oil ratio sensitivity. This comparison indicates that the streamline-based analytic sensitivity can provide reasonable approximations for the purpose of production history matching.

Moreover, it shows that the history matching with a gas-oil ratio term in the three-phase flow model is essential and our approach is applicable to the field-scale model.

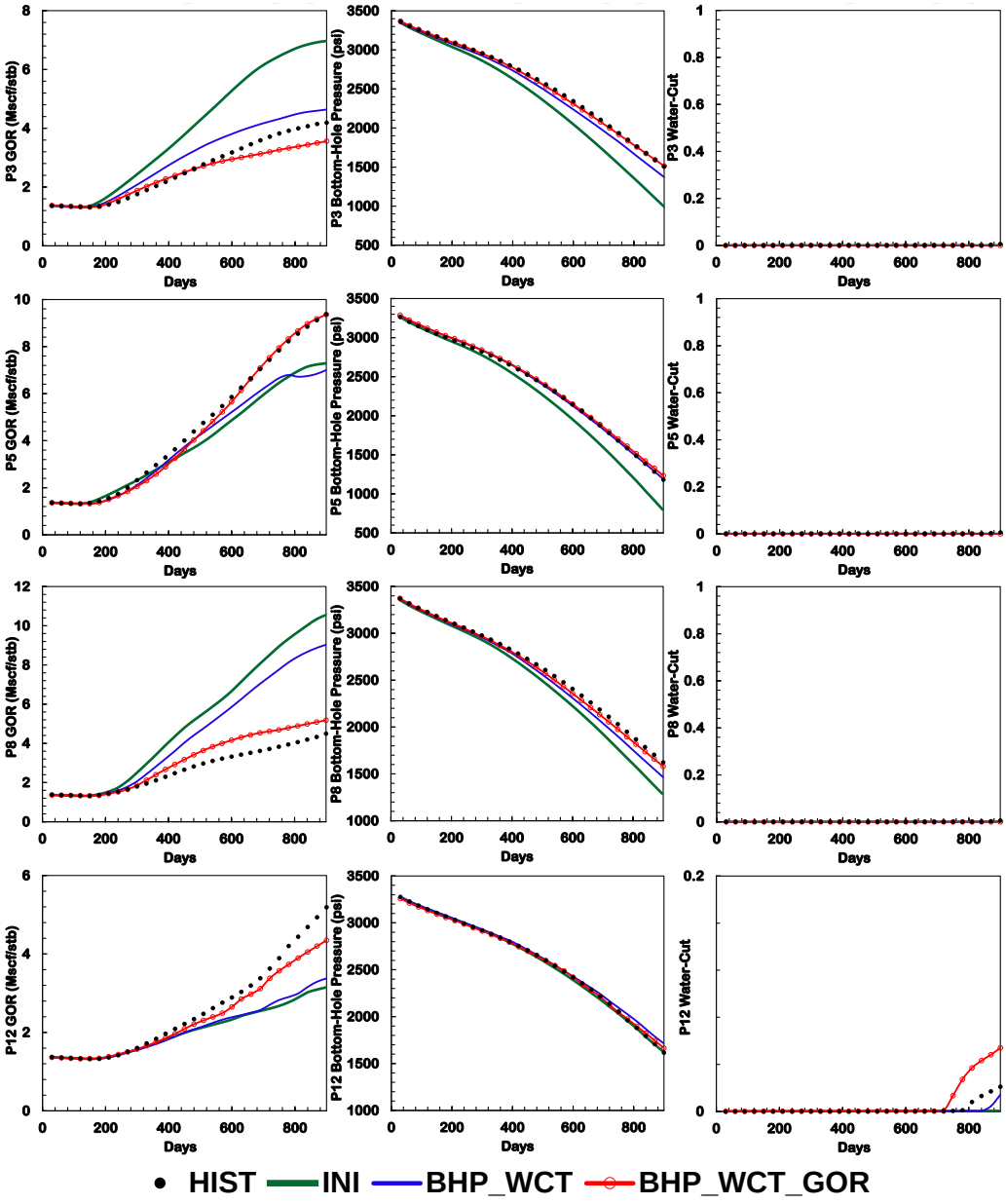

Figure 4.13 GOR (1st column), BHP (2nd column), and WCT (3rd column) of produers (by each row) corresponding to the reference, initial, calibrated model for BHP-WCT matching, and calibrated model for GOR-BHP-WCT matching.

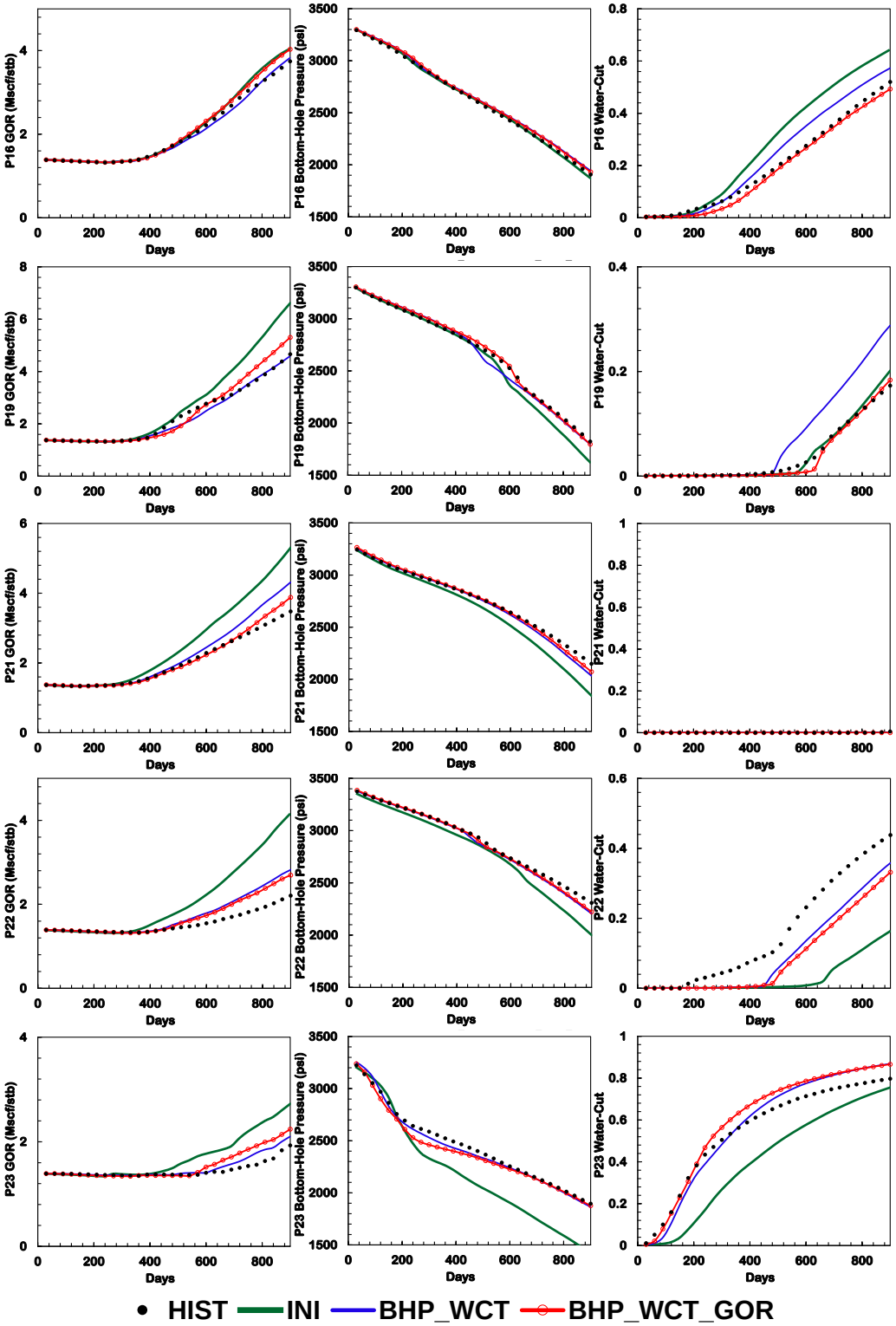

Figure 4.13 continued.

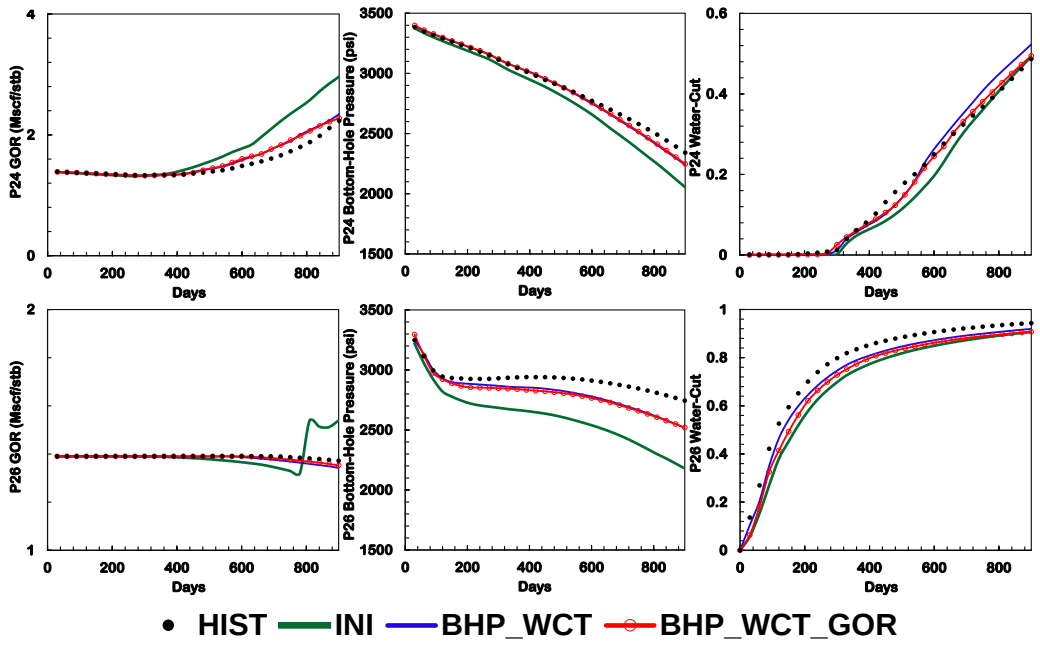

Figure 4.13 continued.

Because we have access to the reference permeability field in the SPE9 case, we can conduct more detailed analyses on the results. First, we check the gas phase streamlines to the producer in Figure 4.14. They have different streamline trajectories and TOF values between the initial and reference models. However, the calibrated models show good agreement in the cover area of gas phase streamline, which is where the gas phase exists. Thus, it makes good gas-oil ratio matching of well responses shown in Figure 4.13. For example, P3 and P21 have smaller areas covered by streamlines after inversion, thus the gas-oil ratio is decreased and closer to the reference data. On the contrary, P5 streamlines stretch out over a broad area and the gas-oil ratio response is increased.

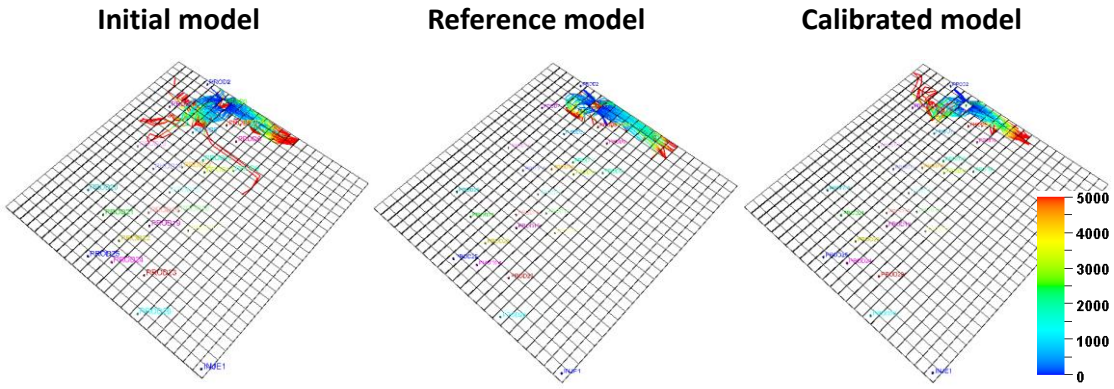

(a) well P3

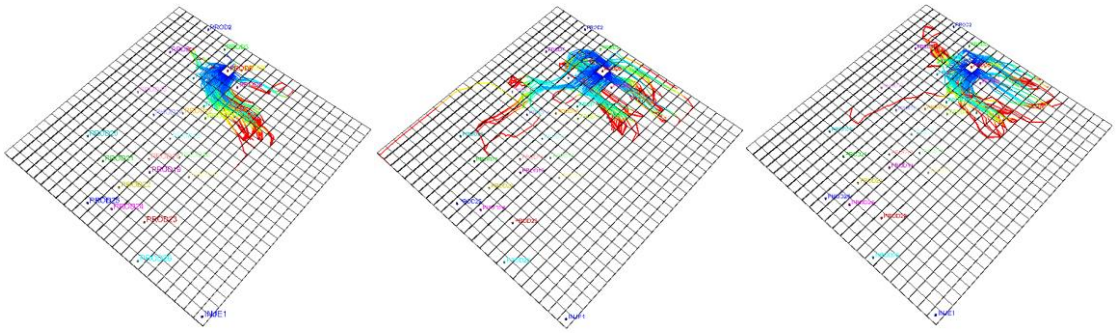

(b) well P5

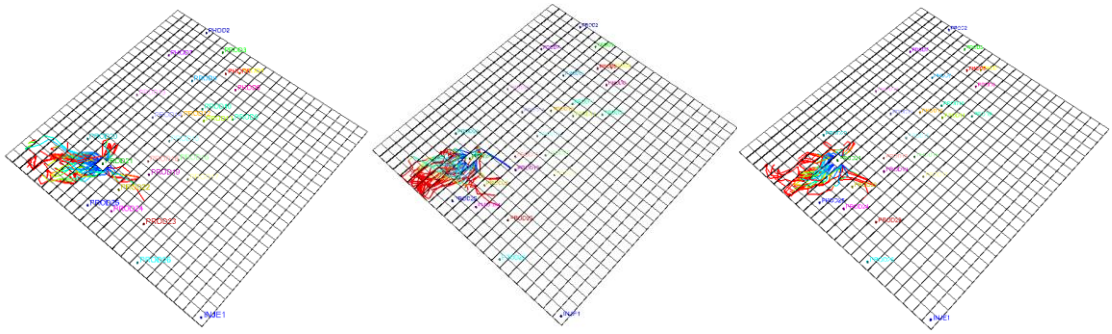

(c) well P21

Figure 4.14 Gas phase streamlines of selected three producers based on initial, referecne, and calibrate model.

Second, we compare the permeability distribution between reference, initial, and calibrated models in Figure 4.15. We select a total of 6 layers; we take two layers from the top, middle, and bottom parts. Based on the permeability field in Figure 4.15, it is difficult to observe the changes made to the initial model, because the inversion algorithm is aimed to preserve the geologic model using penalty terms in Eq. 3.14. In Figure 4.16, we have shown the differences that are change needed (top row) and change made (bottom row) to examine if the change is consistent with the reference model. Change made cannot capture all the differences in change needed. However, our inversion algorithm makes consistent permeability changes in block dotted ellipse areas.

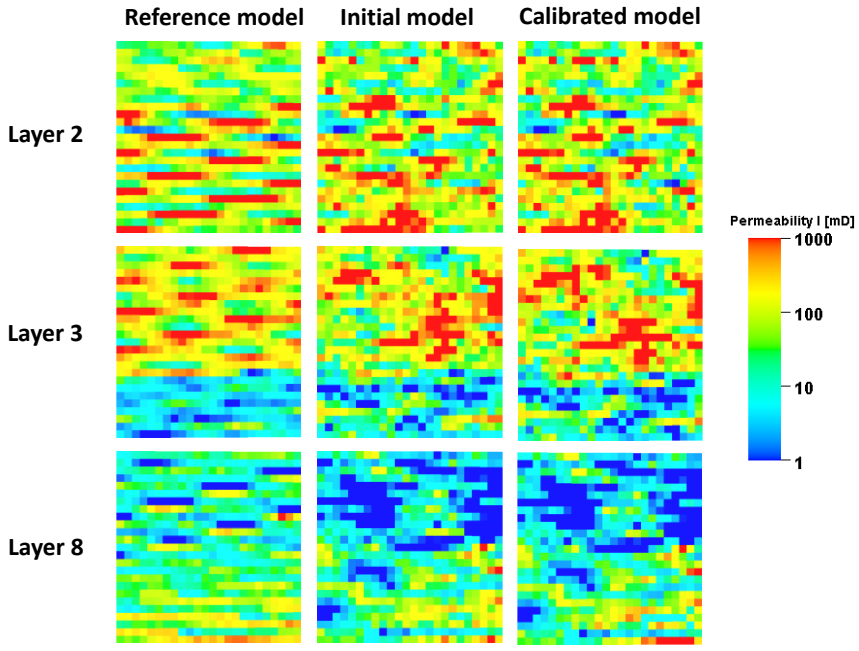

Figure 4.15 Permeability distribution of six layers for reference (1st column), initial (2nd column), and calibrated model (3rd column).

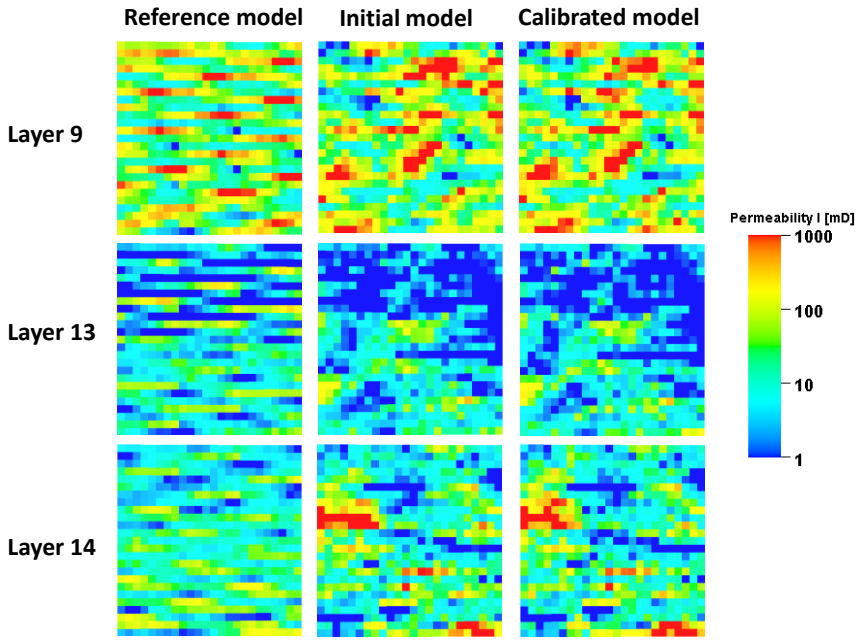

Figure 4.15 continued.

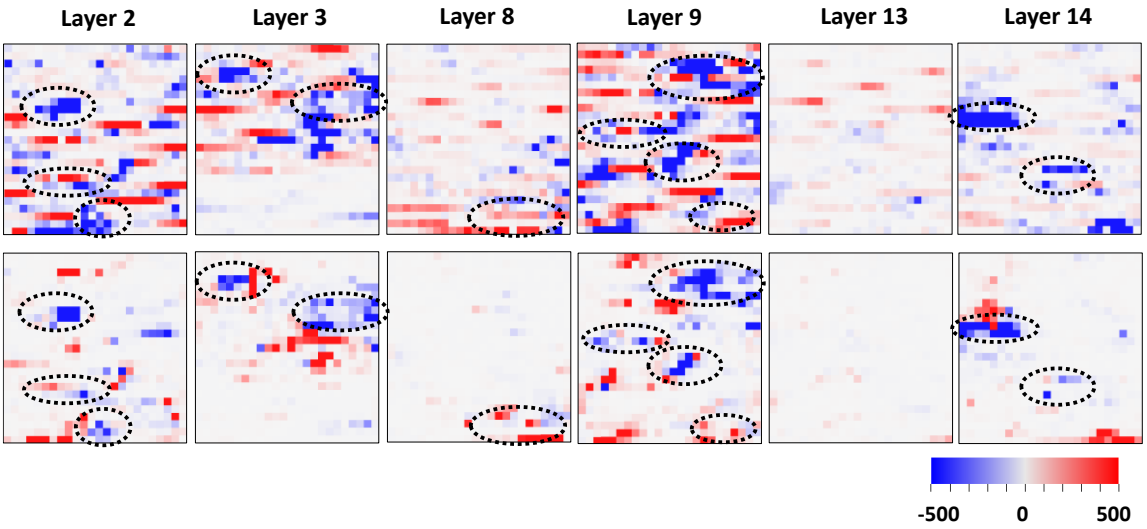

Figure 4.16 Change needed (1st row) and change made (2nd row) after history matching for SPE9 model.

The three-phase history matching with the streamline-based sensitivity works well for calibrating the permeability field of SPE9. Figure 4.12 through Figure 4.14 show that the inversion algorithm with a gas-oil ratio sensitivity successfully reproduces the reservoir responses. However, as might be expected, the permeability distribution has discrepancies between the reference model and the calibrated one. It is due to the combination of several issues. First, this algorithm preserves the initial model. Second, the production data for each well is the sum of the flow rate from each completion. Pressure data is measured at one point of the well trajectory. Therefore, we need additional information like the distributed production data (layer resolution) (Kam and Datta-Gupta, 2014) or PLT (production logging tool) data. If seismic data is available, we are able to capture the high resolution reservoir model (Watanabe et al. 2013).

Case 2: Modified Brugge benchmark model

The original Brugge model we have used in chapter II and chapter III is a two-phase system. For the three-phase history matching test, we modify the Brugge model. Figure 4.17 is PVT data and Figure 4.18 is relative permeability we used for the modified Brugge model.

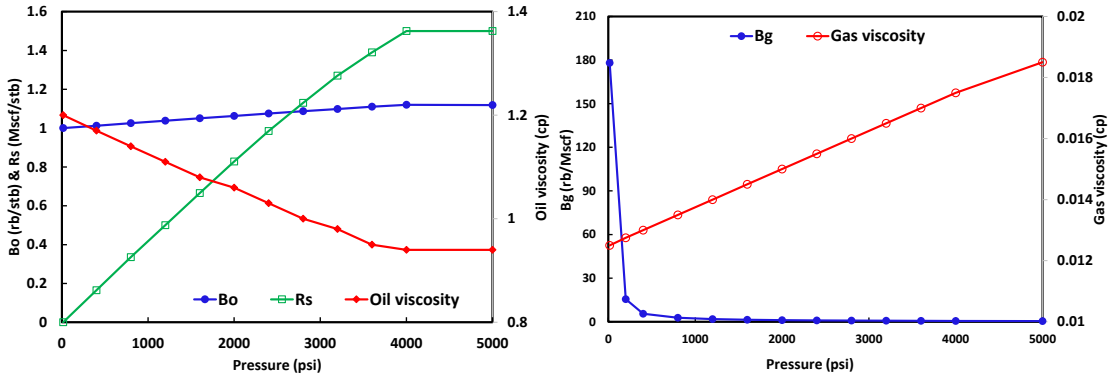

Figure 4.17 Fluid properties for the modified Brugge benchmark model.

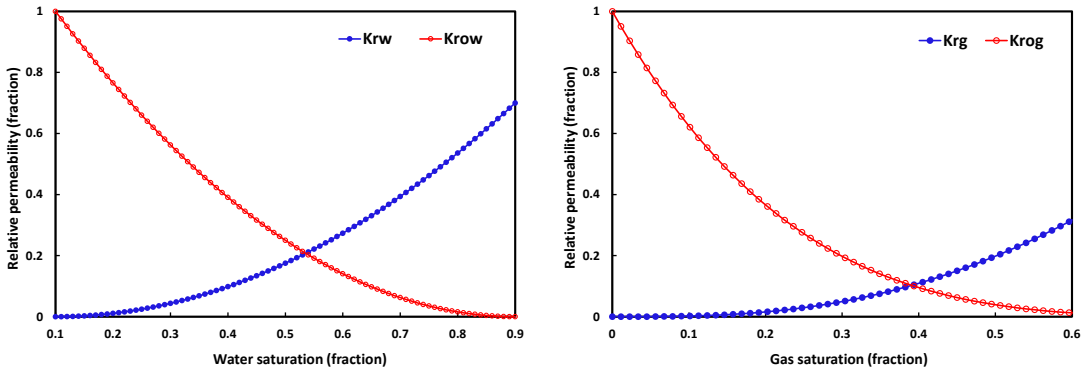

Figure 4.18 Relative permeability model for the modified Brugge benchmark model.

The model description is already shown in chapter II. Here, we selected two models for reference model (No. 103) to make three-phase production data (gas-oil ratio and water-cut) and bottom-hole pressure history. The initial model is realization no.1, that is, the start point of history matching. We changed the type of injector from water to gas to check the applicability of our approach to the field-scale gas injection model. Figure 4.19 shows the permeability distribution of the reference model, the initial model, and the calibrated model after 10 iterations.

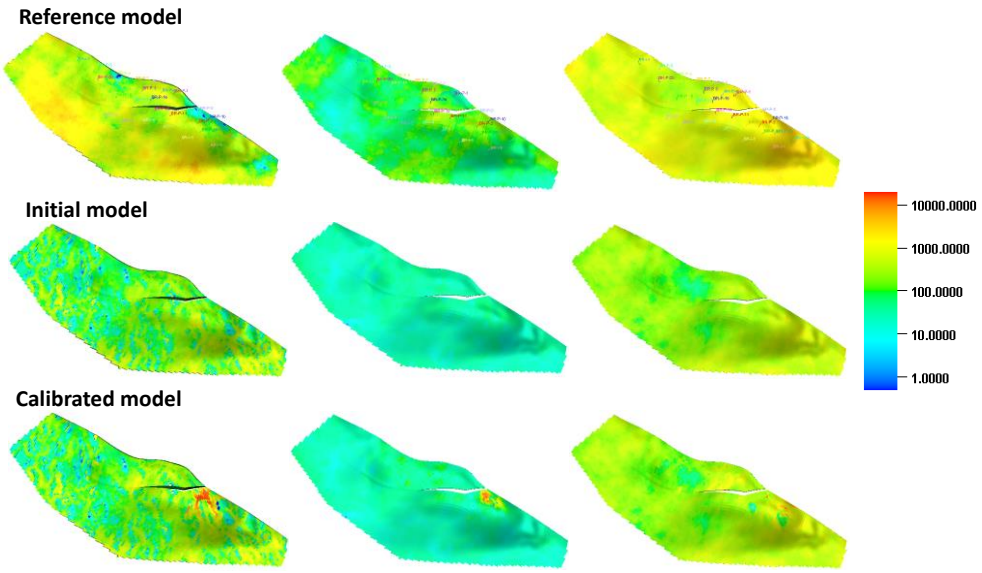

Figure 4.19 Permeability distribution of reference, initial, and calibrated model (by each row) for layer 1 (1st column), layer 4 (2nd column), and layer 7 (3rd column).

Figure 4.20 shows the convergence of data misfit during 10 iterations. Gas-oil ratio and water-cut misfit are reduced 50%, and bottom-hole pressure is decreased around 80% from the original misfit. Although the initial model is far from the reference model particularly the layer 1, the data misfits are successfully reduced. Well responses of ten selected

producers are shown in Figure 4.21. Most of the wells have good agreement with reference well responses. Thus, our approach is also applicable to the field-scale gas injection model for the three-phase history matching problem.

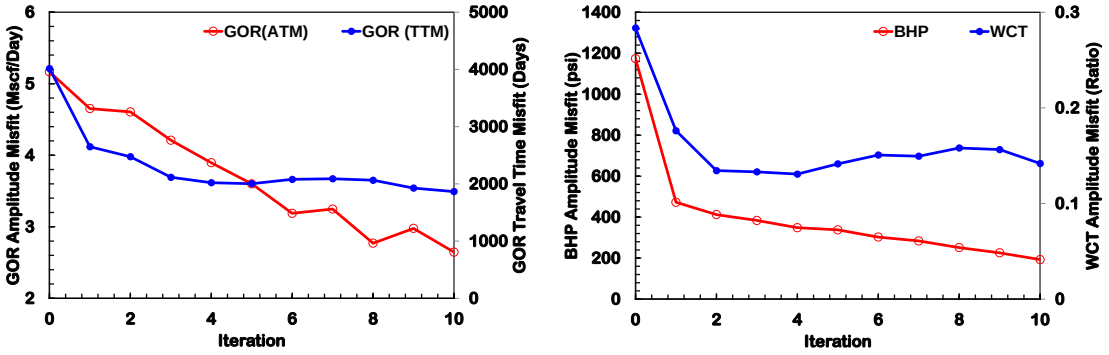

Figure 4.20 Convergence of objective function of GOR (left), BHP and WCT (right) for the three-phase modified Brugge benchmark model.

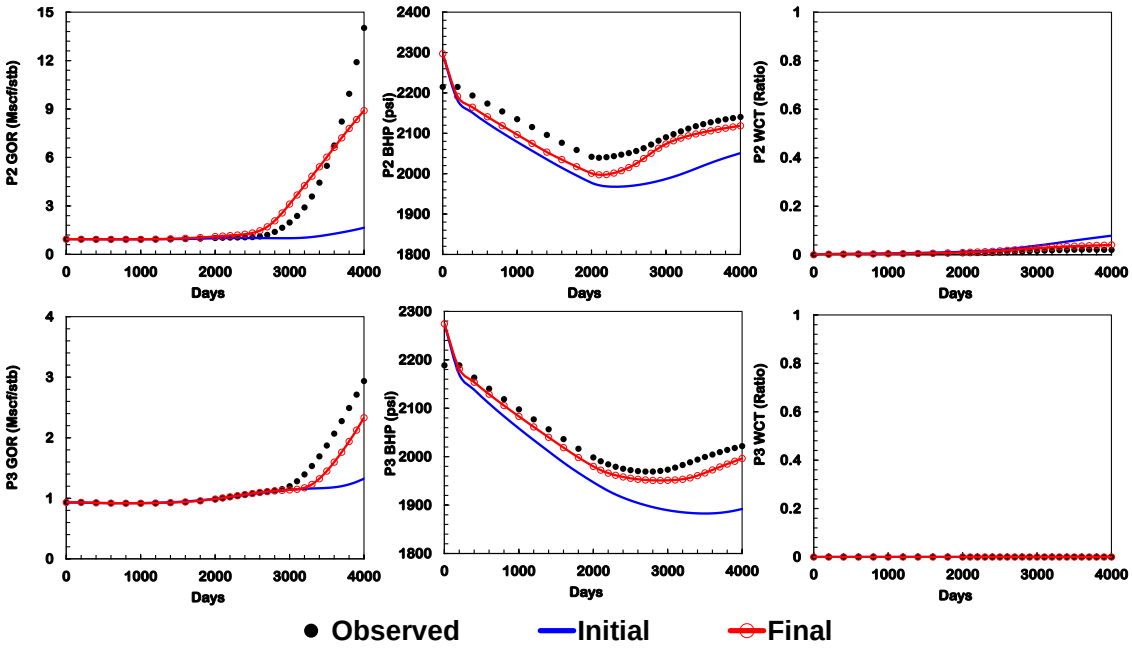

Figure 4.21 GOR (1st column), BHP (2nd column), and WCT (3rd column) of produers (by each row) corresponding to the reference, initial, and calibrated model.

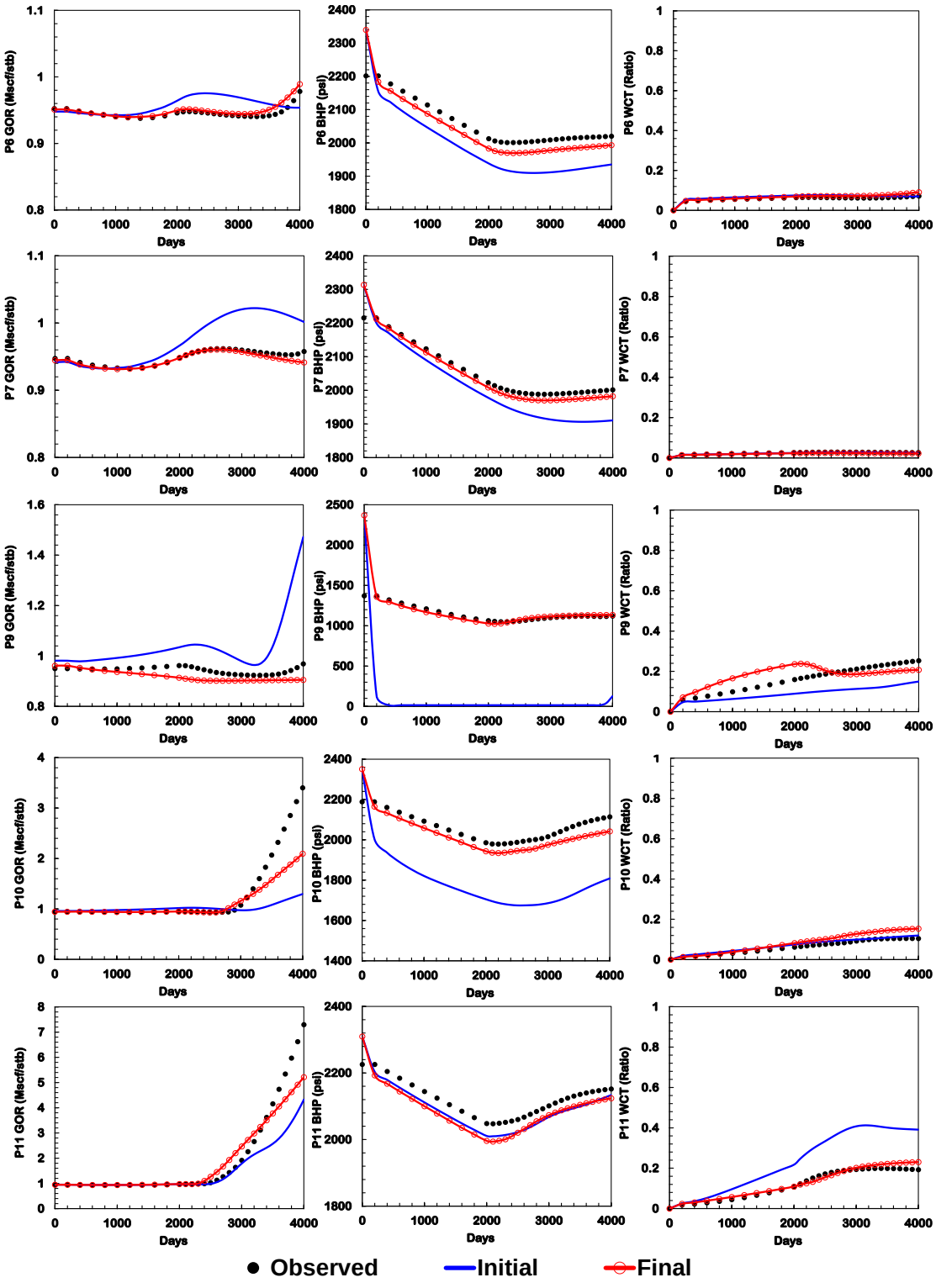

Figure 4.21 continued.

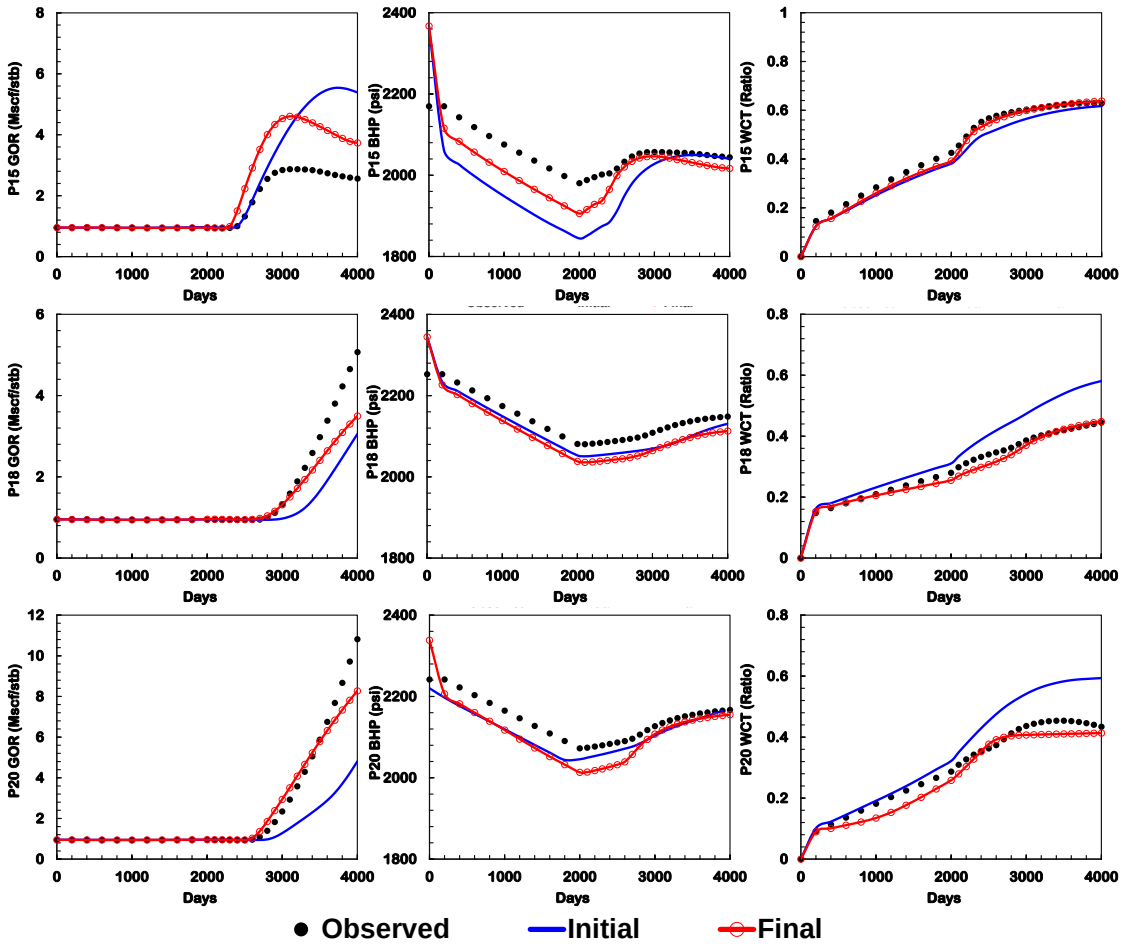

Figure 4.21 continued.

4.5 Multiscale History Matching Workflow for Three-phase Flow (Norne Field Application)

Initially, we apply our streamline-based joint inversion method to Norne field to match gas-oil ratio, bottom-hole pressure, and water-cut. As we have shown in chapter III, the streamline-based pressure and water-cut matching is applicable to the Norne reservoir model. However, we find issues in the application of the three-phase streamline-based workflow to Norne field as below.

- **Inapplicability of GTTI to the gas-oil ratio matching in Norne field**: We applied the GTTI method to the three-phase flow models in previous applications (SPE9 and modified Brugge model). They showed the effectiveness of our streamline-based approach. If the gas-oil ratio data has monotonic responses with small fluctuation, the GTTI approach is applicable because we can correctly calculate the maximum correlation between observed data and shifted simulation response. Although Oyerinde et al. (2009) applied GTTI and showed good matching of gas-oil ratio in the field case, the matching was available because the well response was simple and a monotonic trend. However, Norne field has a non-monotonic trend in gas-oil ratio data like Figure 4.22a and c. Thus, it is difficult to find the correct optimal shift time for the gas-oil ratio matching in Norne field.
- **Potential Conflict between objectives**: As we have seen in previous history matching results for the pressure and water-cut case in the Norne reservoir model, some wells show the conflict between objectives. For example, if one objective (pressure misfit) is decreased, the other one (water-cut misfit) is increased because

of changing reservoir permeability (E-4AH in Figure 3.28). The objectives we are using in the three-phase problem can be potentially conflicting. It will be explained in more details later.

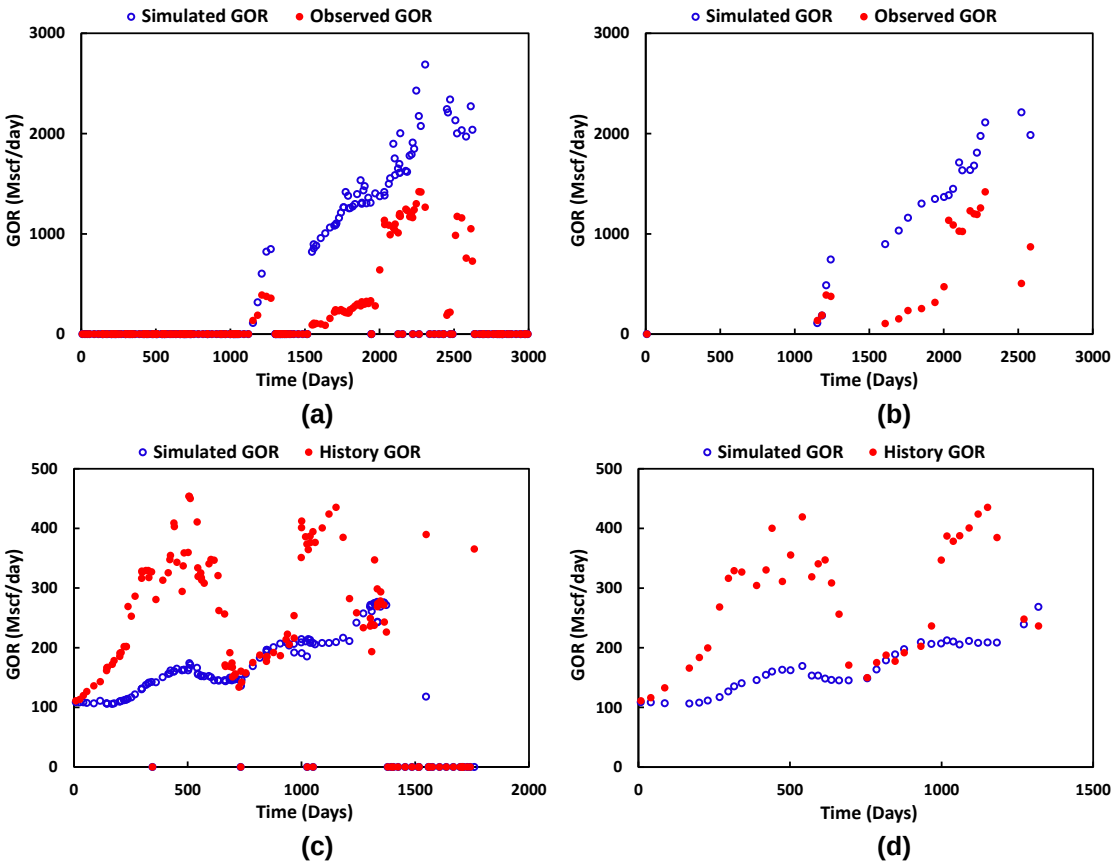

Figure 4.22 GOR responses before (a,c) and after (b,d) transformation for E-3AH (the first row) and D-1H (the second row).

To overcome the GTTI issue, we transform the production data and eliminate high frequency details in gas-oil ratio data. Rey et al. (2009) applied this approach to the water-cut matching for discontinuous and non-monotonic responses. Based on Eq. 4.6 we recalculate the gas-oil ratio response.

$$GOR_n = \frac{\Delta V_{gas}}{\int_t^{t+\Delta t_n} q_o \, dt} \tag{4. 6}$$

where n is number of data point, ΔV_{gas} is a fixed desired volume of gas, and Δt_n is production time for fixed gas volume. This transformation deletes high frequency responses, particularly the shut-in interval, and keeps a main trend, making it more amenable to calculate an optimal travel time in GTTI. For example, well response of E-3AH is more suitable for GTTI after transformation (Figure 4.22a and b). However, most of the well responses still have a non-monotonic trend and a primarily amplitude difference rather than travel time difference (Figure 4.22c and d). Therefore, most wells are unsuitable for applying GTTI to the gas-oil ratio matching in this model.

Finally, we suggest that the pareto-based method (Deb et al. 2002) be used for global matching at first, followed by streamline-based history matching. This is a similar workflow to the multiscale approach in chapter III. The pareto-based multi-objective genetic algorithm (MOGA) with GCT coefficient as parameter for history matching was presented by Park et al. (2013). This approach is well suited to minimize multiple objectives that are potentially conflicting to each other. MOGA is designed to find a set of solutions in the Pareto optimal front which can be useful for the uncertainty analysis. Watanabe et al. (2013) applied this approach to the Norne reservoir model to match seismic data and water-cut sequentially.

In this dissertation, our objective is calibrating pore volume and permeability multipliers globally using MOGA with GCT coefficient, followed by streamline-based permeability updating to match gas-oil ratio, bottom-hole pressure, and water-cut

simultaneously. Our proposed process is primarily focused on the well production data and keeping the matched responses in the global stage (large-scale calibration) by considering all three objectives simultaneously in the local calibration using streamline-based sensitivities.

4.5.1 Global History Matching with Pareto-based Method

Before we start the global history matching, we calibrate the water/oil contact (WOC) that can highly affect the water-cut magnitude. Norne field has total 5 equilibrium regions in Figure 4.23. Rwechungura et al. (2012) lowered the WOC for E-segment wells (3rd region), from 2618.0 m to 2648.2 m. We change two more WOC levels manually; this raises from 2692 m to 2658 m for the 1st region, and from 2693.3 m to 2688.3 m for the 5th region. (In this section, prior model in the results is the one after manual WOC calibration.)

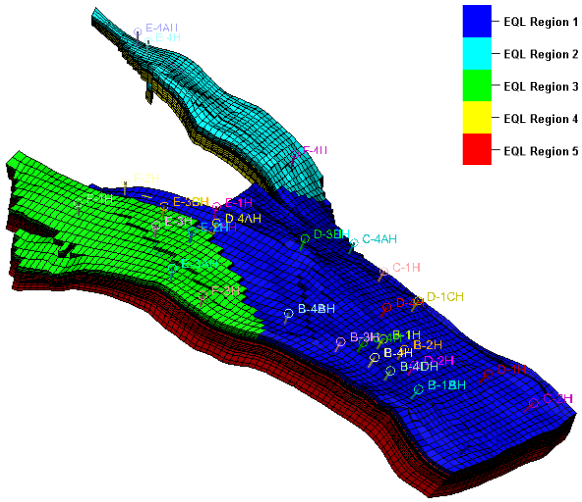

Figure 4.23 Equilibrium regions of Norne field.

Global history matching workflow is shown in Figure 4.24. We update the parameters at each stage using MOGA, a derivative-free method. The detailed algorithm is well described by Deb et al. (2002). Although it is computationally expensive, we do not require any sensitivity calculation. Particularly, we can avoid the gas-oil ratio matching issues when we apply the GTTI to this problem.

At first, we update pore volume (PORV) to match field total production (total field water production (FWPT) and total field gas production (FGPT)) and well bottom-hole pressure. Pore volume of the model was already calibrated to match a reservoir energy by the operator, so we reduced the range of PORV multiplier between 0.5 and 2.0. Our variable is 10 GCT coefficients per layer (total 220 coefficients). After pore volume calibration, we select one of the 1st rank candidates and move to the second stage: calibrating permeability multiplier with updated PORV multiplier. In the second step, we use 20 GCT coefficients (Figure 4.25) per layer (total 440 coefficients) to get higher resolution of reservoir model by matching well production responses (water-cut, gas-oil ratio, bottom-hole pressure). The multiplier fields of the first and second stage in global updating are shown in Figure 4.26.

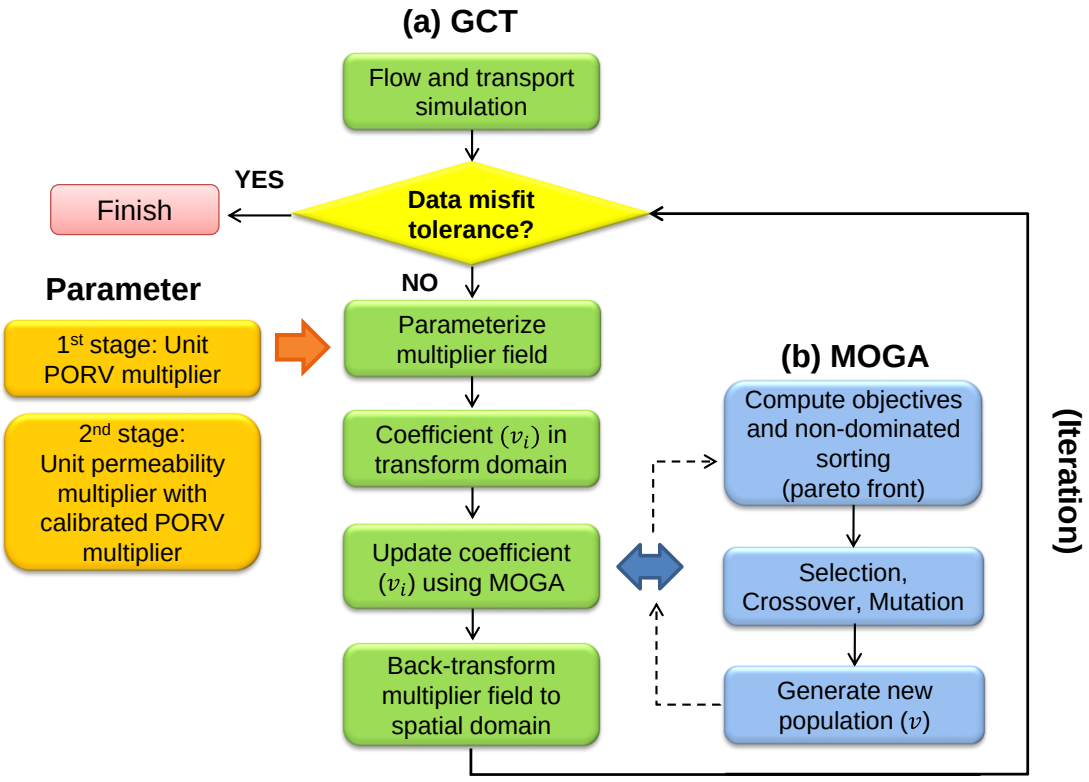

Figure 4.24 Workflow of global matching with MOGA in the Norne reservoir model.

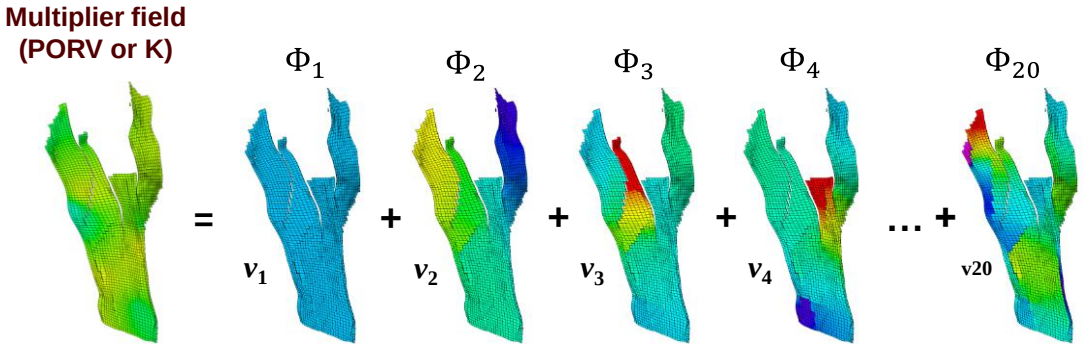

Figure 4.25 Parameterization of the multiplier field as the weighted linear combination of leading GCT basis.

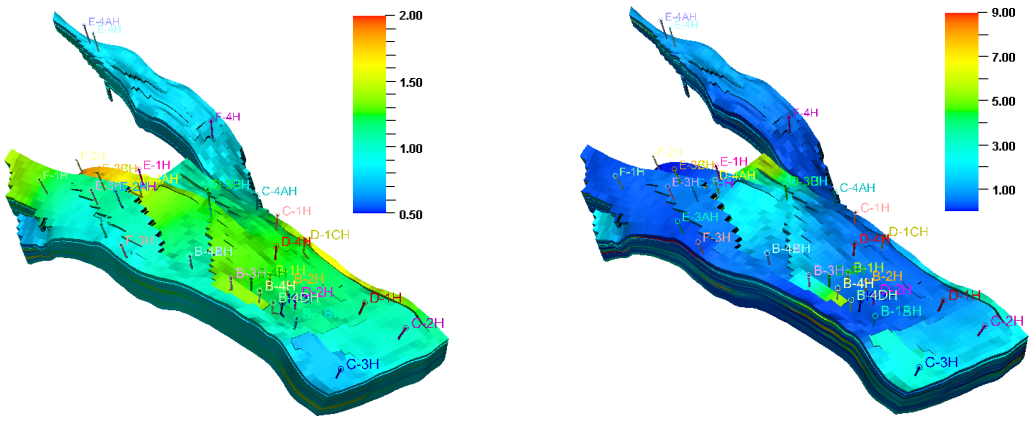

Figure 4.26 Final multiplier field of pore volume (left) and permeability (right) in global matching.

Figure 4.27 shows the population in the first and last generation at each stage. It demonstrates that MOGA makes diverse initial population around the prior model (red dot) at first. It also successfully reduces the misfit of field production rate in the first stage and well responses in the second stage. In addition, it makes the clear pareto-front between three different objectives and the majority of gas-oil ratio misfit reduction and bottom-hole pressure misfit reduction is achieved in the global phase.

The second reason we are using the MOGA in this problem is because both pore volume and permeability multiplier calibration may have conflicting issues. The misfit of bottom-hole pressure and water-cut makes a clear pareto-front (Figure 4.28) that indicates the nature of the trade-off between different objectives. It explains the reason of the final well responses of E-4AH in chapter III (Figure 3.28). Finally, we select one of the candidates in the pareto-front, and then we move to the local calibration based on streamline.

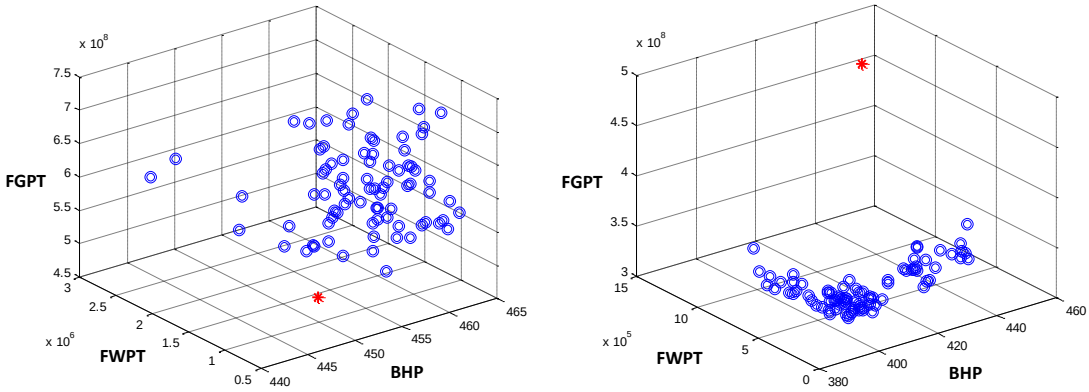

(a) (b)

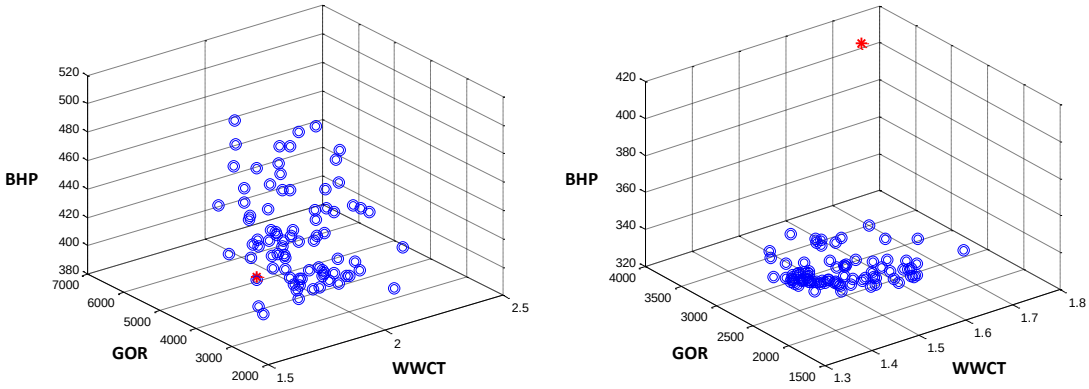

(c) (d)

Figure 4.27 MOGA results comparison between initial population (first column) and final population (second column) by calibration of pore volume multiplier (a and b) and permeability multiplier (c and d). Red dot is the initial model at each stage.

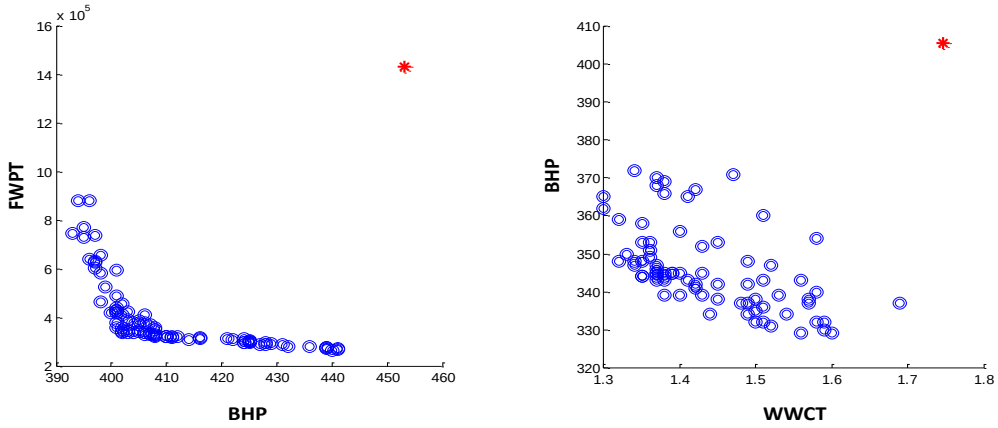

Figure 4.28 Pareto-front between FWPT and BHP (left), and between WCT and BHP (right).

4.5.2 Local History Matching with Streamline-based Method

Now, streamline-based inversion is applied to the calibration of cell by cell permeability. We start with the updated models in global stage and integrate well data such as gas-oil ratio, bottom-hole pressure, and water-cut data using sensitivities derived by streamlines.

The data misfit is continually reduced from the prior model, after global matching, and after local matching (Figure 4.29). As we mentioned, the majority reduction of bottom-hole pressure and gas-oil ratio misfit is achieved in the global matching using MOGA. Streamline-based calibration also improves the bottom-hole pressure and gas-oil ratio. Local history matching primarily improves the water-cut result while maintaining the matched well responses in the global phase.

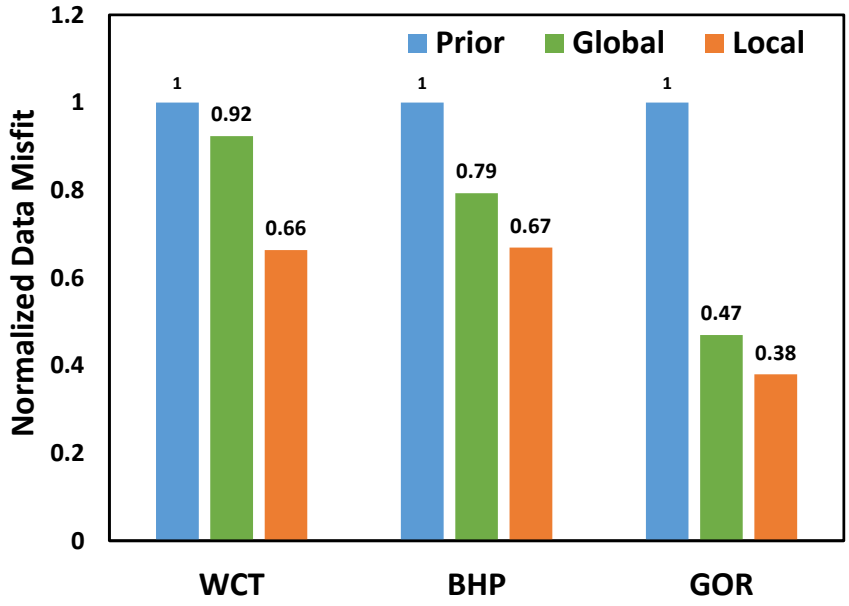

Figure 4.29 The comparison of normalized objective function for WCT, BHP, and GOR among prior, global matching model, and local matching model.

Figure 4.30 shows the well response after history matching. Overall, we have acceptable matches to the observed data. Most of well responses are improved or maintained for three objectives. For the gas-oil ratio, B-1H, D-2H, D-4AH, and E-3AH are key wells because their magnitude of gas-oil ratio responses are much bigger than the other wells. Thus, matching these four wells has a primary effect on the gas-oil ratio misfit reduction. In chapter III, E-4AH showed the conflicting issue. However, the final well response of this approach improves pressure data and maintains well water-cut that has good agreement initially.

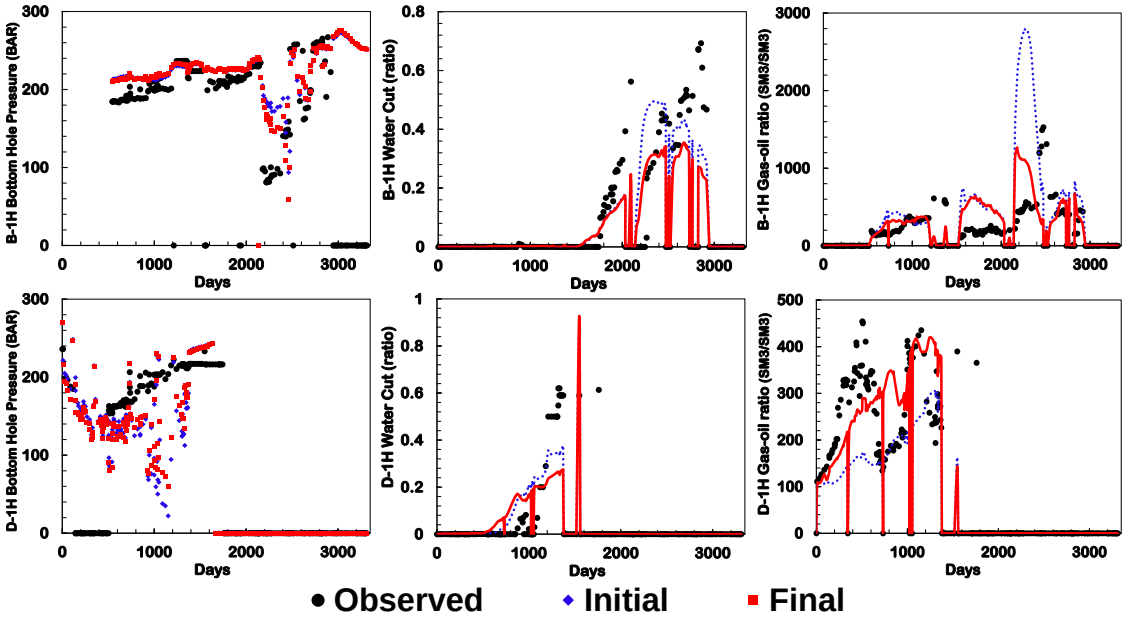

Figure 4.30 BHP (left column), WCT (middle column), and GOR (right column) at each production well corresponding to the reference, initial, and calibrated Norne field model by the three-phase joint inversion with multiscale approach.

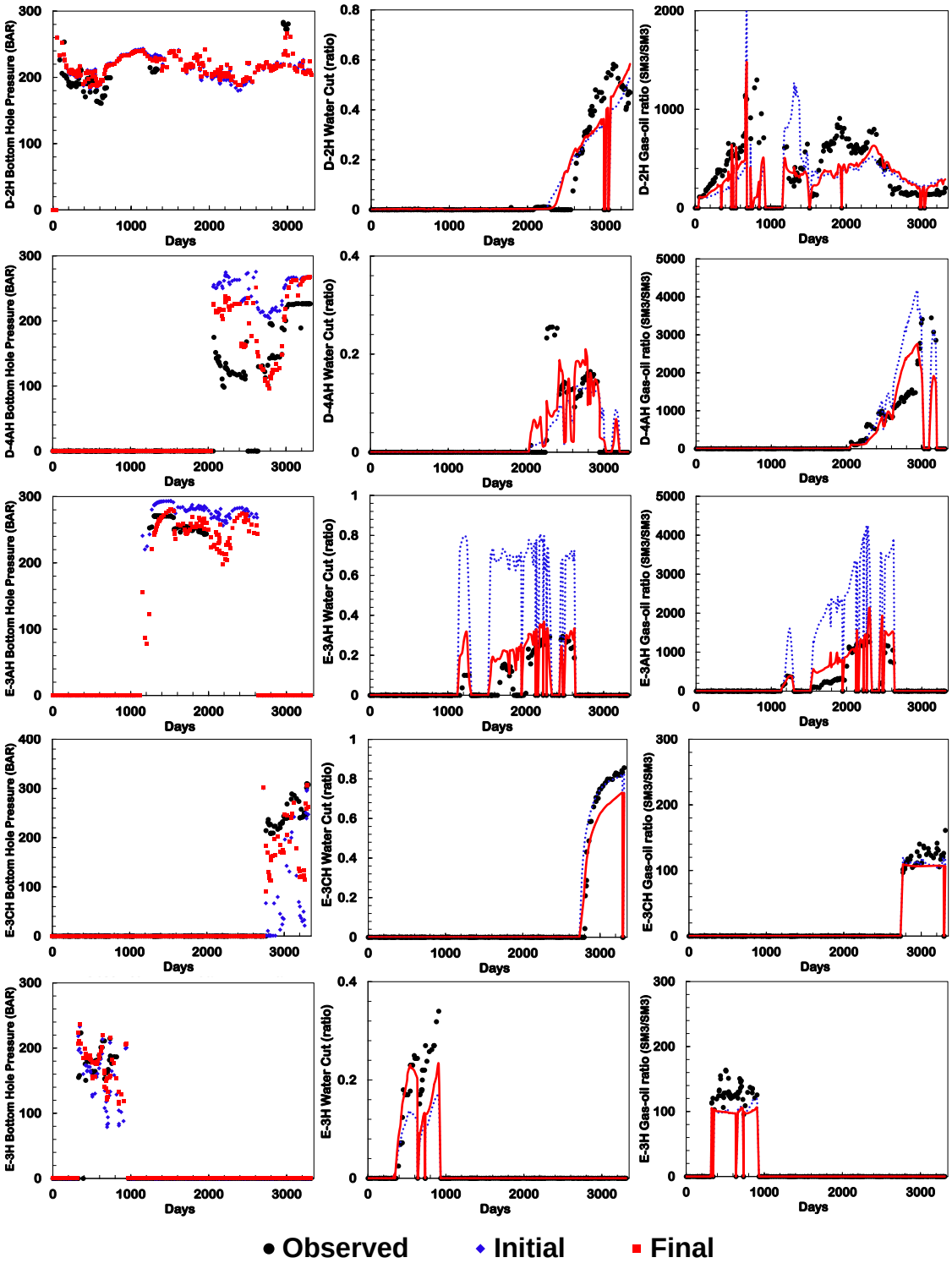

Figure 4.30 continued.

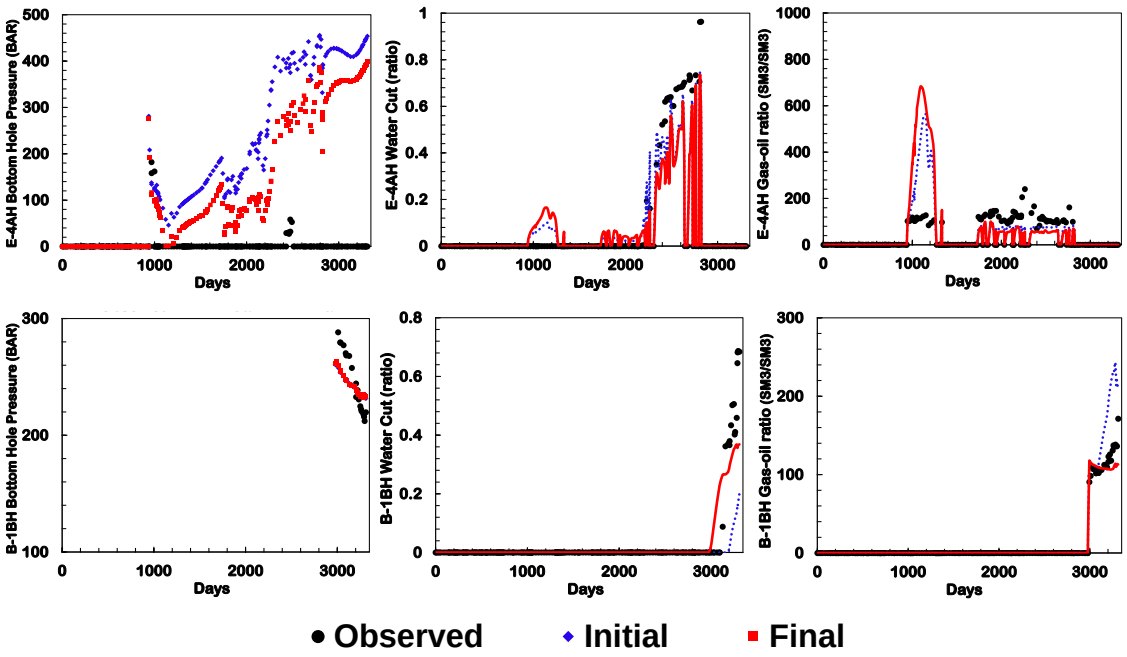

Figure 4.30 continued.

The final permeability field is shown in Figure 4.31 and the permeability change made during the global and local matching are displayed in Figure 4.32. A majority of permeability changes happens in the global phase with MOGA. It captures the large-scale heterogeneity and makes a smooth permeability change as we have shown in chapter III. To maintain the results of global matching in streamline-based local phase, the norm coefficient has a high value in Eq. 3.14. Thus, the local change of permeability is insignificant. An illustration of this permeability preservation is seen in Figure 4.33 through the statistics and histogram of permeability in prior, after global matching, and after local matching models. After global matching, permeability distribution is a little deviated from the prior model. On the contrary, final permeability statistics are very close

to the one after global matching, because local permeability update is minimal for the preservation of the calibration model in global phase.

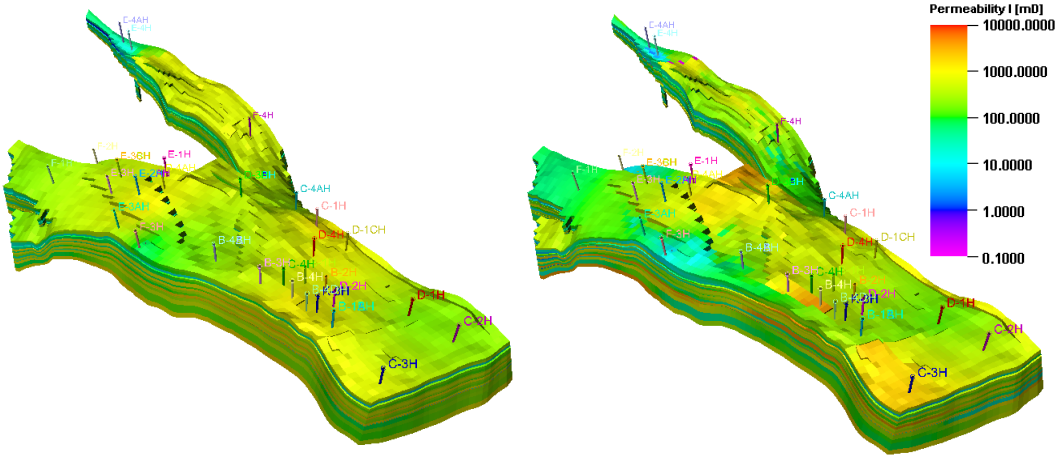

Figure 4.31 Initial (left) and final permeability distribution (right) for Norne reservoir model.

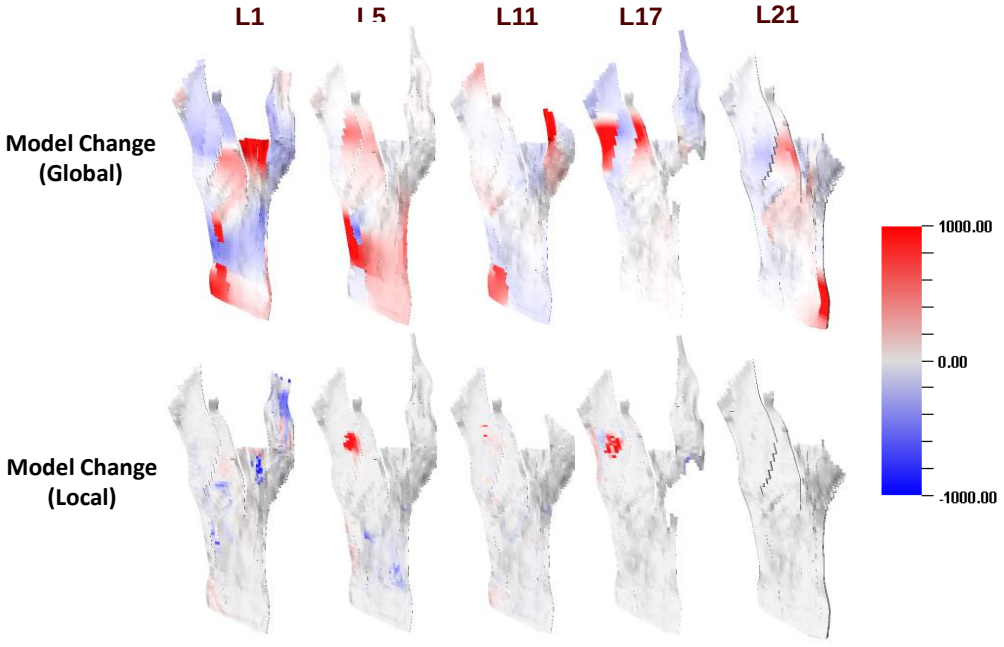

Figure 4.32 Permeability change in global (1st row) and local (2nd row) phase for the selected five layers in Nore reservoir model.

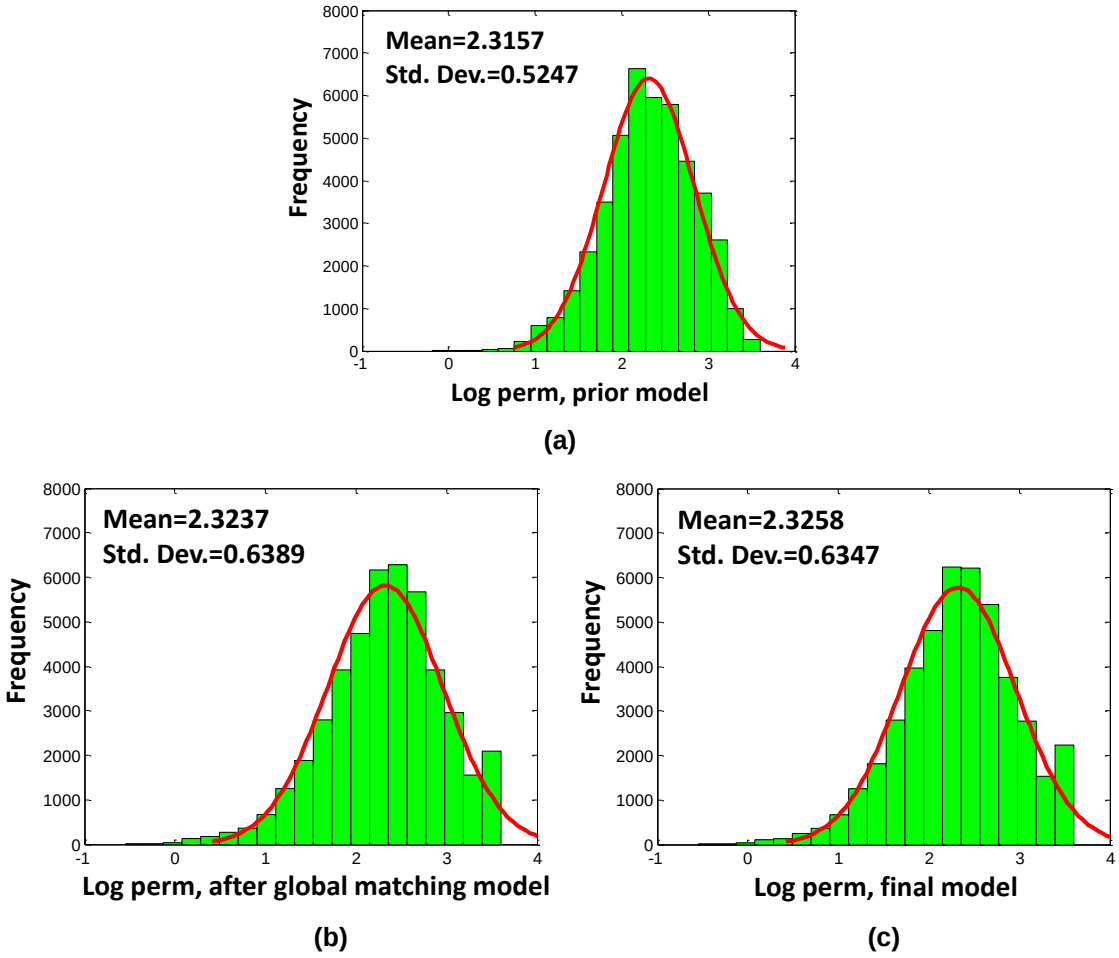

Figure 4.33 Histogram and statstics of the permeability distribution as prior model (a), after global matching (b), and after local matching (c).

4.6 Chapter Conclusions

We have extended the streamline-based joint inversion to the three-phase flow system using the analytical sensitivity of water-cut, bottom-hole pressure, and gas-oil ratio. We demonstrate the applicability and effectiveness of our approach through synthetic and field scale three-phase models. Finally, we apply it to Norne field with the multiscale approach. The major findings from this chapter are summarized below.

1. We analyze the gas-oil ratio sensitivity at first by comparing it with numerical sensitivity (perturbation method). Although the streamline-based analytical sensitivity cannot capture the exact one, it can calculate reasonable approximations for the numerical sensitivity by following the trend of it.
2. We test our analytical sensitivities in the three-phase synthetic models with a water injector or gas injector. The streamline-based joint inversion for gas-oil ratio, bottom-hole pressure, and water-cut reproduces the well responses. It supports that approximate gas-oil ratio sensitivity based on streamline is reliable for the purpose of production history matching.
3. The field scale applications demonstrate the feasibility of our approach for the inversion problem. Adding gas-oil ratio information to the joint inversion of water-cut and bottom-hole pressure creates better convergence of data misfits, particularly gas-oil ratio, and reproduces closer well responses compared to only matching pressure and water-cut. Therefore, the streamline-based three-phase history matching workflow is applicable and effective on the practical history matching problem.

4. In the Norne field application, we have two issues in which GTTI is not applicable due to non-monotonic gas-oil ratio data and multi-objectives in history matching problem can be potentially conflicting. To avoid these issues, we suggest the multiscale approach by combining a multi-objective genetic algorithm (MOGA) for global matching and a streamline-based approach for local calibration. It successfully reduces the data misfit of water-cut, bottom-hole pressure, and gas-oil ratio simultaneously while keeping the prior reservoir properties. The calibrated model has substantially improved well responses.

CHAPTER V

CONCLUSIONS AND RECOMMENDATIONS

5.1 Conclusions

This study summarized the development and applications of streamline-based history matching. We presented how to incorporate diverse data types related to multiphase flow and pressure with the streamline-based inversion process. In addition to the demonstration of our method, we emphasized the applicability of our approach to the field-scale reservoir model to satisfy the industry demands.

First, we have presented the streamline-based transport tomography for high resolution reservoir characterization using a novel tracer technology.

Second, we have proposed a new approach to calculate the streamline-based bottom-hole pressure sensitivity at the wells. It makes the joint inversion with a multiscale approach treatable.

Lastly, the streamline-based joint inversion is extended to the three-phase flow model by integrating gas-oil ratio, bottom-hole pressure, and water-cut data simultaneously.

The summary of all the works and findings are listed below.

- We have proposed a new approach for streamline-based history matching of distributed water arrival time together with the aggregated well production data.
- The distributed water arrival information provides significantly improved flow resolution for reservoir characterization. The calibrated model with transport

tomography reproduces the detailed flow behavior of the reference model more closely.

- The proposed bottom-hole pressure sensitivity based on streamline is validated by a comparison to the adjoint method.
- The joint inversion for bottom-hole pressure and water-cut simultaneously avoids the limitation in a sequential approach and makes significant improvements in inversion results.
- We suggest the joint inversion with a multiscale approach. It shows better convergence of data misfits and improves the well response matching compared to direct fine-scale history matching. It captures the large-scale heterogeneity and makes smooth changes in permeability.
- We showed that the streamline-based gas-oil ratio sensitivity can provide reasonable approximations for the purpose of history matching.
- The field-scale applications demonstrated the feasibility of our streamline-based approach for practical history matching. We examined the impact of adding gas-oil ratio information to the three-phase joint inversion.
- In the Norne field application, we suggested the multiscale approach by combining a multi-objective genetic algorithm (MOGA) for global matching with a streamline-based approach for local calibration. This approach resolves the issues related to the inapplicability of GTTI and the potential conflict between objectives. Therefore, our approach is recommended to the field-scale history matching problem.

5.2 Recommendations

There are several recommendations that can be drawn from this study.

- Including seismic information (acoustic impedance or inversed pressure and saturation data) into our approach of matching the three-phase production data, will improve the resolution of calibrated reservoir models.
- Incorporating different types of data requires normalization. We normalized it based on the inverse of standard deviation of measurement errors. However, typically such measurement errors are not available and the approach needs to be generalized. Particularly, it will be critical when we develop the joint inversion of seismic data with production data.
- Gas-oil ratio sensitivity is a reasonable approximation for the history matching. However, arrival time sensitivity is not applicable to the non-monotonic well response which is common in field cases. We need to develop new algorithms.
- In chapter IV, we tried the global phase by calibrating PORV and permeability multiplier sequentially. However, two variables can contradict. Simultaneous consideration of them can result in a more accurate estimation of reservoir properties.
- Currently, we have an ability to trace streamlines in an irregular grid systems. Thus, we can develop the joint inversion in unstructured grids with mostly coarse grids except for well areas that have fine grids.

NOMENCLATURE

ATM	=	amplitude misfit
BHP	=	bottom-hole pressure
GCT	=	grid connectivity based transformation
GOR	=	gas-oil ratio
GTTI	=	generalized travel time inversion
MOGA	=	multi-objective genetic algorithm
RMSE	=	root mean square error
TOF	=	time of flight
TTI	=	travel time inversion
TTM	=	travel time misfit
WCT	=	water-cut

A	=	Area
B_o	=	oil formation volume factor
B_g	=	gas formation volume factor
c	=	divergence of the velocity field
D	=	depth
E	=	misfit function
f_α	=	total fractional flow of phase α
g	=	gravity acceleration constant

k	=	permeability
L	=	length
$\boldsymbol{L}$	=	spatial difference operator
m	=	reservoir parameter
N_d	=	number of dynamic data observations
p	=	pressure
p_{bhp}	=	bottom hole pressure
q	=	flow rate
R^2	=	coefficient of determination
R_s	=	solution gas/oil ratio
s	=	slowness
S_α	=	saturation of phase α
t	=	time
u_α	=	velocity of phase α
u	=	parameter in spatial domain
v	=	parameter set in transform domain
y^{obs}	=	observed response
$\overline{y^{obs}}$	=	averaged observed response
y^{cal}	=	calculated response
β_1	=	weighting factor for the prior model
β_2	=	weighting factor for the roughness term
Δt	=	travel-time shift

$\Delta\tilde{t}$	=	generalized travel time
λ_t	=	total mobility
τ	=	time of flight
ϕ	=	porosity
$\mathbf{\Phi}$	=	basis matrix
ψ	=	streamline trajectory

REFERENCES

Aanonsen, S.I. 2008. Efficient History Matching Using a Multiscale Technique. *SPE Reservoir Evaluation & Engineering* 11 (1): 154-164.

Annable, M.D., Rao, P., Hatfield, K., Graham, W.D., Wood, A. et al. 1998. Partitioning Tracers for Measuring Residual NAPL: Field-scale Test Results. *Journal of Environmental Engineering* 124 (6): 498-503.

Bhark, E.W., Jafarpour, B., and Datta-Gupta, A. 2011. A Generalized Grid Connectivity–based Parameterization for Subsurface Flow Model Calibration. *Water Resources Research* 47 (6): W06517.

Bhark, E., Rey, A., Datta-Gupta, A., and Jafarpour, B. 2012. A Multiscale Workflow for History Matching in Structured and Unstructured Grid Geometries. *SPE Journal* 17 (3): 828-848.

Cheng, H., Datta-Gupta, A., and He, Z. 2005. A Comparison of Travel-Time and Amplitude Matching for Field-Scale Production-Data Integration: Sensitivity, Nonlinearity, and Practical Implications. *SPE Journal* 10 (1): 75-90.

Cheng, H., Dehghani, K., and Billiter, T.C. 2008. A Structured Approach for Probabilistic-Assisted History Matching Using Evolutionary Algorithms: Tengiz Field Applications. Paper SPE 116212 presented at the SPE Annual Technical Conference and Exhibition, Denver, Colorado, 21-24 September.

Cheng, H., Kharghoria, A., He, Z., and Datta-Gupta, A. 2005. Fast History Matching of Finite-Difference Models Using Streamline-Derived Sensitivities. *SPE Reservoir Evaluation & Engineering* 8 (5): 426-436.

Cheng, H., Osako, I., Datta-Gupta, A., and King, M.J. 2006. A Rigorous Compressible Streamline Formulation for Two and Three-Phase Black-Oil Simulation. *SPE Journal* 11 (4): 407-417.

Cheng, H., Oyerinde, A.S., Datta-Gupta, A., and Milliken, W.J. 2007. Compressible Streamlines and Three-Phase History Matching. *SPE Journal* 12 (4): 475-485.

Cheng, H., Wen, X.-H., Milliken, W.J.M., and Datta-Gupta, A. 2004. Field Experiences with Assisted and Automatic History Matching Using Streamline Models. Paper SPE 89857 presented at the SPE Annual Technical Conference and Exhibition, Houston, Texas, 26-29 September.

Datta-Gupta, A. and King, M.J. 2007. *Streamline Simulation : Theory and Practice*, SPE Textbook series Vol. 11, Society of Petroleum Engineers. Richardson, Texas, U.S.A.

Datta-Gupta, A., Yoon, S., Vasco, D.W., and Pope, G.A. 2002. Inverse Modeling of Partitioning Interwell Tracer Tests: A Streamline Approach. *Water Resources Research* 38 (6): 1079.

Deb, K., Pratap, A., Agarwal, S., and Meyarivan, T. 2002. A Fast and Elitist Multiobjective Genetic Algorithm: NSGA-II. *IEEE Transactions on Evolutionary Computation* 6 (2): 182-197.

Granville, V., Krivanek, M. and Rasson, J.P. 1994. Simulated Annealing: A Proof of Convergence. *Pattern Analysis and Machine Intelligence, IEEE Transactions on* 16 (6): 652-656.

Hastings, W.K. 1970. Monte Carlo Sampling Methods Using Markov Chains and Their Applications. *Biometrika* 57 (1): 97-109.

He, Z., Yoon, S., and Datta-Gupta, A. 2002. Streamline-Based Production Data Integration with Gravity and Changing Field Conditions. *SPE Journal* 7 (4): 423-436.

Hohl, D., Jimenez, E., and Datta-Gupta, A. 2006. Field Experiences with History Matching an Offshore Turbiditic Reservoir Using Inverse Modeling. Paper SPE 101983 presented at the SPE Annual Technical Conference and Exhibition, San Antonio, Texas, USA, 24-27 September.

Hoffman, B.T., Caers, J.K., Wen, X. and Strebelle, S.B. 2006. A Practical Data Integration Approach to History Matching: Application to a Deepwater Reservoir. *SPE Journal* 11 (04): 464-479.

Kam, D. and Datta-Gupta, A. 2014. Streamline-based Transport Tomography Using Novel Tracer Technologies. Paper SPE 169105 presented at the SPE Improved Oil Recovery Symposium, Tulsa, Oklahoma, 12-16 April.

Kang, S., Bhark, E., Datta-Gupta, A., Kim, J., and Jang, I. 2014. A Hierarchical Model Calibration Approach with Multiscale Spectral-Domain Parameterization: Application to a Structurally Complex Fractured Reservoir. Paper SPE 169061 presented at the SPE Improved Oil Recovery Symposium, Tulsa, Oklahoma, 12-16 April.

Killough, J.E. 1995. Ninth SPE Comparative Solution Project: A Reexamination of Black-Oil Simulation. Paper SPE 29110 presented at the SPE Reservoir Simulation Symposium, San Antonio, Texas, 12-15 February.

Kim, J.U., Datta-Gupta, A., Jimenez, E.A., and Hohl, D. 2010. A Dual Scale Approach to Production Data Integration into High Resolution Geologic Models. *Journal of Petroleum Science and Engineering* 71 (3–4): 147-159.

Kulkarni, K.N., Datta-Gupta, A., and Vasco, D.W. 2001. A Streamline Approach for Integrating Transient Pressure Data Into High-Resolution Reservoir Models. *SPE Journal* 6 (3): 273-282.

Li, R., Reynolds, A.C., and Oliver, D.S. 2003. Sensitivity Coefficients for Three-Phase Flow History Matching. *Journal of Canadian Petroleum Technology* 42 (04): 70-77.

Luo, Y. and Schuster, G.T. 1991. Wave-equation Traveltime Inversion. *Geophysics* 56 (5): 645-653.

Maroongroge, V., Saad, N., Pope, G.A., and Sepehrnoori, K. 1995. Use of Inverse Modeling for Conditioning Geostatistical Models to Vertical Tracer Profiles. Paper SPE 30592 presented at the SPE Annual Technical Conference and Exhibition, Dallas, Texas, 22-25 October.

Montes, A., Nyhavn, F., Oftedal, G., Faevelen, E., Andresen, C.A. et al. 2013. Application of Inflow Well Tracers for Permanent Reservoir Monitoring in North Amethyst Subsea Tieback ICD wells in Canada. Paper SPE 167463 presented at the SPE Middle East Intelligent Energy Conference and Exhibition, Dubai, UAE, 28-30 October.

Napalowski, R., Loro, R., Anderson, C., Anderson, C., Dyrli, A.D. et al. 2012. Successful Application fo Well Inflow Tracers for Water Breakthrough Surveillance in the Pyrenees Development, Offshore Western Australia. Paper SPE 158423 presented at the SPE Asia Pacific Oil and Gas Conference and Exhibition, Perth, Australia, 22-24 October.

Oliver, D.S. and Chen, Y. 2011. Recent progress on resevoir history matching: a review. *Computational Geosciences* 15: 185-221.

Oliver, D. S., Reynolds, A. C. and Liu, N. 2008. *Inverse Theory for Petroleum Reservoir Characterization and History Matching*, Cambridge University Press, Cambridge, U.K.

Osdal, B., Husby, O., Aronsen, H.A., Chen, N., and Alsos, T. 2006. Mapping the Fluid Front and Pressure Buildup Using 4D Data on Norne Field. *The Leading Edge* 25 (9): 1134-1141.

Oyerinde, A., Datta-Gupta, A., and Milliken, W.J. 2009. Experiences with Streamline-based Three-phase History Matching. *SPE Reservoir Evaluation & Engineering* 12 (4): 528-541.

Paige, C.C. and Saunders, M.A. 1982. LSQR: An Algorithm for Sparse Linear Equations and Sparse Least Squares. *ACM Transactions on Mathematical Software* 8 (1): 43-71.

Park, H.-Y., Datta-Gupta, A., and King, M.J. 2013. Handling Conflicting Multiple Objectives Using Pareto-Based Evolutionary Algorithm for History Matching of Reservoir Performance. Paper SPE 163623 presented at the SPE Reservoir Simulation Symposium, Woodlands, Texas, 18-20 February.

Peters, L., Arts, R., Brouwer, G., Geel, C., Cullick, S. et al. 2010. Results of the Brugge Benchmark Study for Flooding Optimization and History Matching. *SPE Reservoir Evaluation & Engineering* 13 (3): 391-405.

Pollock, D.W. 1988. Semianalytical Computation of Path Lines for Finite-Difference Models. *Ground Water* 26 (6): 743-750.

Rey, A., Ballin, P.R., Vitalis, C.F., Parke, J., and Datta-Gupta, A. 2009. Assisted History Matching in an Offshore Turbidite Reservoir With Active Reservoir Management. Paper SPE 124950 presented at the SPE Annual Technical Conference and Exhibition, New Orleans, Louisiana, 4-7 October.

Rwechungura, R.W., Bhark, E.W., Miljeteig, O.T., Suman, A., Kourounis, D. et al. 2012. Results of the First Norne Field Case on History Matching and Recovery Optimization Using Production and 4D Seismic Data. Paper SPE 157112 presented at the SPE Annual Technical Conference and Exhibition, San Antonio, Texas, 8-10 October.

Steffensen, I. and Karstadt, P.I. 1996. Norne Field Development - Fast Track from Discovery to Production. *Journal of Petroleum Technology* 48 (4): 296-299, 339.

Stenerud, V.R. and Lie, K.-A. 2006. A Multiscale Streamline Method for Inversion of Production Data. *Journal of Petroleum Science and Engineering* 54 (1–2): 79-92.

Tanaka, S., Kam, D., Datta-Gupta, A., and King, M. J. 2015. Streamline-based History mathing of Arrival Times and Bottom-hole Pressure Data for Multicompnent Compositional Systems. Paper SPE 174750 presented at the SPE Annual Technical Conference and Exhibition, Houston, Texas, 28-30 September. (accepted)

Vasco, D.W. and Karasaki, K. 2006. Interpretation and Inversion of Low-frequency Head Observations. *Water Resources Research* 42 (5): W05408.

Vasco, D.W., Keers, H., and Karasaki, K. 2000. Estimation of Reservoir Properties Using Transient Pressure Data: An Asymptotic Approach. *Water Resources Research* 36 (12): 3447-3465.

Vasco, D.W., Yoon, S., and Datta-Gupta, A. 1999. Integrating Dynamic Data Into High-Resolution Reservoir Models Using Streamline-Based Analytic Sensitivity Coefficients. *SPE Journal* 4 (4): 389-399.

Vega, L., Rojas, D., and Datta-Gupta, A. 2004. Scalability of the Deterministic and Bayesian Approaches to Production-Data Integration Into Reservoir Models. *SPE Journal* 9 (03): 330-338.

Watanabe, S. and Datta-Gupta, A. 2012. Use of Pahse Streamlines for Covariance Localization in Ensemble Kalman Filter for Three-phase History Mathing. *SPE Reservoir Eavluation & Engineering* 15 (3): 273-289.

Watanabe, S., Han, J., Datta-Gupta, A., and King, M.J. 2013. Streamline-Based Time Lapse Seismic Data Integration Incorporating Pressure and Saturation Effects. Paper SPE 166395 presented at the SPE Annual Technical Conference and Exhibition, New Orleans, Louisiana, 30 September-2 October.

Williams, B. and Vilela, A. 2012. Wireless Reservoir Surveillance Using Intelligent Tracers. Paper SPE 152660 presented at the SPE Latin American and Caribbean Petroleum Engineering Conference, Mexico City, Mexico, 16-18 April.

Williams, M.A., Keating, J.F., and Barghouty, M.F. 1998. The Stratigraphic Method: A Structured Approach to History Matching Complex Simulation Models. *SPE Reservoir Evaluation & Engineering* 1 (2): 169-176.

Yin, J., Park, H., Datta-Gupta, A., King, J.M., and Choudhary, M.K. 2010. A Hierarchical Streamline-Assisted History Matching Approach With Global and Local Parameter Updates. Paper SPE 132642 presented at the SPE Western Regional Meeting, Anaheim, California, 27-29 May.

Yoon, S., Malallah, A.H., Datta-Gupta, A., Vasco, D.W., and Behrens, R.A. 2001. A Multiscale Approach to Production-Data Integration Using Streamline Models. *SPE Journal* 6 (2): 182-192.

APPENDIX A

ANALYSIS OF GAS-OIL RATIO ARRIVAL TIME SENSITIVITY

We validated gas-oil ratio (GOR) arrival time sensitivity in chapter IV. Here, we conduct additional analyses to clarify when the formulation (Eq. 4.5) is applicable. Adedayo et al. (2009) showed that the divergence of flux dominates the GOR sensitivity at early times and the fractional flow term dominates the sensitivity when the flow is fully developed (Figure A.1). They used the numerical sensitivity (left column in the figure) to show the dominance in the analysis.

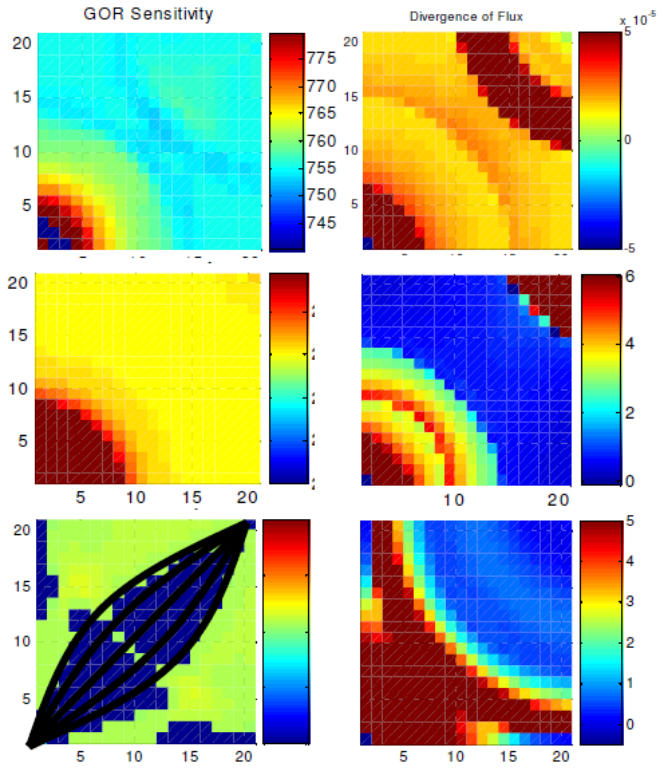

Figure A.1 Comparison between GOR sensitivity and divergence of flux (Adedayo et al. 2009)

Watanabe and Datta-Gupta (2012) also showed this characteristic in cross-covariance map between cell permeability and well GOR response (Figure A.2).

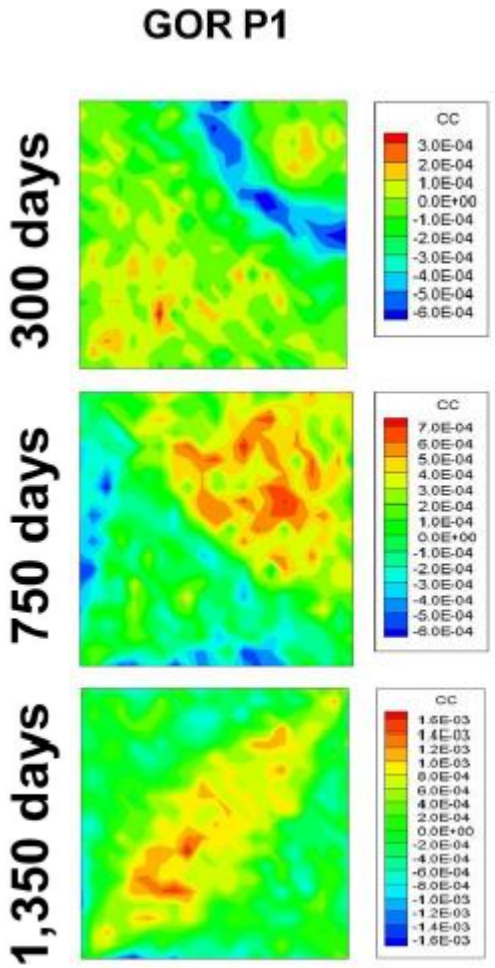

Figure A.2 Cross-covariance map between permeability and GOR at three different times (Watanabe and Datta-Gupta, 2012).

Here, we analyze when the streamline-based GOR arrival time sensitivity formulation is applicable using the models in section 4.3. Figure 4.2 and Figure 4.3 are the sensitivities after water breakthrough. They have showed good agreement with the numerical sensitivity. However, when the water front has not arrived the producer (the flow is not

fully developed), there are issues in the analytical sensitivity. First, we test the BHP-BHP case, which means injector and producer are constrained by pressure. Figure A.3 shows the behavior of properties used in the sensitivity formulation (Eq. 4.5). The numerical and analytical sensitivities are not matched in this condition. The analytical sensitivity has two peaks; the first one is because of the water front and the second is because of the gas phase ($p_{cell} < p_b$). The water front makes the difference between two sensitivities. The behavior of the numerical sensitivity is similar with the shape of divergence of flux (rising sharply), though the location of peak does not exactly match.

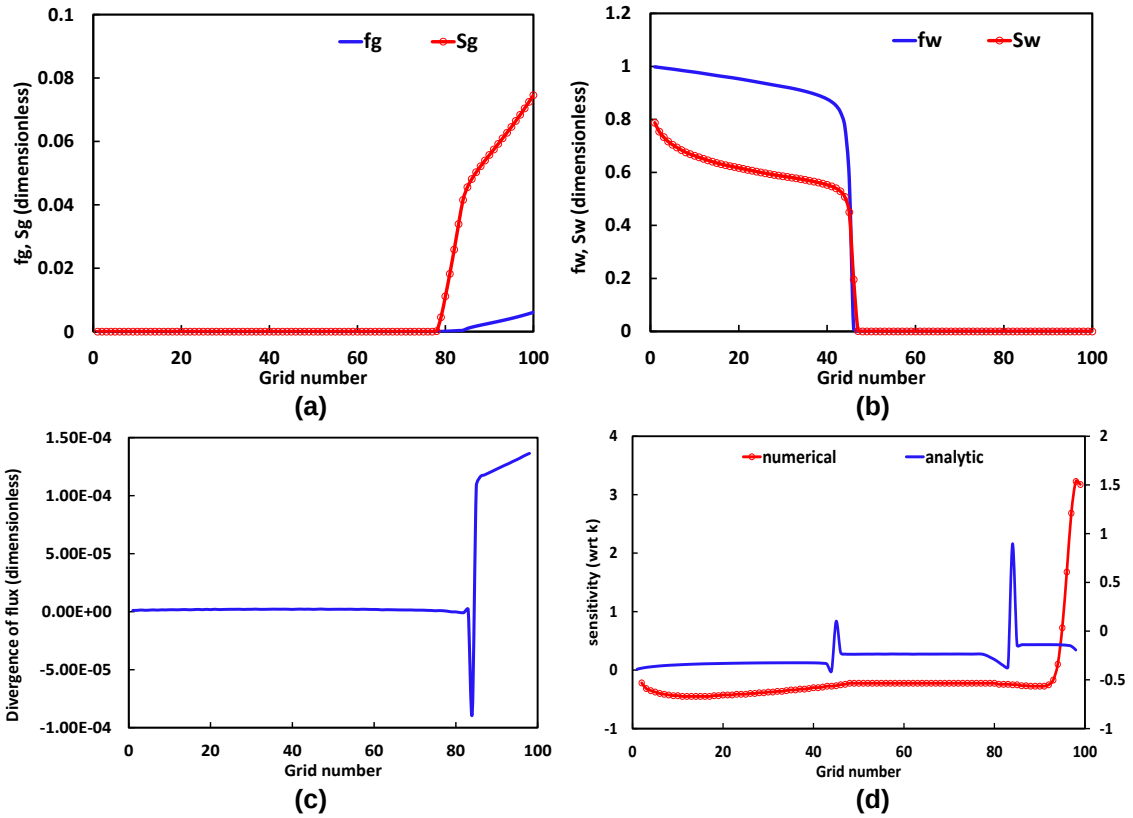

Figure A.3 (a) Fractional flow and saturation of gas phase, (b) fractional flow and saturation of water phase, (c) divergence of flux, and (d) sensitivity comparison before water breakthrough in 1D BHP-BHP case.

Figure A.4 shows the behavior of properties and sensitivities after water breakthrough in BHP-BHP case (same condition with Figure 4.2). The sensitivities show the small fluctuation when gas phase exists, but they are not dominated by the divergence term and show good agreement in Figure A.4 (d).

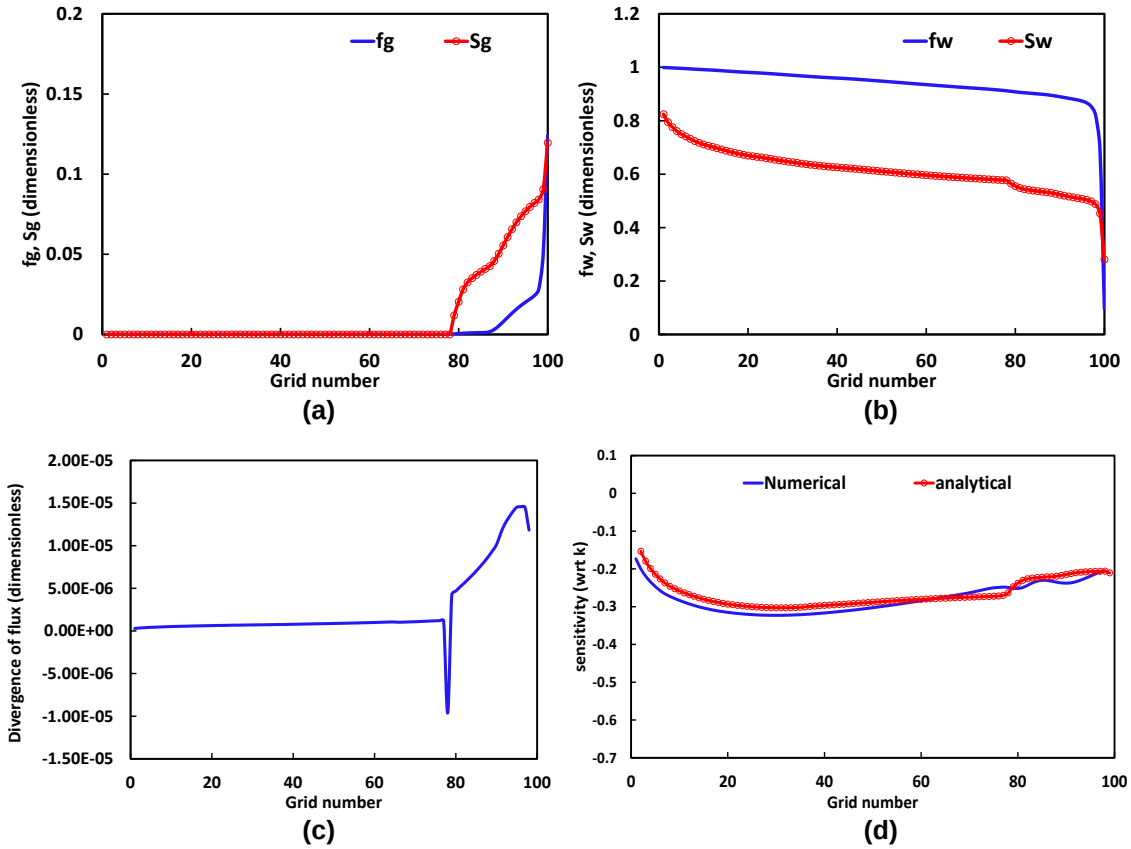

Figure A.4 (a) Fractional flow and saturation of gas phase, (b) fractional flow and saturation of water phase, (c) divergence of flux, and (d) sensitivity comparison after water breakthrough in 1D BHP-BHP case.

Figure A.5 and Figure A.6 show the analysis with BHP-Rate case, which is the same as the model in Figure 4.3. This case also has differences when the flow is not fully developed. Figure A.5 indicates the divergence term has a large effect on the analytical

sensitivity. The peak of divergence is due to gas phase soaring, which is related to the water front. However, the numerical sensitivity shows the different behavior when the gas phase is released. It also has an upsurge as closing to the water front, which is similar location with peak of divergence. But the numerical sensitivity increases much smoother and broader compared to the divergence behavior and analytical sensitivity. In this condition, the numerical sensitivity does not seem to be only dominated by the divergence of flux. The producer is constrained by rate, so it can be affected by pressure change due to the permeability perturbation.

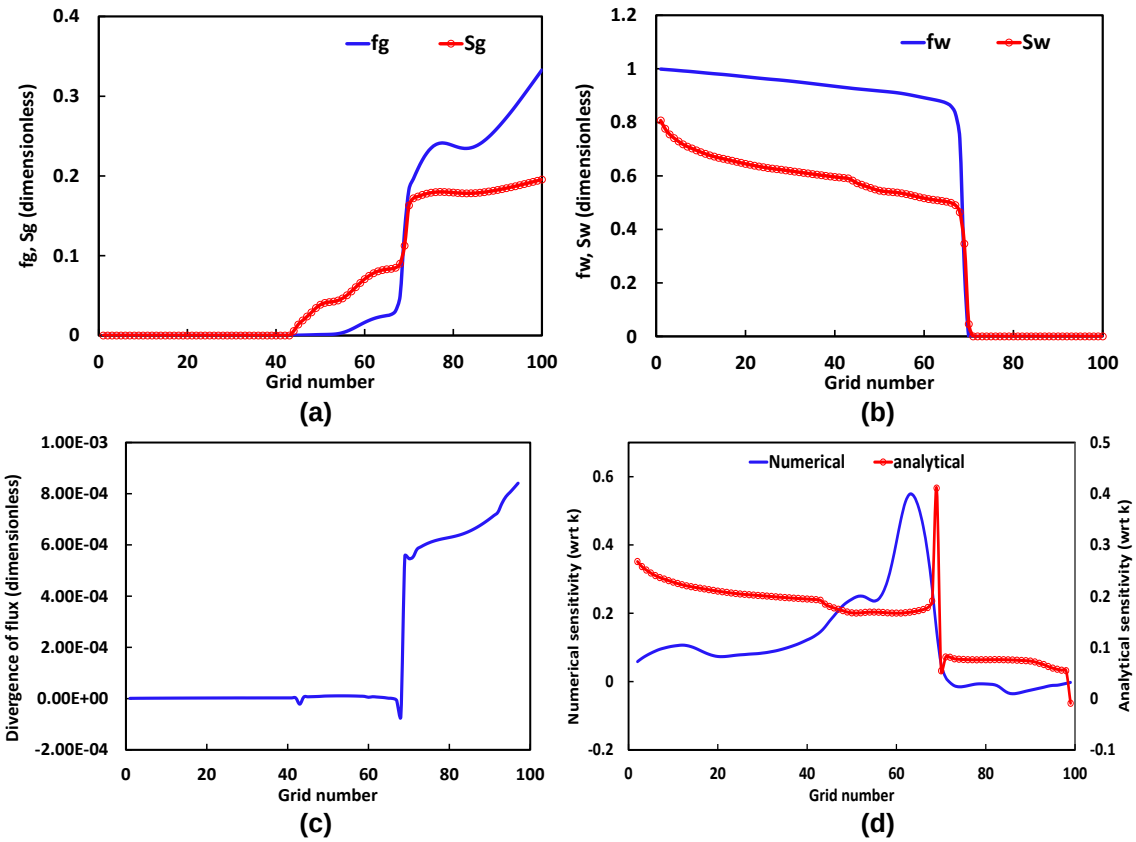

Figure A.5 (a) Fractional flow and saturation of gas phase, (b) fractional flow and saturation of water phase, (c) divergence of flux, and (d) sensitivity comparison before water breakthrough in 1D BHP-Rate case.

However, when the flow is fully developed the sensitivities have good agreement (similar trend) in Figure A.6 (d). Both numerical and analytical sensitivities have different behavior with the divergence of flux.

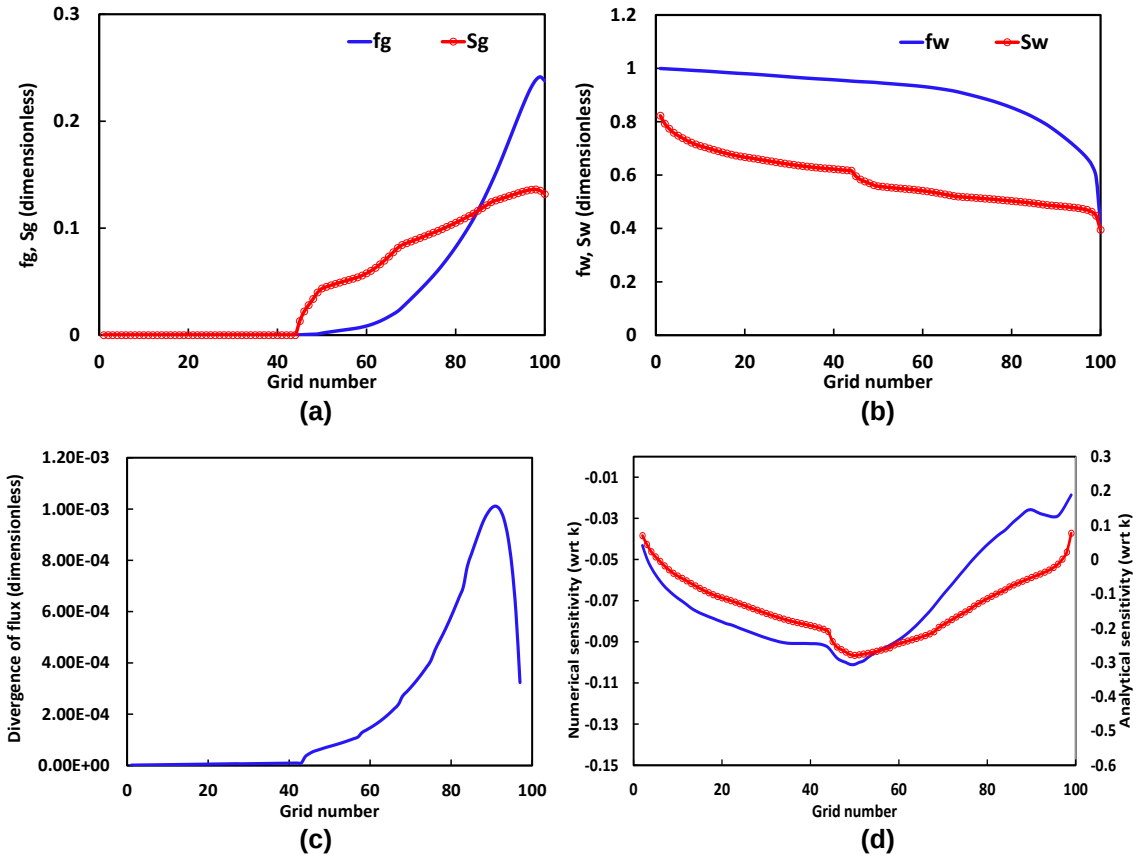

Figure A.6 (a) Fractional flow and saturation of gas phase, (b) fractional flow and saturation of water phase, (c) divergence of flux, and (d) sensitivity comparison after water breakthrough in 1D BHP-Rate case.

In Figure 4.5, we have showed that the analytic sensitivity has good agreement with numerical sensitivity after water breakthrough with the 2D homogeneous model. Figure A.7 shows two conditions: before the water breakthrough (top) and after water breakthrough (bottom). In Figure A.7 (a) on the right, the analytical sensitivity exhibits

vaguely a similar trend as the numerical sensitivity by showing an arc. However, the analytical sensitivity has the flow-dominated behavior along the diagonal direction between wells, which is the same trend as the streamline trajectory. The numerical sensitivity (Figure A.7 (a) on the left) seems to be dominated by the divergence that is shown in Figure A.1. Therefore, we have a different shape of the sensitivity before the water breakthrough. On the other hand, we have good agreement when the flow is fully developed (Figure A.7 (b)).

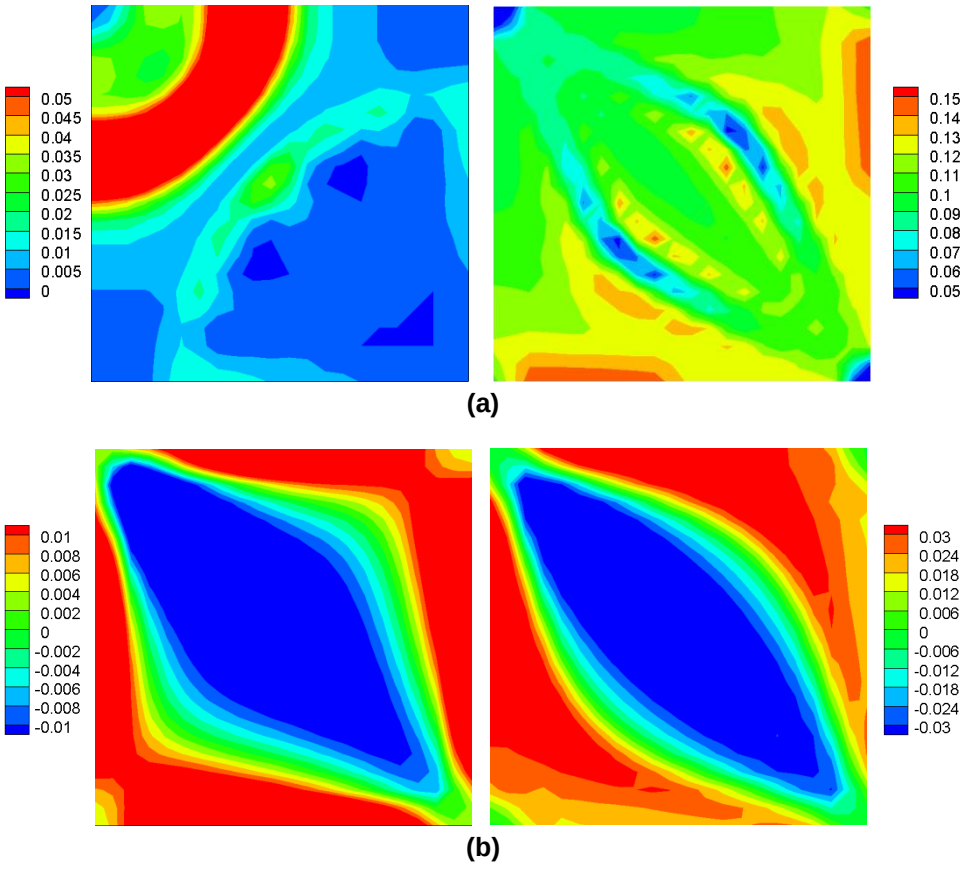

Figure A.7 Comaprison of sensitivity between numerical (left) and analytical based on streamline (right) at (a) before water breakthrough and (b) after water breakthrough in 2D Rate-Rate case.

Our GOR arrival time sensitivity formulation makes reasonable approximations when the flow is fully developed and it is applicable to the history matching problem (Chapter IV). However, it has a limitation: the analytical sensitivity cannot represent the numerical sensitivity when the flow is not fully developed (before the water breakthrough). Thus, we need additional efforts to figure out this issue.

- The water front makes an effect on the analytical sensitivity when the flow is not fully developed. It is one of the reasons in the sensitivity differences.
- The pressure effect by the permeability perturbation is considered implicitly because the saturation and fractional flow etc. in the Eq. 4.5 are the function of pressure. In history matching, the analytical sensitivity can be applicable because we add pressure sensitivity separately in this dissertation. However, we need to think about the necessity of the pressure term explicitly to obtain the accurate sensitivity regardless of the development of the flow.

APPENDIX B

USER MANUAL MULTI-PURPOSE SOFTWARE (DESTINY) FOR STREAMLINE TRACING, HISTORY MATCHING AND RESERVOIR MANAGEMENT

B.1 Introduction

This is manual for streamline-based tool called "DESTINY". The applications in this dissertation have been carried out using it and all new features of streamline-based history matching are implemented. The DESTINY has been developed for multi-purpose; streamline tracing, history matching, and reservoir management & development. Here, I briefly show how it works and objective of this software. In addition, how to construct input data for DESTINY because it has new input after implementing the new features shown in this dissertation.

B.2 Overview of DESTINY

Figure B.1 shows the DESTINY workflow. It interfaces with several commercial simulators under window and Linux system. In this dissertation, we use ECLIPSE developed by Schlumberger for a simulation and Petrel and Tecplot for a visualization.

B.3 Objectives

The main objectives of DESTINY are to trace streamline even in complex corner point and faulted (non-neighbor connection) geometry as well as the sensitivity

coefficient computation of generalized travel time inversion (He et al., 2002; Cheng et al., 2005; Oyerinde et al., 2007).

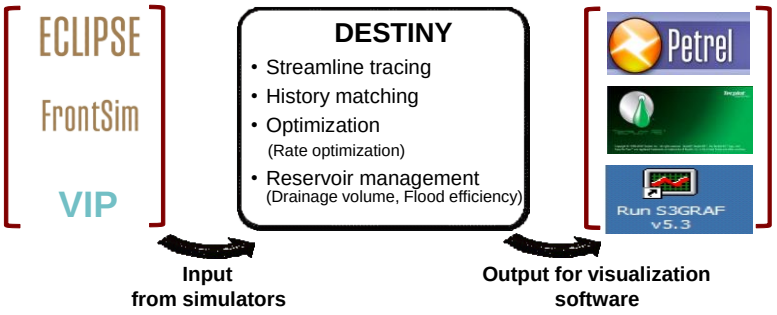

Figure B.1 Overview of DESTINY working environment.

In addition, DESTINY provides reservoir management tool such as drainage and swept volume calculation. Besides, it has ability to do rate optimization either for injection rate or for production rate based on simple analytic approach (Park and Datta-Gupta, 2011). Following summarizes main features in DESTINY (Figure B.2):

- Streamline Tracing and Visualization in corner point geometry and faulted cells from finite difference velocity field
- Streamline-based assisted History Matching for calibration of high resolution geologic models to production data.
- Reservoir Management/Optimization for analyzing and optimizing drainage/swept volumes, well connectivity using flood efficiency maps
- Reservoir Development for optimal infill well placement

Figure B.2 DESTINY main features.

B.4 Structure of input data

DIP file is an input file for DESTINY where we enter correct information about the simulation model that we are going to run and specify task with keywords, as we desire. This section gives details about keywords in input file.

DIP_DATA_FILE

File with general model information

This keyword defines the file holding the main ECLIPSE input deck. This file will be used to make the system call to run ECLIPSE in batch mode and should have the full ECLIPSE input data structure.

DIP_STREAMLINE_NUM

Number of Streamlines and output

The keyword is followed by a line with two records. The records are defined as follows,

1st INTEGER Number of Streamlines to be used

2nd BOOLEAN Defines if output files with streamlines is desired. The default streamline output in DESTINY satisfies binary FLOVIZ/PETREL formats

DIP_FORWARD_SIMULATOR

Defines simulator to be used

The keyword is followed by a line with five records. The records are defined as follows,

1st STRING Define which simulator is to be used for tracing and inversion. DESTINY is interfaced to work with *ECLIPSE/VIP/FRONTSIM* (Use simulator name to select the proper system calls)

2nd BOOLEAN Define if utility/debug files are required (*TRUE*:: REMOVE || *FALSE*::KEEP). It is recommended to leave this record as *FALSE*

3rd STRING Define which format is used for Summary / Restart files from simulator (*BINARY / ASCII*). Default is *BINARY*.

4th *STRING* Define if we want to run the FORWARD simulator or not. If 'STOP' is selected there must be and available set of output files including summary file and restart files etc. (RUN/STOP)

5th *BOOLEAN* "PRE-SCREENING BOOLEAN" which to ask if user want to check the data setup for running DESTINY(TRUE/FALSE) ; TRUE means we will screen data setup and show prescreening report. If it is OK, we keep run simulation. Otherwise, we stop

simulation and show a report that asks user to make correction on data set.

DIP_TRACING_SETTING

Defines setting for tracing

The keyword is followed by a line with thirteen records. The records are defined as follows,

1st STRING Phases involved in forward model. This will set DESTINY readers to scan phase fluxes as reported by the selected simulator. Use mnemonics OIL, WAT and GAS in any order followed by PHASE

2nd STRING Phases involved in tracing. This will set DESTINY to perform tracing based on single/multi phases. Use mnemonics *OIL*, *WAT* and *GAS* in any order followed by *PROD* if streamlines are starting from producers only. Use mnemonics *OIL*, *WAT* and *GAS* in any order followed by *SINK* if streamlines are starting from any cell.

3rd STRING Define if tracing is to be done at *(ALL)* schedule dates or at a *(SINGLE)* date.

4th STRING If *SINGLE* date tracing is selected in 3rd argument, this record sets the schedule date in which tracing is to be done.

5th FLOAT Set a flag to request *(ASCII/BINARY)* output from streamlines. No action will be taken when *BINARY* is selected.

6th STRING Define if the number of streamlines per completion is defined

based on flux *(STCFLUX)* or should be uniformly *(STCUNI)* distributed. Default is defined based on fluxes, even if the keyword is not included in DIP file.

7th STRING Define the type tracing to tackle faults and NNC connections. The default in DESTINY for inversion purposes is POLLOCK's construction (*POLLOCK/ MODPOLLOCK/LBLJIMENEZ*)

8th STRING Define the type discretization for tracing. The default in DESTINY is *HORIZNRAND* (Random discretization in Horizontal). (*HORIZNRAND/HORIZONTAL/VERTICAL/SQUARE*)

9th BOOLEAN Define if inversion process is applied (*TRUE*: TRACING ONLY ||*FALSE*: INVERSION APPLIED). Keep this as "TRUE" for tracing and reservoir management purposes.

10th STRING (*FEMAP/FALSE)*

FEMAP is going to additionally print both Flux connectivity map and average of TOF map. *FALSE* is printing NORMAL streamlines (this is normal and default)

11th STRING (*NORMAL/INJ2PROD*)

This option switches tracing option to the injector to producer. The default is to trace from producer to injector.

12th BOOLEAN This option is to define whether we consider "free gas only" or not. If "*TRUE*" is chosen, we do not consider "Dissolved gas".

13th BOOLEAN Set as *TRUE* if we are going to use 'COARSEN' keyword and use it for tracing and inversion

DIP_ECLRUN_SETTING

This setting aims to provide correct command to call simulator. Depending on working system (either Linux or window, also depending on setting up in their own system), the command to call simulator is different as shown in example below. Thus, in this setting we can specify about how to call simulator by command. If this setting is void, then DESTINY will activate its own default command which is $eclipse (for window) and @eclipse (for Linux run).

DIP_SENS_TUNING

Defines setting for sensitivity tuning

The keyword is followed by a line with seven records on each line. The records are defined as follows,

1st STRING When set to *TRUE* sensitivity normalization for equalization of the sensitivities is applied. The normalization facilitates the inversion algorithm based on data misfit.

2th FLOAT Normalizing value for bottom hole pressure sensitivity in joint inversion.

3th FLOAT Normalizing value for gas-oil ratio sensitivity in joint inversion.

4th STRING When set to *PERCCUTOFF*, a percentile based cutoff will be

applied to WWCT sensitivities on a well-basis. It is used to reduce unusual high and low sensitivity values. Default record is *NONE*

5th FLOAT Define the lower percentile for the WWCT sensitivity cut-off.

6th FLOAT Define the upper percentile for the WWCT sensitivity cut-off.

7th STRING When set to *TOFCUTOFF*, a time of flight based cutoff will be applied to WWCT sensitivities on a well-basis. Used to eliminate the sensitivities in stagnation region which may cause distort inversion performance. Default record is *NONE*

8th FLOAT Defines the threshold of the time of flight for the water cut/gas oil ratio sensitivity cut-off. This Maximum Time of Flight cut off value is automatically calculated by multiplication of actual producing time period with input multiplier value.

9th FLOAT Define the threshold of the time of flight for the bottom hole pressure sensitivity cut-off.

10th *BOOLEAN* Flag to sensitivity files print out. If set to *FALSE*, the sensitivity files are not going to be generated even not calculated. (*TRUE/FALSE*)

DIP_DATA_MISFIT

Defines misfit tolerance to stop inversion

The keyword is followed by a line with two records. The records are defined as follows,

1st FLOAT Overall travel time misfit defined along all wells (WCT)

2nd FLOAT Overall amplitude misfit defined along all wells (WCT)

3rd FLOAT Overall amplitude misfit defined along all wells (BHP)

These values will be used to stop the inversion whenever the specified tolerance is satisfied.

DIP_INV_TUNNING

Defines tuning parameters for running LSQR minimization

The keyword is followed by a line with five records. The records are defined as follows,

1st FLOAT Number of LSQR iterations

2nd FLOAT Decrease factor to be applied over the norm and smoothing constraints through iterations.

3rd FLOAT Maximum weight given to permeability changes at each iteration.

4th FLOAT Minimum weight given to permeability changes at each iteration.

5thFLOAT Default weight given to permeability changes in the each iteration

DIP_INV_CONSTRAINTS

Defines norm and smoothing constraints to minimize objective function

The keyword is followed by three lines with three records on each line. The records are defined as follows,

1st FLOAT FLOAT FLOAT Norm constraint

2nd FLOAT FLOAT FLOAT Horizontal smoothing constraint

3rd FLOAT FLOAT FLOAT Vertical smoothing constraint

DIP_INV_INTEGRATION #INT

Defines type of production data integration (added new options for Chapter II,III, and IV)

The keyword is followed by an integer (*#INT*). This integer defines the number of subsequent lines to be scanned. The records are defined as follows,

1st STRING Define which inversion type is applied (*WWCT/WGOR/BHP/BHPWCT/BHPGOR/BHPWCTGOR*)

2nd *STRING* Define inversion method, specifically method to calculate data misfit. 'RATE' or 'PRESSURE' depends on the well constraint for BHP inversion (Chapter III). 'COMP' is needed for transport tomography in Chapter II. (*GTT/TTM/AMP/GTTRATE/GTTPRESSURE/GTTCOMP/ TTMCOMP)*

3rd *FLOAT* Defines no. of iteration to run

DIP_INV_SETTINGS

Defines setting for inversion

The keyword is followed by a line with five records. The records are defined as follows,

Keyword to define WWCT inversion settings

1st *FLOAT* This will be the WWCT value selected for TTM misfit evaluation

2nd	*BOOLEAN*	Flag to include WWCT sensitivities in INVERSION, leave this field at TRUE (*TRUE/FALSE*)
3rd	*STRING*	When set to *PERM_RANGE*, a permeability range specified below will be applied to perm range for inversion process (*NONE/PERM_RANGE*)
4th	*FLOAT*	Define the lower limit for permeability (LOWER LIMIT OF PERM)
5h	*FLOAT*	Define the upper limit for permeability (UPPER LIMIT OF PERM)

DIP_INV_PARAMETER

Defines setting for GCT inversion (Chapter III – multiscale approach)

The keyword is followed by a line with two records. The records are defined as follows,

Keyword to define GCT inversion (global matching) settings

1st	*FLOAT*	Number of basis
2nd	*STRING*	File name to read basis values